의학박사 학위논문

Role of Type I interferon in infection of *Mycobacterium abscessus* to macrophages

대식세포에서 *Mycobacterium abscessus* 감염에 대한 제 1 형 인터페론 역할에 관한 연구

2019 년 2 월

서울대학교 대학원

의과학과 의과학전공

김 보 람

ABSTRACT

Mycobacterium abscessus complex (MAB) is a rapidly growing *Mycobacterium* (RGM), whose clinical significance as an emerging human pathogen has been increasing worldwide. It has two types of colony morphology, a smooth (S) type producing high glycopeptidolipid (GPL) content, and a rough (R) type which produces low levels of GPLs and is associated with increased virulence. The mechanism responsible for their difference in virulence is poorly known, while these pathogenic mechanisms should be proved at the molecular level.

In this study, I demonstrated that phagosomal escape of rough MAB-R strains in macrophage after phagosomal rupture can lead to Type I interferon (IFN) production. In addition, MAB-R strains enhance Type I IFN production and NLRP3 activation via mitochondrial stress mediated by release of oxidized mitochondrial DNA into cytosol.

By ultrastructural examination of murine macrophages infected with MAB strains, I found that MAB-R strains can replicate more actively in the macrophage phagosome than the S variants and that they could escape into cytosol subsequent to phagosomal rupture. The cytosolic access of MAB-R strains following phagosomal rupture brings about increased Type I IFN production via cGAS-STING signaling and cell death, which results in their cell-to-cell spreading. This behavior can provide an additional niche for the intracellular survival of MAB-R strains. In addition, I found that their enhancement of cell death mediated by cell spreading is dependent on Type I IFN signaling through comparison of wild-type and IFNAR1 knockout mice. This result indicated that a transition of MAB-S strains into MAB-R variants increases their virulence via elevated Type I IFN

production, which leads to enhancing their survival in infected macrophage via cell death mediated cell-to-cell spreading.

Next, I sought to explore experimentally that mitochondria stress caused by bacterial phagosomal rupture could contribute into enhanced Type I IFN secretion and NLRP3 inflammasome activation by MAB-R strains.

I showed that MAB-R strains lead to more mitochondrial stress and more release of oxidized mtDNA into cytosol compared to MAB-S strains in murine macrophage. It also leads to the enhanced NLRP3 inflammasome mediated by IL-1β and IRF3 dependent Type I IFN secretions in the infection of MAB-R strains. Treatment of infected macrophages with a mitochondria-specific antioxidant, mito-TEMPO reduced cytosolic oxidized mtDNA and inhibited both innate cytokines, IL-1β and Type I IFN by MAB-R strains, suggesting a pivotal role of mitochondrial stress in their innate cytokine inductions by MAB-R strains.

Finally, I found that treatment of cytochalasin D, which interferes with actin mediated bacterial phagocytosis, lead to inhibition of mitochondrial stress mediated by Type I IFN and IL-1β productions, suggesting a crucial role in actin dependent phagocytosis in MAB-R mediated mitochondrial stress.

Taken together, my study suggests that a transition of MAB-S strains into MAB-R variants increases their virulence via enhanced Type I IFN production, which leads to enhanced bacterial survival in infected macrophage via cell death mediated cell-to-cell spreading. Furthermore, MAB-R strains can lead to enhanced Type I IFN and IL-1β production via mitochondrial stress induction by actin dependent bacterial phagocytosis. This study further proposes that not only a novel insight

into the difference in virulence between MAB-R and -S variants but also hints about their treatment strategy.

Keywords: *Mycobacterium abscessus*, rough strains, phagosomal rupture, Type I interferon, cell death, cell-to-cell spread, mitochondrial stress, inflammasome.
Student number: 2012-21785.

CONTENTS

Abstract i

Contents iv

List of tables and figures vi

List of abbreviations viii

Introduction 1

Material and Methods 5

1. **Ethics statement** 5
2. **Mice** 5
3. **Cell culture** 5
4. **Preparation of Mouse Bone Marrow-derived Macrophages (BMDMs)** 5
5. **Preparation of Mouse Bone Marrow-derived Dendritic cells (BMDCs)** 6
6. **Bacterial strains and growth conditions** 7
7. **Confocal microscopy analysis** 8
8. **Construction of *Mycobacterium-E. coli* shuttle vectors for the expression of EGFP** 9
9. **Infection with mycobacterial strains and bacterial counts** 10
10. **Bacterial staining** 10
11. **Transmission electron microscopy** 11
12. **Immunoblotting assay** 11

13. Type I IFN bioassay and luciferase reporter assay 12
14. Apoptosis analysis 12
15. Cellular fractionation and detection of cytosolic DNA 13
16. Enzyme-linked immunosorbent assay 14
17. RNA purification and qRT-PCR 14
18. Measurement of mitochondrial membrane potential and mitochondrial ROS detection 15
19. Measurements of oxidative DNA damage quantitation 16
20. Statistical analysis 16

Results 17

1. MAB-R strains show greater intracellular growth and innate immune response in murine macrophage than MAB-S strains17
2. Increased multiplication of MAB-R strains in the macrophage phagosome leads to bacterial phagosomal escape after phagosomal rupture 21
3. Live MAB-R stains induce Type I IFN secretion in an IRF3-dependent manner 31
4. Live MAB-R stains enhance cell death in murine macrophage36
5. The caspase dependent apoptotic cell death by MAB-R strains contribute into their cell-to-cell spread 41
6. Enhanced cell-to-cell spreading of MAB-R strains is due to an IFNAR1-dependent pathway..... 47

7. MAB-R strains exert enhance mitochondrial stress compared to MAB-S strains..... 51
8. MAB-R strains lead to increased cytosolic mtDNA and cytosolic oxidized mtDNA compared to MAB-S strains 55
9. Enhanced IL-1ß secretion by MAB-R strains is due to both increased NLRP3 expression and inflammasome activation. 58
10. MAB-R strains lead to enhanced Type I IFNs in infected murine macrophages via actin dependent phagocytosis..... 68

Discussion **76**

References **83**

Abstract in Korean..... **95**

LIST OF TABLES AND FIGURES

Table 1. Primers sequences used in RT-qPCR 15

Table 2. Primers sequences used in cytosolic mtDNA 15

Figure 1. Comparison of intracellular survival and inflammatory cytokine production of MAB-R and -S strains of various subspecies or genotypes in infected murine macrophage 20

Figure 2. Morphological evidence of phagosomal escape and subsequent phagosomal rupture in MAB-R-infected murine macrophage..... 27

Figure 3. Detection of mycobacterial DNA from the cytosolic region of MAB-R-infected murine macrophages by PCR..... 31

Figure 4. Live MAB-R strains induce Type I IFN secretion via the cGAS-STING-IRF3 axis 35

Figure 5. Live MAB-R stains enhance apoptotic cell death in murine macrophage 40

Figure 6. Enhanced apoptotic cell death by a MAB-R strain contributes to its cell-to-cell spread..... 46

Figure 7. The cell-to-cell spread in MAB-R infection depends on Type I IFN signaling..... 50

Figure 8. MAB-R strains induce severe mitochondrial damages compared to MAB-S strains..... 54

Figure 9. Increased cytosolic mtDNA and oxidized DNA by MAB-R

strains in macrophage cell 57

Figure 10. Cytokine production by live or heat-killed mycobacteria in murine macrophages 60

Figure 11. Production of IL-1β induced MAB-R via NLRP3 inflammasome 61

Figure 12. mtROS enhance type I IFN production and cell-to-cell spread in MAB-R infection macrophage cells 67

Figure 13. Actin-dependent phagocytosis contributes to cell-to-cell spreading by MAB-R strains 73

Figure 14. Schematic of a phagocyte infected with MAB and the different events related Type I IFN production and NLRP3 inflammasome 75

LIST OF TABLES AND FIGURES

Table 1. Primers sequences used in RT-qPCR 15

Table 2. Primers sequences used in cytosolic mtDNA 15

Figure 1. Comparison of intracellular survival and inflammatory cytokine production of MAB-R and -S strains of various subspecies or genotypes in infected murine macrophage 20

Figure 2. Morphological evidence of phagosomal escape and subsequent phagosomal rupture in MAB-R-infected murine macrophage..... 27

Figure 3. Detection of mycobacterial DNA from the cytosolic region of MAB-R-infected murine macrophages by PCR..... 31

Figure 4. Live MAB-R strains induce Type I IFN secretion via the cGAS-STING-IRF3 axis. 35

Figure 5. Live MAB-R stains enhance apoptotic cell death in murine macrophage 40

Figure 6. Enhanced apoptotic cell death by a MAB-R strain contributes to its cell-to-cell spread..... 46

Figure 7. The cell-to-cell spread in MAB-R infection depends on Type I IFN signaling..... 50

Figure 8. MAB-R strains induce severe mitochondrial damages compared to MAB-S strains. 54

Figure 9. Increased cytosolic mtDNA and oxidized DNA by MAB-R

strains in macrophage cell. 57

Figure 10. Cytokine production by live or heat-killed mycobacteria in murine macrophages. 60

Figure 11. Production of IL-1β induced MAB-R via NLRP3 inflammasome 61

Figure 12. mtROS enhance type I IFN production and cell-to-cell spread in MAB-R infection macrophage cells. 67

Figure 13. Actin-dependent phagocytosis contributes to cell-to-cell spreading by MAB-R strains 73

Figure 14. Schematic of a phagocyte infected with MAB and the different events related Type I IFN production and NLRP3 inflammasome 75

LIST OF ABBREVIATIONS

AFB: acid-fast bacillus

ATCC: American Type Culture Collection

BM: bone-marrow

BMDC: Bone marrow-derived dendritic cell

BMDM: Bone marrow-derived macrophages

CIP: Collection de I'Institut Pasteur

cGAS: cyclic GMP-AMP Synthase

CFP-10: 10-kDa culture filtrate protein

CFU: colony-forming unit

Ct: cycle threshold

DAMP: Damage-associated molecular pattern

EGFP: Enhanced Green Fluorescent Protein

ELISA: enzyme-linked immunosorbent assay

ESAT-6: 6 kDa early secretory antigenic target

GPL: glycopeptidolipid

h.p.i.: hours post infection

hsp65: heat shock protein 65 kDa

IL-1β: Interleukin 1 beta

IFN: interferon

IRF3: interferon regulatory factor 3

KO: knock out

MAB: *Mycobacterium abscessus*

MACS: magnetic-activated cell sorting

mtROS: Mitochondrial reactive oxygen species

Mtb: Mycobacterium tuberculosis

M.O.I.: multiplicity of infection

LAMP-1: Lysosomal-associated membrane protein 1

NLRP3: NACHT, LRR and PYD domains-containing protein 3

NTM: non-tuberculous mycobacteria

OADC: oleic acid albumin dextrose catalase

OD: optical density

PCI: phenol-chloroform isoamyl alcohol

PCR: polymerase chain reaction

PRR: pattern recognition receptors

qRT-PCR: quantitative real-time polymerase chain reaction

***rpoB*:** RNA polymerase β-subunit gene

SEM: scanning electron microscopy

SNUMC: Seoul National University College of Medicine

STS: staurosporine

TBK1: TANK Binding Kinase 1

TEM: transmission electron microscopy

TLR: Toll-like receptor

INTRODUCTION

Mycobacterium abscessus complex (MAB) is now recognized as a major pathogen leading to pulmonary infection within the rapidly growing mycobacteria (RGMs) (1-3) and is a common pathogen in lung diseases, especially in cystic fibrosis patients (4-6). In South Korea, MAB lung diseases have also been increasing in frequency and account for 70 ~ 80% of RGM-induced lung diseases (7, 8). MAB is also one of the major pathogens leading to nosocomial infections (9). MAB infections are difficult to treat due to both natural broad-spectrum resistance and acquired resistance, with disparate antibiotic susceptibility patterns being observed between different clinical strains (10, 11).

MAB consists of diverse subspecies or genotypes. Currently, the MAB group can be divided into two subspecies, *M. abscessus* subsp. *abscessus* (hereafter, S-Abs) and *M. abscessus* subsp. *bolletii*. *M. abscessus* subsp. *bolletii* was proposed to include the two former species *M. massiliense* (S-Mas) and *M. bolletii* (S-Bol) (12, 13). S-Mas can be further subdivided into two *hsp*65 genotypes (Type I and Type II) (14).

MAB consists of two phenotypes: smooth colony (MAB-S) and rough colony (MAB-R), with or without glycopeptidolipid (GPL) gene synthesis (15, 16). In relation to these phenotypes, there have been reports of infection experiments using various cells such as macrophages and bronchial epithelial cells, and studies on the etiology of the pathogenesis in mouse models (16-18). MAB-S has an advantage in survival due to GPL-based biofilm formation, leading to inhibit bacteria-induced

apoptosis (2). So, the MAB-R variant without outer GPL induces could induce enhanced apoptotic cell death mediated invasion ability than MAB-S (17, 18). However, the underlying mechanism regarding the disparity between the pathogenic potential of MAB-R and -S types remains unknown.

Virulent *Mycobacterium tuberculosis* (*Mtb*) strains have ability to escape into the cytosol from the phagosome via the type VII secretion system ESX-1 (19, 20), which is responsible for the secretion of the 6-kDa early secreted antigenic target (ESAT-6), and its protein partner, the 10-kDa culture filtrate protein (CFP-10). *Mycobacterium marinum* can escape into the cytosol via a similar strategy as virulent *M. tuberculosis* (21). Active phagosomal rupture in antigen-presenting cells (APCs) such as macrophages or dendritic cells induced by the ESX-1 system present in the genome of pathogenic mycobacteria can expose bacterial DNA in the cytosol, which in turn drives the transcription of IFN-β via the cGAS–STING–TBK1–IRF3 axis and enhanced IL-1β secretion via NLRP3 inflammasome activation (3, 22). The activation of both Type I IFN signaling and inflammasome systems might synergistically contribute to the enhanced virulence of pathogenic mycobacteria via damping excessive inflammation and tissue damage. Furthermore, ESX-1–derived phagosomal rupture can result in toxicity and enhanced host cell death, also contributing to the virulence of pathogenic mycobacteria via increased intracellular bacterial growth (23-25).

Several previous studies consistently demonstrated that the MAB-R type survived more efficiently during infection into macrophage or dendritic cells than the MAB-S type (15, 18, 26, 27). Therefore, I hypothesized that enhanced survival of MAB-R strains in APCs may be due to the bacteria cytosol access and subsequent

phagosomal rupture. However, the previous complete genome studies of several MAB strains revealed that no orthologs corresponding to *M. tuberculosis* ESX-1 genes are in their genomes (28), suggesting there may be an alternative strategy facilitating cytosol access of the MAB-R type. Here, I elucidated the underlying mechanism that likely explains the distinct pathogenic potentials between the MAB-R and -S types, mainly focusing on Type I IFN signaling of MAB-R strains, the MAB-R access to cytosol rupture and their enhanced survival in macrophage via host-cell death mediated cell-to-cell spreading.

In addition, exposed bacterial DNAs of escaped bacteria into cytosol could in turn lead to exposing bacterial DNAs in cytosol, leading to driving secretion of Type I IFN via cGAS–STING sensing and enhanced IL-1β secretion via NLRP3 inflammasome activation. However, a recent study has reported that Type I IFN secretion was varied depending on *M. tuberculosis* strains despite there being no difference in bacterial cytosol access via phagosome rupture between them, suggesting the presence of other factors affecting Type I IFN secretion in *Mtb* infection (29). Indeed, other authors proved that mitochondrial stress mediated release of mtDNA into cytosol may play a more pivotal role in Type I IFN secretion via cGAS-STING axis rather than cytosol bacterial DNA. In NLRP3 dependent inflammasome activation, contribution of the cytosol exposed oxidized mtDNA has also been proved (30, 31). Besides its role in classical energy production as cell factor, mitochondria can also play a very pivotal role in signaling controls innate and adaptive immune responses (32). In particular, mitochondrial components such as mtDNA can activate the NLRP3 inflammasome and TLR9 to induce an inflammatory response as damage-associated molecular patterns

(DAMPs). In addition, it also can exert an innate antiviral response by inducing Type I IFN secretion via cGAS-STING-TBK-IRF3 axis (33-35).

So, here, I elucidated underlying mechanism for the likely explanation of distinct pathogenic potentials between MAB-R and -S stains, mainly focusing on Type I IFN signaling via both mechanisms, one for exposed bacterial DNAs into cytosol by bacteria escape from phagosome into cytosol and the other for mitochondrial stress mediated release of mtDNA into cytosol.

MATERIALS AND METHODS

1. Ethics statement

All animal treatment was in accordance with the institutional recommendations in the National Guidelines for the care and use of laboratory animals. The protocol was approved by the Institutional Animal Care and Use Committee (IACUC; approval No. of SNU-170717-7) of the Institute of Laboratory Animal Resources at Seoul National University.

2. Mice

Male C57BL/6 mice and C57BL/6 IFNAR KO mice (~25 g, 6 weeks old) were purchased from Orient-Bio (Seongnam, South Korea). All mice were housed and maintained in a specific pathogen-free facility at Seoul National University College of Medicine. All mice were used for experiments at 8 ~12 weeks of age.

3. Cell culture

J774A.1 (murine macrophage) and L929 cells (mouse fibroblast, CCL-1) were maintained in Dulbecco's modified Eagle's medium (DMEM) containing 10% fetal bovine serum and penicillin/streptomycin (100 U/ml) and kept at 37°C and 5% CO2 in humid incubator.

4. Preparation of Mouse Bone Marrow-derived Macrophages (BMDMs)

Bone marrow-derived macrophages (BMDMs) were generated from the bone-marrow (BM) of 8-12 weeks-old C57BL/6J mice. BM cells were obtained from femurs and tibia of mice and flushed out with serum-free DMEM media (Gibco). The single cell suspension was then filtered through a nylon cell strainer (70-µm Nylon mesh; BD Pharmingen, Franklin Lakes, NJ, USA), washed twice with HBSS media. Pellet the cells by centrifugation (350 x *g*, 5 minutes) and aspirate the supernatant. Resuspend the pellet with Red Blood Cell Lysis Buffer (sigma) and Incubate 3 minutes at room temperature and Stop the reaction by diluting the Lysis Buffer with V/V ml of serum-containing DMEM media. Spin the cells (350 x *g*, 5 minutes) and discard the supernatant. BMDMs were differentiated from bone marrow precursors cultured for 4 days in complete DMEM containing 10% FBS, 1% sodium pyruvate, 4 mM glutamine, and 1% penicillin-streptomycin (100 units/ml) supplemented with 10% L929 cell-conditioned media. Total BM cells were cultured in microbiological 12- or 24-well plates (Sterilin) and kept at 37 °C and in 5% CO2 in a humid incubator.

5. Preparation of Mouse Bone Marrow-derived Dendritic cells (BMDCs)

Bone marrow-derived dendritic cells (BMDCs) were generated from the bone marrow (BM) of 8-12 weeks-old C57BL/6J mice. The BM cells were flushed out of the femurs and tibias with serum-free Iscove's modified Eagle medium (IMDM; Gibco Invitrogen). The single cell suspension was then filtered through a nylon cell strainer (70-µm Nylon mesh; BD Biosciences, San Jose, CA, USA), washed twice with HBSS media. BMDCs were differentiated with complete IMDM supplemented with 10% FBS (Gibco, Invitrogen), recombinant mouse GM-CSF

(20 ng/ml, PeproTech, Rocky Hill, NJ, USA) and mouse IL-4 (20 ng/ml; PeproTech), penicillin (100 units/ml; Gibco Invitrogen), streptomycin (100μg/ml; Gibco Invitrogen), gentamicin (50μg/ml; Gibco Invitrogen), L-glutamine (2 mM; Gibco Invitrogen), and β–mercaptoethanol (50 nM; Gibco Invitrogen) and seeded at a concentration of 1×10^6 cells per well in a 24-well plate in a final volume of 2 ml of complete IMDM. Half of the medium was replaced every other day with an equal volume of complete IMDM for 6 days. All the cells expressing $CD11C^+$ in the different wells were isolated using appropriate magnetic-activated cell sorting (MACS) kits according to the manufacturer's instruction (Miltenyi Biotec). $CD11c^+$ cells were collected and used in all experiments.

6. Bacterial strains and growth conditions

The mycobacterial strains used in this study are as follows: 5 type strains of *Mycobacterium abscessus* (ATCC 19977^T rough and smooth type), *Mycobacterium abscessus* subsp. *massiliense* (CIP 108297^T), *Mycobacterium smegmatis* ATCC 19420^T, *Mycobacterium bovis* BCG Tokyo strain (BCG), and *Mycobacterium marinum* JCM 17638^T. 13 clinical isolates of *Mycobacterium abscessus* smooth (S-Abs_S; Asan 53040 and Asan 58582) and rough (As S-Abs_R; Asan 52550 and Asan 58116), *Mycobacterium abscessus* subsp. *massiliense* Type I smooth (S-Mas_I-S; Asan 15 and Asan 51312, Asan 51843), type I-Rough (S-Mas_I-R; Asan 16 and Asan 22, Asan 34), type II-Rough (S-Mas_II-R; Asan 4 and Asan 50594, Asan 62188). All the strains were cultured from low-passage frozen stocks (at −70°C) to exponential phase and subcultured in 7H9 broth (supplemented with 10% ADC) or on 7H10 agar plates (supplemented with 10% OADC) at 37°C for each

experiment. RGM were grown in Middlebrook 7H9 broth supplemented with Tween 80 and 10% ADC (BD) by shaking incubation for 3-5 days (SGM; for 14-28 days) at 37°C. To obtain single-cell bacterial suspensions, all the strains were washed and resuspended in phosphate-buffered saline (PBS) with 0.05% Tween 80 (PBS-T) and passed through a 27-gauge needle three to five times. The concentration was determined by measuring the optical density at 600 nm (OD 600) as a function of CFU/ml. To inactivate various mycobacteria strains, I heated them at 100°C in a boiling-water bath for 30 minutes.

7. Confocal microscopy analysis

To evaluate co-localization with bacteria containing phagosome and lysosome, I prepared J774A.1 cells on chamber plates (Nunc™ Lab-Tek™ II Chamber Slide™ System). The cells infected for 24 h.p.i. with CFSE (#C34554, Invitrogen) stained bacteria [MAB-R (M. abscessus type strain ATCC 19977 rough strain) MAB-S (M. abscessus type strain ATCC 19977 smooth strain] at an M.O.I of 10. After infection, the cells were washed with PBS and then fixed with 4% paraformaldehyde for 10 minutes at room temperature. To visualize the phagosomal lysosome, the fixed infected cells were permeabilized with a 0.1% Triton X-100 for 10 minutes and blocked with 1% BSA for 30 minutes room temperature. The cells were labeled with rat anti-LAMP1 antibody (#25245, Abcam) and incubated for 18 hours at 4°C and then labeled with Goat anti-Rat IgG (H+L), Alexa Fluor® 633 conjugate, dilution 1:1000 for 45 minutes at room temperature. Nuclei were stained with 300 nM DAPI (#D1306, Invitrogen) for 5 minutes at room temperature. The samples were washed with PBS and mounted on

a glass slide with Vectashield solution (Vector Laboratories) and observed using a confocal laser scanning microscope system (Olympus-FV1000).

8. Construction of *Mycobacterium-E. coli* shuttle vectors for the expression of EGFP

Using the pAL5000-TOPO vector, an EGFP-expressing *Mycobacterium-Escherichia coli* shuttle vector was generated as previous study (36). Briefly, the *EGFP* gene was amplified from the pIRES2-EGFP vector (Clontech, Mountain View, CA, USA; Cat No., 6029–1), and the *hsp65* promoter gene was amplified from genomic DNA of *M. bovis* BCG. The *EGFP* gene with the *hsp65* promoter was amplified from the pMyong2-EGFP^{h} vector and ligated into pAL5000-TOPO using *HindIII* and *BamHI* restriction sites. The *hsp65* promoter and *EGFP* gene were amplified by overlapping PCR. To generate three different types of recombinant strains expressing *EGFP* (Asan 50594, *M. smegmatis* and BCG), the pAL5000-TOPO-EGFP plasmid was electroporated into competent bacteria (Asan 50594, *M. smegmatis* and BCG) using the Gene Pulser II electroporation apparatus (Bio-Rad, Hercules, CA, USA). Transformants were selected on Middlebrook 7H10 medium (Difco Laboratories, Detroit, MI, USA) (37) supplemented with OADC and containing 100 μg/ml kanamycin. Typically, colonies of transformants were selected from the plates, transferred into 7H9 broth medium (Difco Laboratories, Detroit, MI, USA) supplemented with 0.5% glycerol, 0.05% Tween-80, 10% ADC and 100 μg/ml kanamycin and cultured for 3~5 days. The growth rate of the recombinant mycobacteria strains was determined by measuring the medium OD at 600 nm.

9. Infection with mycobacterial strains and bacterial counts

The J774A.1 cells, BMDMs, and immature BMDCs were infected with mycobacterial strains at an M.O.I. of 10 and incubated for 2 hours to allow the phagocytosis of the bacteria (The meaning of 0 hr I referred to means this time point). The infected cells were washed three times with PBS and to remove extracellular mycobacteria, cells were incubated with fresh culture medium containing 50 μg/ml amikacin (27, 55). The term h.p.i. (hours post infection) refers to the incubation time after a fresh antibiotic medium change. After further incubation, the cells were detached by PBS with 0.5% Triton-X-100 or by scraping at each time point. The cell pellets were diluted in PBS and plated onto 7H10 agar plates (supplemented with OADC) to determine the CFUs. The cell culture supernatants were collected and stored in a deep freezer (at −70 °C) for determining the cytokine levels.

10. Bacterial staining

The bacterial infected cells were prepared on chamber plates (Nunc™ Lab-Tek™ II Chamber Slide™ System), and the plates were then placed on a dryer with their smeared surface upwards, where they were air-dried for approximately 30 minutes and then heat-fixed. The specimens were covered with carbol fuchsin stain and then heated until vapor just began to rise (i.e., approximately 60 °C). Additional stain was added if necessary, and the heated stain remained on the slide for 5 minutes. The stain was removed by washing with clean water. The smear was covered with 3% v/v acid alcohol (or 20% sulfuric acid) for 20 seconds and washed

off with clean water. Methylene blue was then applied to counterstain any cells that had been decolorized. The smear was then examined with microscope using the 100 × oil immersion objective (10 × eye piece for a total of 1000 × magnification), and the smear was systematically scanned.

11. Transmission electron microscopy

Infected cells were washed with PBS and fixed with 2% paraformaldehyde (v/v) and 2% glutaraldehyde (v/v) in 0.05 M Na cacodylate-HCl buffer (pH 7.2) at 4 °C for 2~4 hours. Primary fixed samples were washed three times with 0.05 M Na cacodylate-HCl buffer (pH 7.0) at 4 °C for 10 minutes. The fixed samples were postfixed with 1% osmium tetroxide (w/v) in Na cacodylate-HCl buffer (pH 7.2) at 4 °C for 2 hours. Then, fixed samples were washed two times with distilled water at room temperature. The pelleted cells were block-stained with 0.5% uranyl acetate (w/v) at 4 °C for 30 minutes and dehydrated with 30, 50, 70, 80, 90, 100, 100, and 100% at room temperature for 10 minutes each. The samples were transferred two times with 100% propylene oxide at room temperature for 15 minutes, 1:1 propylene oxide/Spurr's resin (2 hours), 1:2 propylene oxide/Spurr's resin (4 hours or overnight), and 100% Spurr's resin (2 hours) to infiltrate. In the following step, samples were embedded in molds filled with a mixture of Spurr's epoxy resin and polymerized for 24 hours at 70 °C. The polymerized blocks were cut on a ultramicrotome (MT-X, RC, Tucson, AZ, USA), and sections were stained with 2% uranyl acetate (7 minutes) followed by Reynolds' lead citrate (7 minutes) and then examined on a JEOL transmission electron microscope (Japan) at 80 kV accelerating voltage.

12. Immunoblotting assay

Infected cell lysates were collected for protein analysis, and cells were lysed in RIPA buffer (Cell Signaling) containing complete EDTA-free protease inhibitor (Roche) and phosphatase inhibitor cocktail (Roche). Protein concentrations were determined using a bovine serum albumin (BSA) protein assay (Bio-Rad). Cellular proteins separated by SDS–polyacrylamide gel electrophoresis were electrotransferred to nitrocellulose (NC) membranes and subjected to immunoblot analysis with various primary antibodies. Immunoblot analysis was done with various primary antibodies: anti-rabbit IRF3 (#4302; Cell Signaling), anti-rabbit pIRF3 (#29047; Cell Signaling), anti-rabbit cGAS (#31659; Cell Signaling), anti-rabbit STING (#29047; Cell Signaling), anti-rabbit Actin (sc-1616; Santa Cruz Biotechnology), and anti-rabbit GAPDH (sc-25778; Santa Cruz Biotechnology) antibodies.

13. Type I IFN bioassay and luciferase reporter assay

Supernatants from infected cells were overlaid on top of L929 IFN reporter cells containing the ISRE-luciferase construct (38) and incubated for 4 hours (48- or 96-well plates). The reporter cells were lysed in Reporter Lysis Buffer (Promega, Madison, WI, USA) for 30 minutes at room temperature and mixed with firefly luciferin substrate (Promega, Madison, WI, USA), and luminescence was measured on an illuminometer (TECAN).

14. Apoptosis analysis

Cells were seeded in 12-well plates and infected the following day with the different strains as explained before. The supernatant was completely aspirated and washed with PBS 2 times, trypsinized cells were collected, and cells were used to analyze apoptosis by flow cytometry. Phosphatidylserine (PS) exposure and membrane integrity were analyzed by using Annexin V and 7-AAD (BD Biosciences) and flow cytometry according to the manufacturers' instructions. Briefly, cells were washed with PBS and incubated with Annexin V and 7-AAD in Annexin V Binding buffer for 15 minutes. Then, 400 µl of Annexin V Binding buffer was added to each tube, and the samples were analyzed by flow cytometry (FACS LSRFortessa X-20).

15. Cellular fractionation and detection of cytosolic DNA

BMDM and J774A.1 cells were infected in 6-well plates. Cytosolic cell fractions were isolated using the manufacturer's protocol for the Qproteome Cell Compartment Kit (QIAGEN). Briefly, cell pellets were resuspended in ice-cold PBS by pipetting up and down and then centrifuged three times at 500 × *g* at 4 ℃ for 10 minutes; this process was repeated three times. The supernatant was carefully removed and discarded, and the pellets were resuspended in Protease Inhibitor Solution lysis buffer, vortexed and incubated at 4°C for 10 minutes on an end-over-end shaker. The lysate was centrifuged at 1000 × *g* for 10 minutes at 4°C, and the supernatant was carefully transferred into a new microcentrifuge tube, where it was stored on ice. This supernatant primarily contained cytosolic proteins. To extract DNA from the fractionized supernatant, I performed the PCI method (39). To detect mycobacterial DNA, I specifically targeted the mycobacterial *hsp65*

gene (14) and applied PCR (40). A set of primers HspF3 (forward; 5'-ATC GCC AAG GAG ATC GAG CT-3') and HspR4 (reverse; 5'-AAG GTG CCG CGG ATC TTG TT- 3') was used.

16. Enzyme-linked immunosorbent assay

Cells were infected in 6-, 12-, and 24-well plates. Post infection cell culture supernatants were collected from infected cells and stored at -70 °C. Paired antibodies and standard recombinant mouse IL-1β, TNF-α, IL-6, IL-10 (eBioscience), and IFN-β (BioLegend) were used to determine cytokine concentrations according to the manufacturers' instructions.

17. RNA purification and qRT-PCR

Total RNA was extracted from cells using TRIzol (Invitrogen) according to the manufacturer's instructions. For quantitative real-time PCR analysis, cDNA was amplified using specific primers for IFI204, IFN-β, STING and SYBR green PCR Master Mix (Applied Biosystems, Grand Island, NY, USA) and processed using an ABI 7500 (Applied Biosystems, Grand Island, NY, USA). The results were acquired as cycle threshold (Ct) values and represented the average of at least two independent experiments. The relative amount of mRNA ($2^{\Delta\Delta Ct}$) was obtained by normalizing its level to that of the β-actin gene in each experiment. The specific primer sequences are listed in Table 1. (41, 42). To detect cytosolic mtDNA, the specific primer sequences are listed in Table 2. The relative level of gene expression was calculated by the 2-dCt or the ddCt method, where actin was used

for normalization. The RT-qPCR graphs represent the average of at least two independent experiments.

Table 1. Primers sequences used in RT-qPCR

IFN-β	forward	5’-ATGGTGGTCCGAGCAGAGAT-3’
	reverse	5’-CCACCACTCATTCTGAGGCA-3’
IFI204	forward	5’-GAGCAAGGCGGCTAAGGAA-3’
	reverse	5’-GCTGTGGAGTATTGGTGACTG-3’
STING	forward	5'-AAATAACTGCCGCCTCATTG-3′
	reverse	5'-ACAGTACGGAGGGAGGAGG-3′
IRF-3	forward	5'-GGCTTGTGATGGTCAAGGTT-3’
	reverse	5’-CATGTCCTCCACCAAGTCCT-3’
β-actin	forward	5’-GTGACGTTGACATCCGTAAAGA-3’
	reverse	5’-GCCGGACTCATCGTACTCC-3’

Table 2. Primers sequences used in cytosolic mtDNA

β-Actin	forward	5’-GTGACGTTGACATCCGTAAAGA- 3’
	reverse	5’-GCCGGACTCATCGTACTCC-3’
mtDNA Dloop-1	forward	5'-AATCTACCATCCTCCGTGAAACC-3’
	reverse	5’-TCAGTTTAGCTACCCCCAAGTTTAA-3’
mtDNA Dloop-2	forward	5'-CCCTTCCCCATTTGGTCT-3’
	reverse	5’-TGGTTTCACGGAGGATGG-3’
mtDNA Dloop-3	forward	5'-TCCTCCGTGAAACCAACAA-3’
	reverse	5’-AGCGAGAAGAGGGGCATT-3’
mtDNA CytB	forward	5’-GCTTTCCACTTCATCTTACCATTTA-3’
	reverse	5’-TGTTGGGTTGTTTGATCCTG-3’
mtDNA 16S	forward	5’-CACTGCCTGCCCAGTGA-3’
	reverse	5’-ATACCGCGGCCGTTAAA-3’
mtDNA ND4	forward	5’-AACGGATCCACAGCCGTA-3’
	reverse	5’-AGTCCTCGGGCCATGATT-3’

18. Measurement of mitochondrial membrane potential and mitochondrial ROS detection

Cells stained with the cationic dye TMRM (Invitrogen) or mitochondrial superoxide indicator MitoSOX (Invitrogen) as described in the manufacturer's protocol. Cells were loaded with 200 nM of TMRM for 30 minutes or 5 μM of MitoSOX for 30 minutes and washed three times with PBS. TMRM and MitoSOX fluorescence was measured using the FACS Calibur (Becton-Dickinson, San Diego, CA) and were gated and analyzed using forward and side-scatter plots on 10,000 live events.

19. Measurements of oxidative DNA damage quantitation

Extract DNA from infected cell by commercial DNA Extration kit (G-spin™ Total DNA Extraction Mini Kit, Intron). The DNA samples were incubated at 95 °C for 5 minutes and raplidly chilling on ice for single-stranded DNA. Digest the DNA sample 5 units of nuclease P1 for 2 hours at 37°C in a final concentration of 20 mM sodium acetate, pH 5.2 and treatment of 5 units of alkaline phosphatase for 1 hour at 37 °C in a final concentration of 100 mM Tris pH 7.5. The reaction mixture samples centrifuged for 5 minutes at 6000×*g* and the supernatant is used for measurement of oxidative DNA damage quantitation. To measurement oxidative DNA damage quantitation, the manufacturer's protocol for using OxiSelect™ Oxidative DNA Damage ELISA Kit 8-OHdG Quantitation (Cell biolab).

20. Statistical analysis

Statistical analysis was performed using GraphPad Prism 5 software and Microsoft

Excel software. All experiments were performed at least two times and the data are presented as the mean ± standard deviation (SD). Asterisks indicate significance as determined by the ANOVA with Tukey's correction and the Student's *t*-test calculated as described in figure legends (*$P < 0.05$; **$P < 0.01$, and ***$P < 0.001$).

RESULTS

MAB-R strains show greater intracellular growth and innate immune response in murine macrophage than MAB-S strains

Previously, MAB-R strains have been reported to better survive in macrophage and lead to more proinflammatory cytokines than MAB-S strains (26). However, variation in survival- or inflammation-inducing capacity between subspecies or genotypes of MAB has not been addressed. Therefore, I evaluated the intracellular growth (Figure 1A-C) and pro- (TNF-α and IL-6) and anti- (IL-10) inflammatory cytokine secretion (Figure 1D-F) of MAB-R and -S strains of various subspecies or genotypes [S-Abs smooth strains (S-Abs_S): *M. abscessus* type strain ATCC 19977 smooth strain, Asan 53040 and Asan 58582; S-Abs rough strains (S-Abs_R): *M. abscessus* type strain ATCC 19977 rough strain, Asan 52550 and Asan 58116; S-Mas type I-Smooth (S-Mas_I-S): type strain, Asan 15, Asan 51312, and Asan 51843; S-Mas type I-Rough (S-Mas_I-R): Asan 16, Asan 22, and Asan 34; and S-Mas type II-Rough (S-Mas_II-R): Asan 4, Asan 50594, and Asan 62188] in murine

macrophage J774A.1 cells as a function of the multiplicity of infection (M.O.I.) (Figure 1A-B). The survival of intracellular mycobacteria was examined with a colony-forming unit (CFU) assay. The results showed that irrespective of subspecies or genotypes, MAB-R strains formed significantly higher levels of CFUs than MAB-S strains in J774A.1 cells. A similar growth trend was also shown in a bone marrow-derived macrophage (BMDM) cells (Figure 1C). Of note, MAB-R and -S strains showed different intracellular growth kinetics. Briefly, there were no significant differences in intracellular growth between MAB-S and MAB-R infected cells at 0 hr (it means time points after incubation for 2 hr to allow the phagocytosis of the bacteria). MAB-R strains showed a marked increase in intracellular growth in BMDM as infection time increased (0 to 6 h and 6 to 24 h), but in contrast, MAB-S strains were almost invariable in intracellular growth in BMDM between 3 time points (0, 6 and 24 h). It suggests that the increased number of MAB-R strain in phagocytes may be due to its active replication within phagocytes.

To check the capacity of MAB-R and -S strains to induce the innate immune response, I measured cytokine production from supernatants of infected cells with 10 M.O.I at 24 h.p.i by enzyme-linked immunosorbent assay (ELISA). Both of the pro-inflammatory cytokines TNF-α and IL-6 were more induced in two different macrophages (J774A.1 cells and BMDMs) and in BMDCs infected with MAB-R strains than in those infected with MAB-S strains (Figure 1D-F). In addition, the anti-inflammatory cytokine IL-10 was also more induced in MAB-R strain-infected cells (Figure 1D-F). The expression of GPL, which is known to inhibit TLR2 signaling (43), is reduced in the MAB-R strains, and thus the expression of

cytokines induced by MAB-R strains is increased, compared to MAB-S strains. Together, these results indicated that MAB-R strains showed increased intracellular growth and innate immune responses in murine macrophage than MAB-S strains, irrespective of the taxonomic status of subspecies or genotype. It also suggests M AB-R strains may promote enhanced airway inflammation compared to MAB-S strains

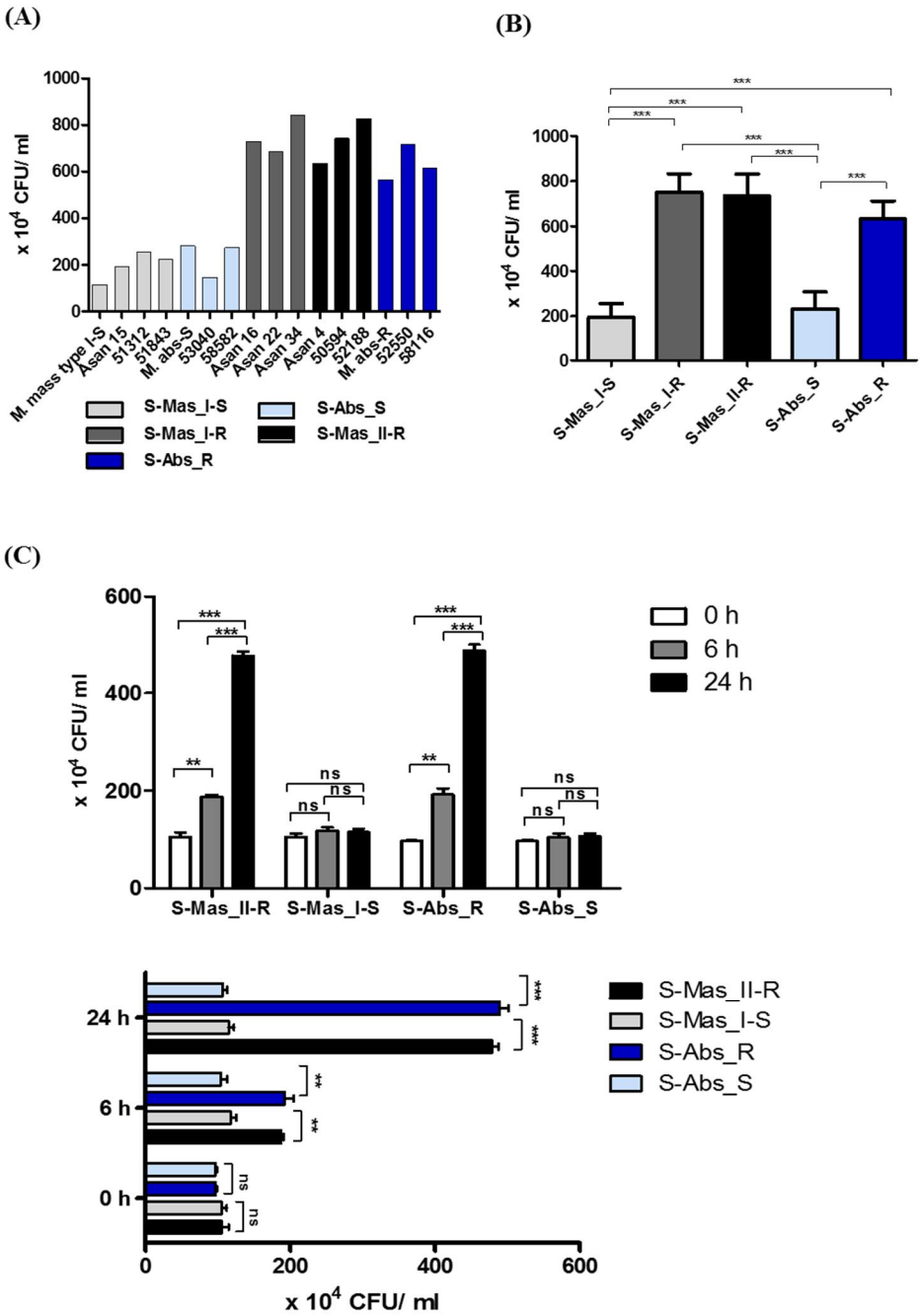
(A)
x 10^4 CFU/ ml
1000
800
600
400
200
0
M. mass type I-S
Asan 15
51312
51843
M. abs-S
53040
58582
Asan 16
Asan 22
Asan 34
Asan 4
50594
52188
M. abs-R
52550
58116
S-Mas_I-S
S-Mas_I-R
S-Abs_R
S-Abs_S
S-Mas_II-R
(B)
x 10^4 CFU/ ml
***
S-Mas_I-S
S-Mas_I-R
S-Mas_II-R
S-Abs_S
S-Abs_R
(C)
x 10^4 CFU/ ml
600
400
200
0
0 h
6 h
24 h
**
ns
S-Mas_II-R
S-Mas_I-S
S-Abs_R
S-Abs_S
x 10^4 CFU/ ml

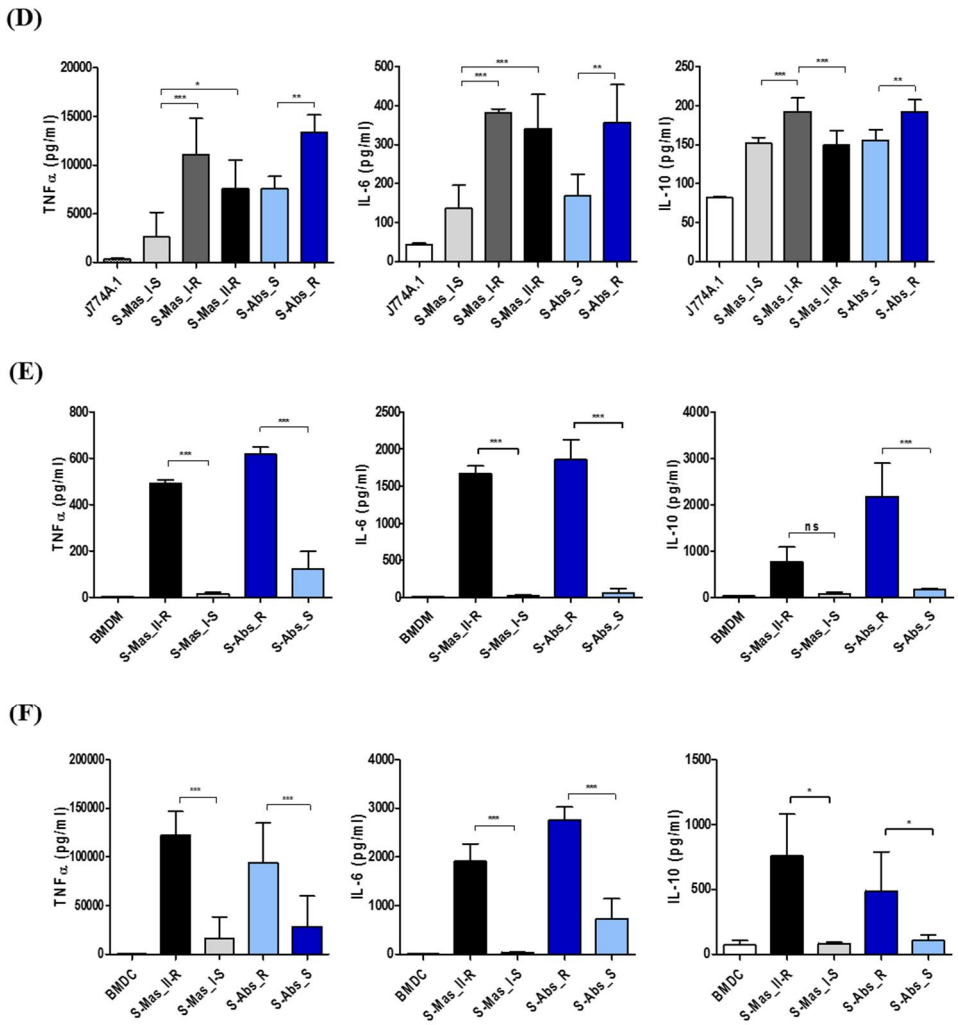

Figure 1. Comparison of intracellular survival and inflammatory cytokine production of MAB-R and -S strains of various subspecies or genotypes in infected murine macrophage. (A) CFU assays of MAB-R and -S strains of various subspecies or genotype [S-Abs smooth strains (S-Abs_S): *M. abscessus* type strain ATCC 19977 smooth strain, Asan 53040 and Asan 58582; S-Abs rough strains (S-Abs_R): *M. abscessus* type strain ATCC 19977 rough strain, Asan 52550 and Asan 58116; S-Mas type I-Smooth (S-Mas_I-S): type strain, Asan 15, Asan 51312, and Asan 51843; S-Mas type I-Rough (S-Mas_I-R): Asan 16, Asan 22, and

Asan 34; and S-Mas type II-Rough (S-Mas_II-R): Asan 4, Asan 50594, and Asan 62188] in infected J774A.1 cells at 37°C for 24 h.p.i. (B) The mean number of CFUs of various subspecies or genotypes of MAB surviving in infected J774A.1 cells. (C) Comparison of the number of CFUs from MAB-R [S-Abs_R (*M. abscessus* type strain ATCC 19977 rough strain) and S-Mas_II-R (Asan 50594)] and MAB-S strains [S-Abs_S (*M. abscessus* type strain ATCC 19977 smooth strain) and S-Mas_I-S (Asan 51843)] at 37°C at different time points (0, 6 and 24 h) after infection of BMDM at 10 M.O.I. (D-F) Comparison of the mean value of proinflammatory cytokine production (TNF-α, IL-6, and IL-10) between various MAB-R and -S strains (10 M.O.I, at 24 h.p.i) from infected J774A.1 cells (D), BMDMs (E), and BMDCs (F). The results are representative of two independent experiments and represent means ± SD. *P* values were determined by one-way ANOVA with Tukey's multiple comparison test (B and D-F) and paired Student's *t*-test (C) using GraphPad prism program: ns, nonsignificant; $*P < 0.05$; $**P < 0.01$, and $***P < 0.001$.

Increased multiplication of MAB-R strains in the macrophage phagosome leads to bacterial phagosomal escape after phagosomal rupture

To better understand the mechanism underlying the different growth kinetics during macrophage infections of MAB-R and -S strains (Figure 2A-B). I conducted transmission electron microscopy (TEM) and acid-fast bacillus (AFB) staining of infected murine macrophage. First, J774A.1 cells were infected with MAB-R and -S strains at an M.O.I. of 10 for 24 h (see Experimental procedures). After extensive washing to eliminate the residual extracellular bacteria, cells were fixed and

processed for AFB staining. The results showed that while only a few MAB-S strains were phagocytized and confined into small phagosomes, several MAB-R strains were clustered in a few large phagosomes (Figure 2A). Furthermore, while the number of surviving MAB-S cells were almost always invariant at different time points [(0.5, 2, 4, 8, and 18 h.p.i. (hours post-infection)], the numbers of MAB-R cells within phagosomes appear to be increased with infection time, suggesting their active replication in phagosome (Figure 2B). I hypothesized that this AFB staining data is not MAB-S but MAB-S, actively replicated in phagosomes in the initial phase of macrophage infection and that then bacterial overgrowth beyond the phagosome capacity could lead to phagosomal rupture. To further prove this hypothesis, BMDMs were infected with MAB-R and -S strains, and the intracellular localization of the bacteria was examined 24 h.p.i. by TEM. As previously reported (44), in MAB-S strains, single bacteria were located in a phagosome, and the outermost electron translucent zone (ETZ) (marked as a small arrow) (Figure 2C), which is a major part of the mycobacterial cell wall, was thick and poised all around the phagosome membrane. In contrast, MAB-R strains displayed a very thin ETZ, and several bacteria (up to more than 10 bacilli) were located in a larger phagosome (Figure 2C-F). I randomly selected 30 phagosomes in MAB-R or MAB-S infected BMDMs and compared their bacterial numbers in each phagosome (Figure 2D). As a result, I found that bacteria number in phagosome of MAB-R infected BMDMs is significantly higher in that in phagosome of MAB-S infected BMDMs, suggesting active replication of MAB-R strains in phagosome. I also found several pieces of TEM evidence supporting active multiplication through the binary fission of MAB-R in a phagosome of

BMDM (Figure 2E), suggesting that the increased initial intracellular growth of MAB-R strains in macrophage may be due to the its active multiplication within the phagosome (bacterial replication indicated with an asterisk). In addition, my TEM-based study also showed that while MAB-S strains were primarily localized within membrane-bound vesicles within the phagosome, a few MAB-R strains could move from the phagosome into the cytosol of macrophages (marked as a black arrow) (Figure 2E). Furthermore, I also found that in some cases of MAB-R-infected macrophages, bacteria were released into the space, even with a concomitant rupture of the cell membrane (Figure 2F-G), which is consistent with a previous report that the bacterial cytosol access after phagosomal rupture could lead to cell-to-cell spreading via cell membrane ruptures (19). Furthermore, to prove cytosol access of MAB-R strain, I investigated colocalization of MAB-R strains and a late endosome marker (45), LAMP-1 via confocal microscopy. As shown in Figure 2E, the colocalization of MAB-R with LAMP-1 was significantly lower than that of MAB-S (Figure H), which cannot escape into cytosol, strongly supporting TEM based finding of phagosome escape of MAB-R strains. To further prove the phagosomal escape of MAB-R strains during infection, I evaluated the mycobacterial DNA in the nuclear and cytosol fractions in cytosol isolated from infected cells (Figure 3C) after phenol-chloroform isoamyl alcohol (PCI) DNA extraction (see Experimental procedures). As shown in Figure 3, I detected mycobacterial *hsp65* DNA in the cytosol fraction of macrophages with either one of two MAB-R strains [S-Abs_R (*M. abscessus* type strain ATCC 19977 rough strain) and S-Mas_II-R (Asan 50594)] or with *M. marinum*, which is known to be capable of phagosomal escape (21, 46) and served as a positive control; this DNA

was not detected in this fraction from macrophages infected with either of two MAB-S strains [S-Abs_S (*M. abscessus* type strain ATCC 19977 smooth strain) and S-Mas_I-S (Asan 51843)], *M. smegmatis* or BCG (Figure 3A, B), further supporting my TEM finding of phagosomal escape by MAB-R strains. Together, these data indicated that MAB-R strains but not MAB-S strains lead phagosomal escape and subsequent phagosomal rupture, which may be due to active multiplication of MAB-R strains in macrophage phagosomes.

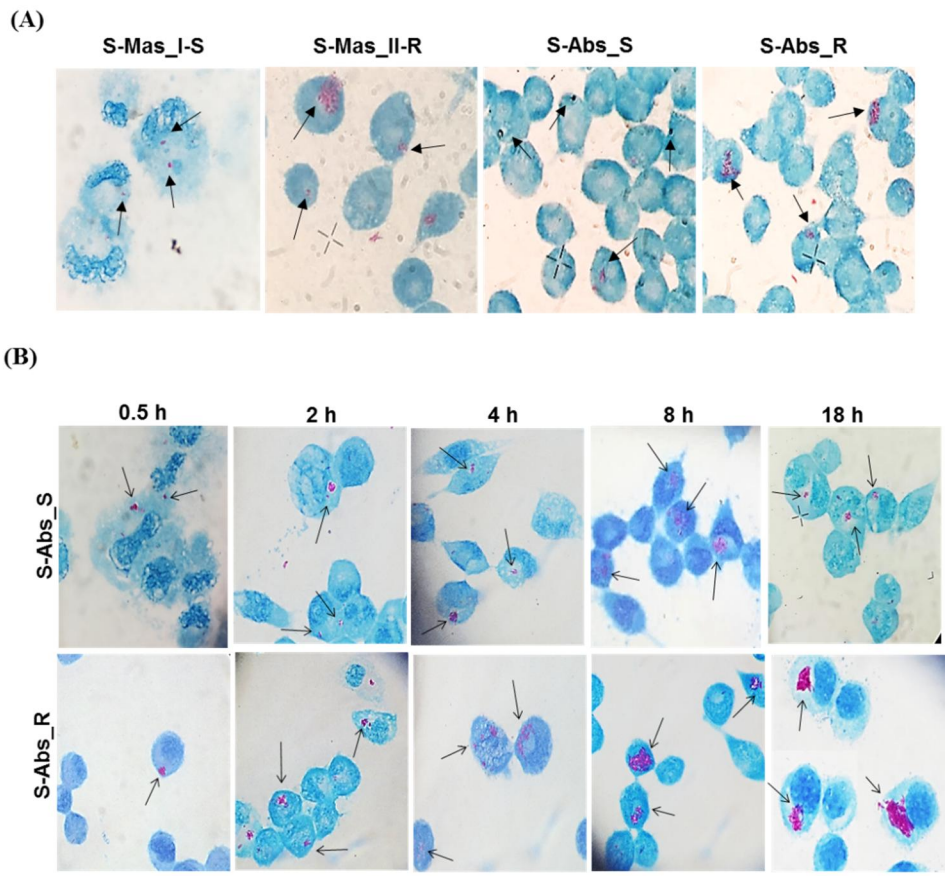

(C)

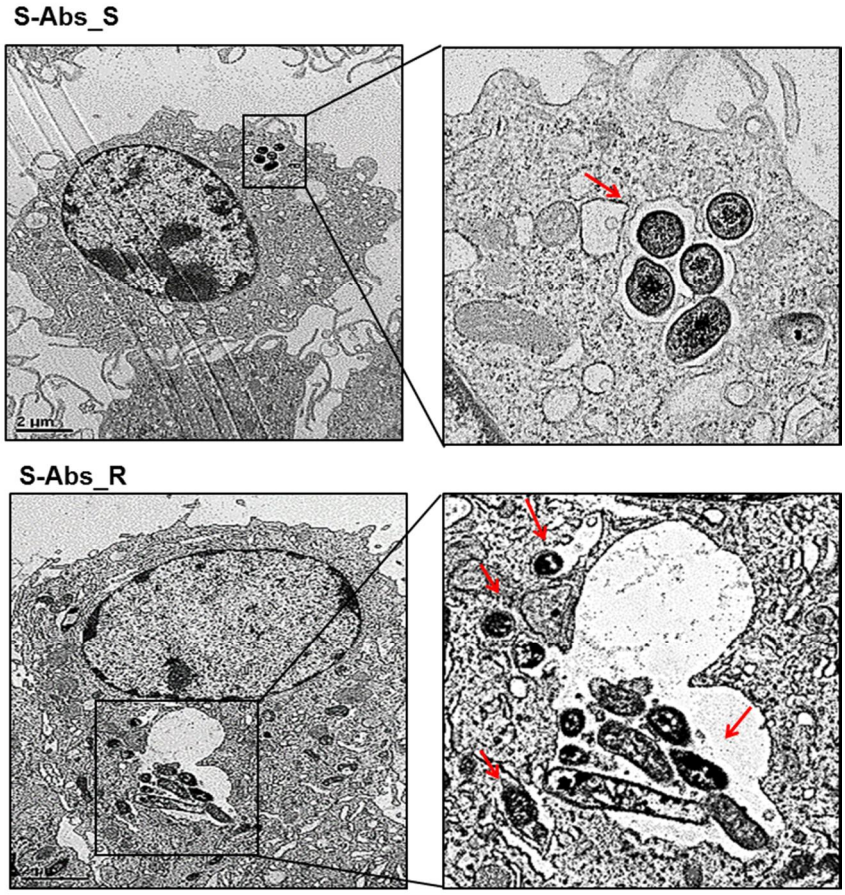
S-Abs_S
2 μm
S-Abs_R

(D)

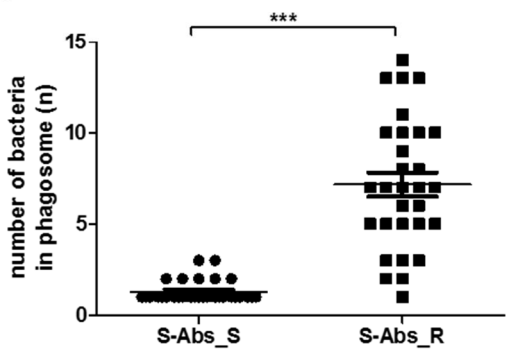
***
number of bacteria in phagosome (n)
15
10
5
0
S-Abs_S
S-Abs_R

(E)

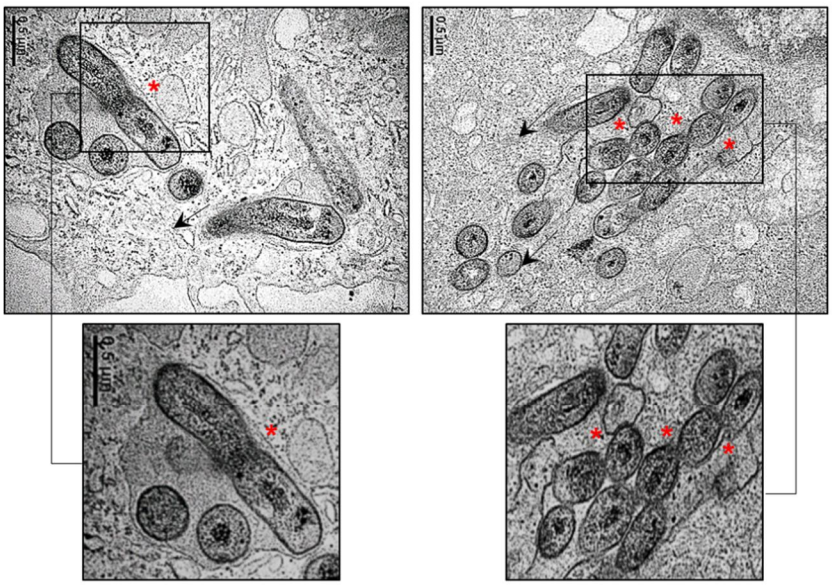

(F)

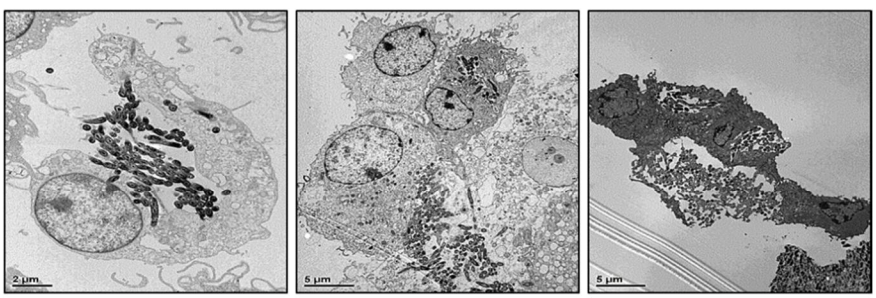

(G)

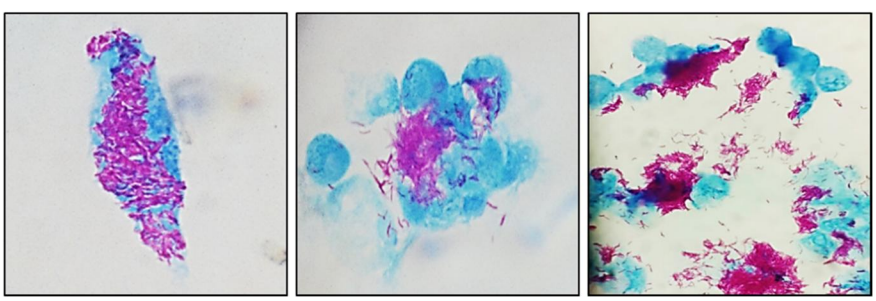

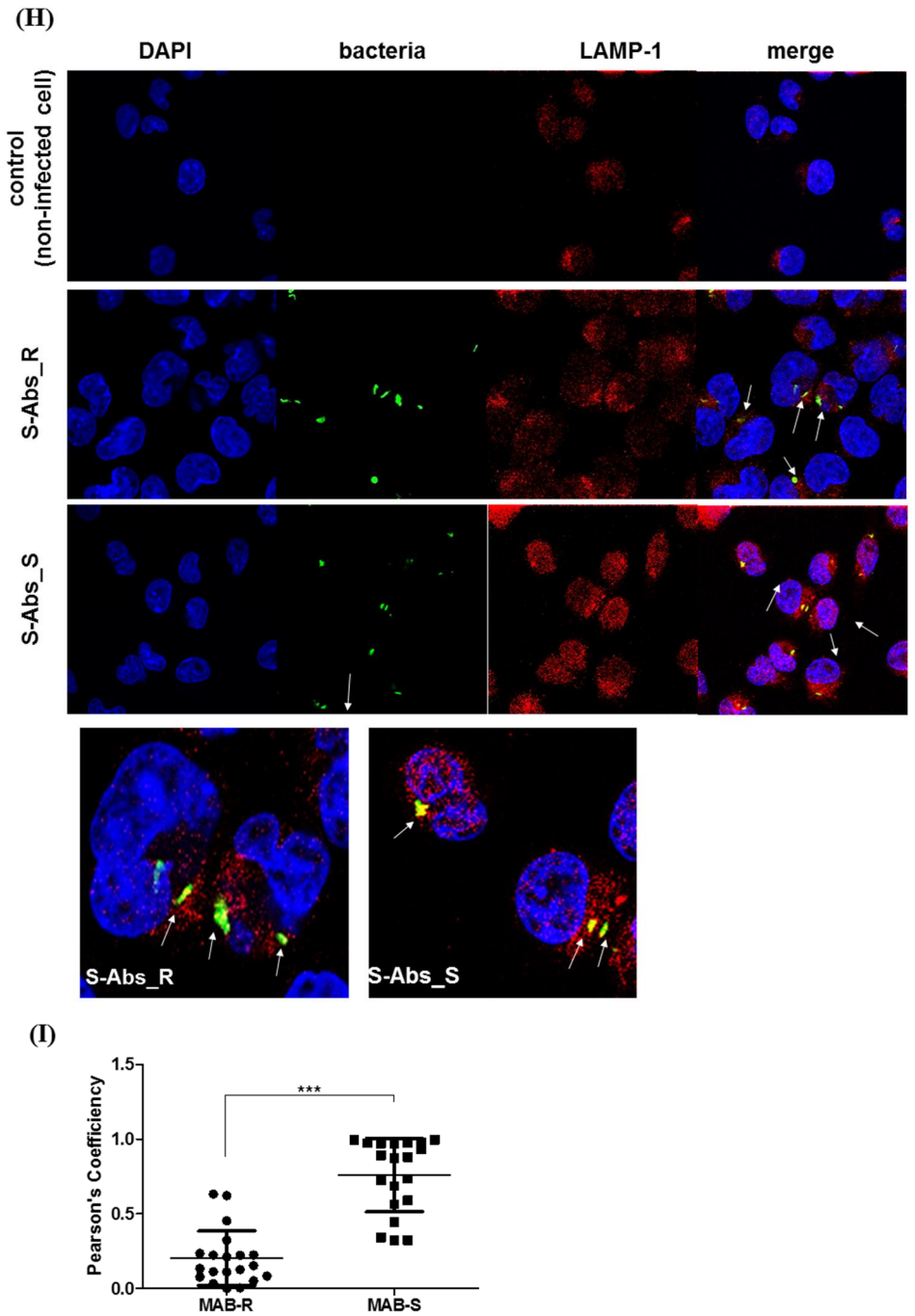

Figure 2. Morphological evidence of phagosomal escape and subsequent phagosomal rupture in MAB-R-infected murine macrophage. (A) AFB stain images of macrophages infected with MAB-R strains [S-Abs_R (*M. abscessus* type

strain ATCC 19977 rough strain) and S-Mas_II-R (Asan 50594)] and MAB-S strains [S-Abs_S (*M. abscessus* type strain ATCC 19977 smooth strain) and S-Mas_I-S (Asan 51843)] at 10 M.O.I. for 24 h.p.i. The black arrow indicates mycobacteria (red-stained rods) in methylene blue-stained J774A.1 cells. (B) Comparison images of J774A.1 cells infected with 10 M.O.I. of S-Abs_R (M. abscessus type strain ATCC 19977 rough strain) and S-Abs_S (M. abscessus type strain ATCC 19977 smooth strain) at different time points (0.5, 2, 4, 8, and 18 h.p.i.). (C-F) Representative TEM images of BMDM cells infected with S-Abs_R (*M. abscessus* type strain ATCC 19977 rough strain) and S-Abs_S (*M. abscessus* type strain ATCC 19977 smooth strain) strains at 10 M.O.I. at 24 h.p.i. Phagosome morphology and magnified images are shown (red box region and red arrow). Bar indicates 0.5 or 2 μm (C). (D) The graph shows the result of intracellular bacterial numbers in each phagosome by counted randomly selected 30 phagosomes in MAB-R or -S infected BMDMs. (E) Representative images of phagosome infected with an S-Abs_R (*M. abscessus* type strain ATCC 19977 rough strain). I marked a red asterisk to indicate bacterial replication in the phagosome. In this image, S-Abs_R was divided into two bacteria in the phagosome, reflecting active replication in the phagosome (red asterisk). S-Abs_R were also removed (black arrow) from the phagosome to the cytosol in macrophage. Bar indicates 0.5 μm. (F) BMDM infected with S-Abs_R (M. abscessus type strain ATCC 19977 rough strain) (10 M.O.I.) for 24 h. TEM analysis shows the infected cell morphology and extracellular images of bacteria leaving. Bar indicates 2 or 5 μm. (G) AFB stain images of J774A.1 cells infected with S-Abs_R (*M. abscessus* type strain ATCC 19977 rough strain) (10 M.O.I.) for 24 h. All data are based on at least 20 cells per

time point and are a representative result out of three independent experiments. (H) J774A.1 cells were infected with 10 M.O.I of CFSE (green) stained bacteria [MAB-R (*M. abscessus* type strain ATCC 19977 rough strain) MAB-S (*M. abscessus* type strain ATCC 19977 smooth strain] for 24 h.p.i. and then stained with DAPI (blue) and LAMP-1(red), representative images is shown. Non-infected J774A.1 cells were used as negative control. The white arrows showed co-localization of intracellular bacteria with LAMP-1 (yellow). (I) Quantification of Pearson's colocalization coefficient between MAB-R or -S and LAMP-1. The 20 bacteria randomly selected were analyzed and are a representative result out of two independent experiments. Results are means ± SD and ***$P < 0.001$ (Student's t-test).

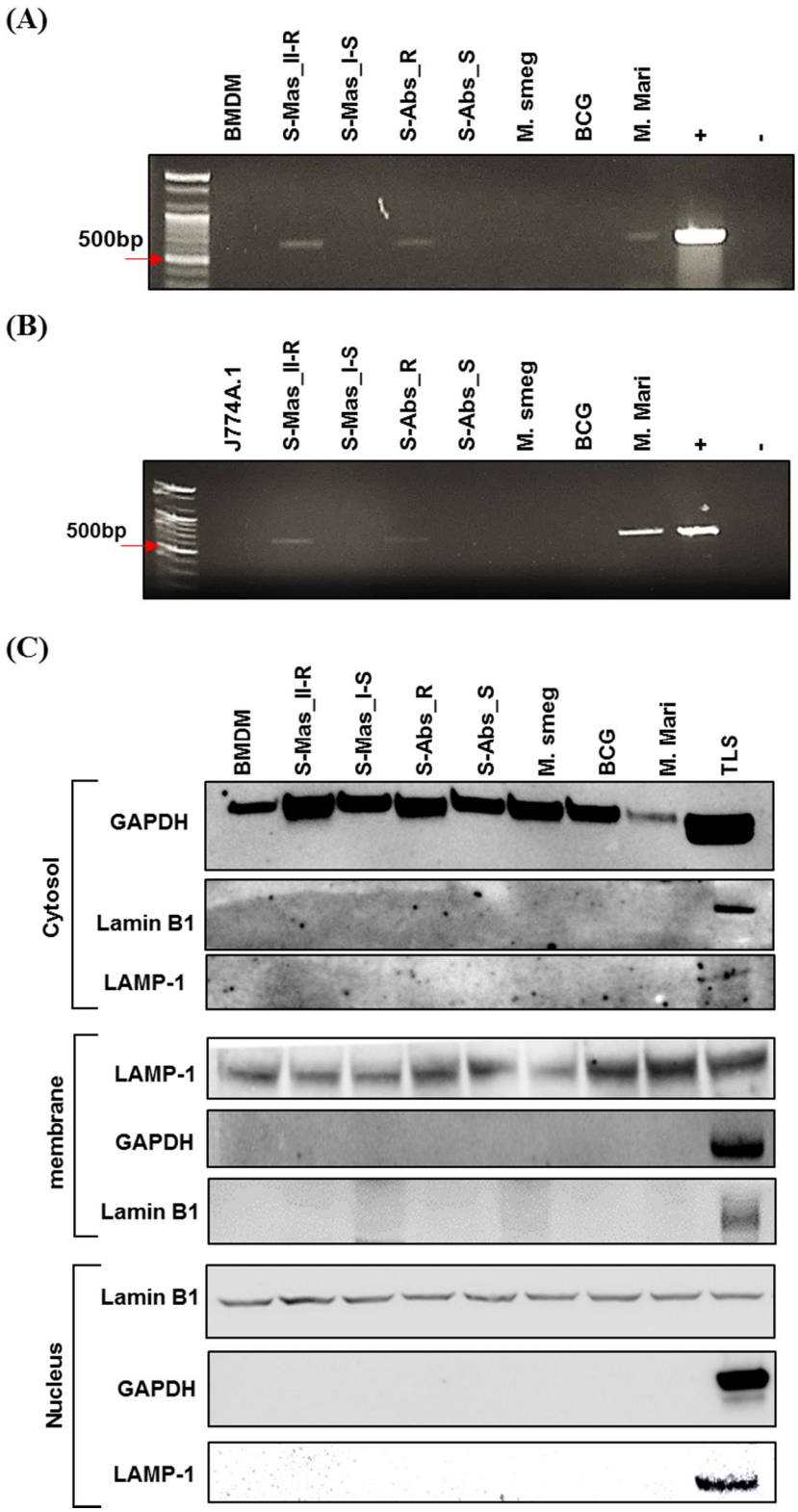
(A)
BMDM
S-Mas_II-R
S-Mas_I-S
S-Abs_R
S-Abs_S
M. smeg
BCG
M. Mari
+
-
500bp
(B)
J774A.1
S-Mas_II-R
S-Mas_I-S
S-Abs_R
S-Abs_S
M. smeg
BCG
M. Mari
+
-
500bp
(C)
BMDM
S-Mas_II-R
S-Mas_I-S
S-Abs_R
S-Abs_S
M. smeg
BCG
M. Mari
TLS
Cytosol
GAPDH
Lamin B1
LAMP-1
membrane
LAMP-1
GAPDH
Lamin B1
Nucleus
Lamin B1
GAPDH
LAMP-1

Figure 3. Detection of mycobacterial DNA from the cytosolic region of MAB-R-infected murine macrophages by PCR. (A-B) BMDMs (A) and J774A.1 cells (B) infected with MAB-R and -S strains [S-Mas_II-R (Asan 50594), S-Mas_I-S (Asan-51843 S-Abs_R (*M. abscessus* type strain ATCC 19977 rough strain), S-Abs_S (*M. abscessus* type strain ATCC 19977 smooth strain)], M.smeg (*M. smegmatis)*, BCG (*M. bovis* BCG), and M.mari (*M. marinum*) at 37°C for 24h.p.i. Cytosolic DNA (from cytosol fractionation) was extracted by the phenol-chloroform-isoamyl alcohol (PCI) method. Cytosolic DNA was detected by PCR amplification of the *hsp65* (603 bp) gene. (+; mycobacterial DNA, -; containing only primers) (C) Cytosolic cell fractions were isolated using the manufacturer's protocol for the Qproteome Cell Compartment Kit (QIAGEN). Western blotting was performed to confirm the separation of the cytoplasm and membrane, nucleus. To confirm this separation and exclude contamination during cell fraction isolation, GAPDH, LAMP-1 and Lamin B1 were used as a cytoplasmic marker, a phagosomal marker, and a nuclear marker, respectively. BMDM (non-infected cell), S-Mas_II-R: Asan 50594, S-Mas_I-S: Asan 51843, S-Abs_R: *M. abscessus* type strain ATCC 19977 rough strain, S-Abs_S: *M. abscessus* type strain ATCC 19977 smooth strain, M.smeg: *M. smegmatis*, BCG: *M. bovis* BCG, M.mari: *M. marinum*, and TLS: BMDM total lysate.

Live MAB-R stains induce Type I IFN secretion in an IRF3-dependent manner

The cytosol access of mycobacterial strains such as virulent *M. tuberculosis* or *M. marinum* in macrophage via phagosomal rupture induce Type I IFN secretion (3,

22-25). Therefore, to address whether MAB-R strains capable of cell escape in macrophage also causes IFN secretion, I checked the IFN-β secretion capacity of MAB-R strains in BMDM or J774A.1 cells by two different methods, a luciferase assay in L929 IFN reporter cells (38) and IFN-β ELISA. I found that irrespective of subspecies or genotypes, MAB-R strains always had a higher level of IFN-β secretions than MAB-S strains and other mycobacterial species known to be not capable of phagosomal escape in macrophage infections such as *M. smegmatis* or BCG in J774A.1 cells or BMDMs (Figure 4A). In L929 IFN reporter cells, a similar trend was shown, proving the validity of these findings (Figure 4B). Next, to check whether Type I IFN secretion of MAB-R strains depends on active multiplication, I compared IFN-β secretion levels between live and heat-killed (HK) MAB-R strains (Figure 4C). Only live, not HK, MAB-R strains induced IFN-β secretions, but MAB-S, *M. smegmatis* and BCG did not cause IFN-β secretion irrespective of whether they were HK or live cells, suggesting that phagosomal escape of MAB-R strains via active multiplication in macrophage phagosome may contribute to IFN-β secretions.

The mycobacterial DNA released into the macrophage cytosol has been reported to lead to IFN-β secretion via cGAS-STING-IRF3 axis signaling (3, 22, 23). To address this issue, I investigated the IRF3 activation of MAB-R strains by western blotting (Figure 4D-F). This data showed that only two MAB-R strains, S-Abs_R (*M. abscessus* type strain ATCC 19977 rough strain) and S-Mas_II-R (Asan 50594), induced IRF-3 activation in infected BMDMs. I also found increased levels of the activated forms of STING (33-35 kDa) and cGAS (62 kDa) in these two MAB-R strains, consistent with the previous result that cytosolically exposed

DNA induced Type I IFN secretion via the cGAS -STING axis (3, 47). The similar trend was also found in infected BMDCs (Figure 4E). Next, I examined the activation capacity of Type I IFN-related gene expression in different mycobacterial strains by quantitative RT-PCR 24 h.p.i. of BMDM (Figure 4F). These data showed that transcription of the IFI204, IFNβ, STING, gene was induced via infection of only 3 strains, two strains of MAB-R [S-Abs_R (*M. abscessus* type strain ATCC 19977 rough strain) and S-Mas_II-R (Asan 50594)] and *M. marinum*, and not by infection of other mycobacterial strains ([S-Abs_S (*M. abscessus* type strain ATCC 19977 smooth strain) and S-Mas_I-S (Asan 51843)] and *M. bovis* BCG), further proving the enhanced Type I IFN signaling by MAB-R strains. But, there were no significant differences in IRF3 transcription levels between MAB-R strains and other mycobacteria (Figure 4F), suggesting enhanced production Type I IFN of MAB-R strains may be due to IRF3 activation, rather than enhanced expression of IRF3. Together, these data suggested that cytosolic DNA of MAB-R strains followed by active multiplication-mediated phagosomal rupture induces Type I IFN secretion via cGAS-STING-IRF3 axis signaling.

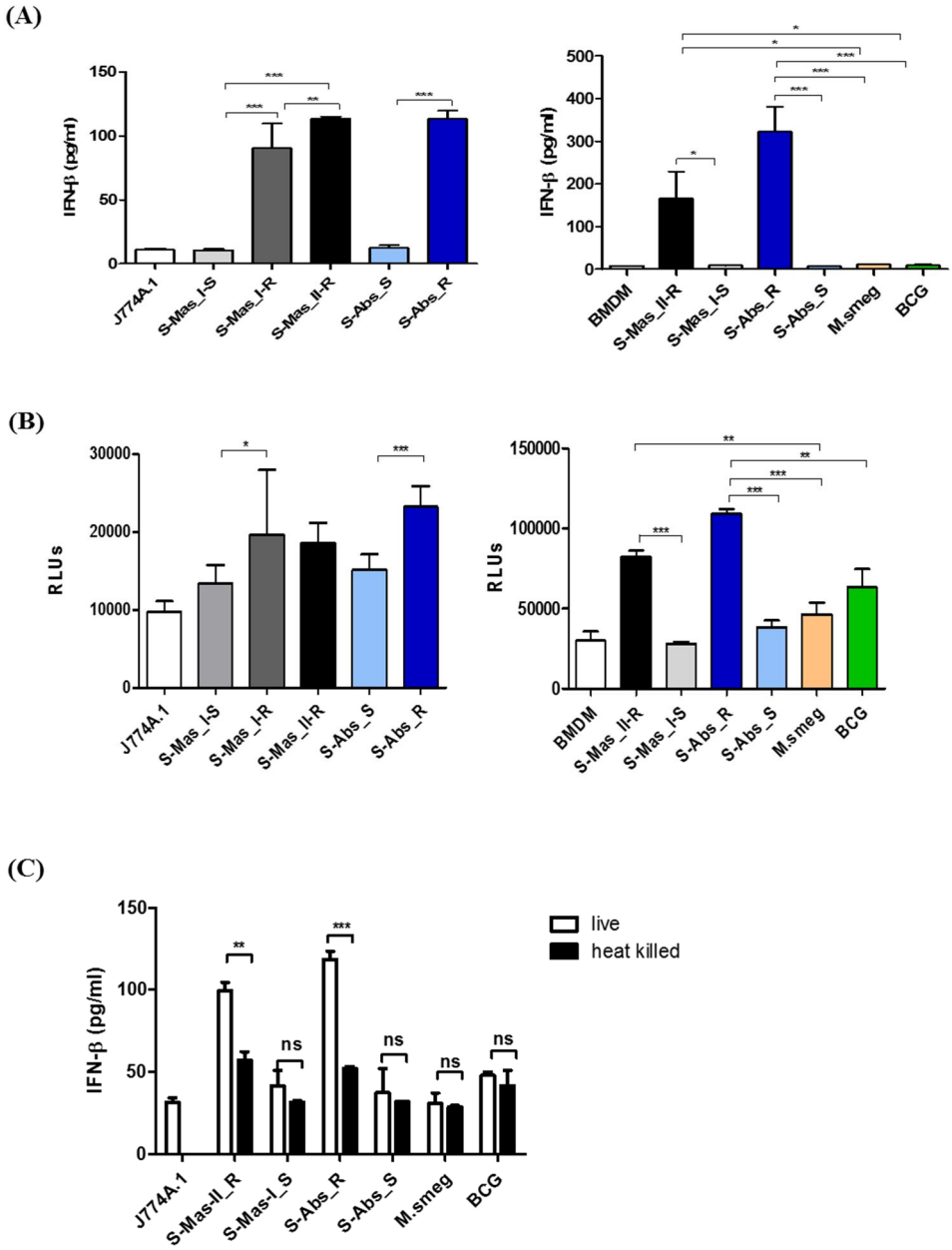
(A)
IFN-β (pg/ml)
J774A.1
S-Mas_I-S
S-Mas_I-R
S-Mas_II-R
S-Abs_S
S-Abs_R
BMDM
M.smeg
BCG
(B)
RLUs
(C)
live
heat killed
ns

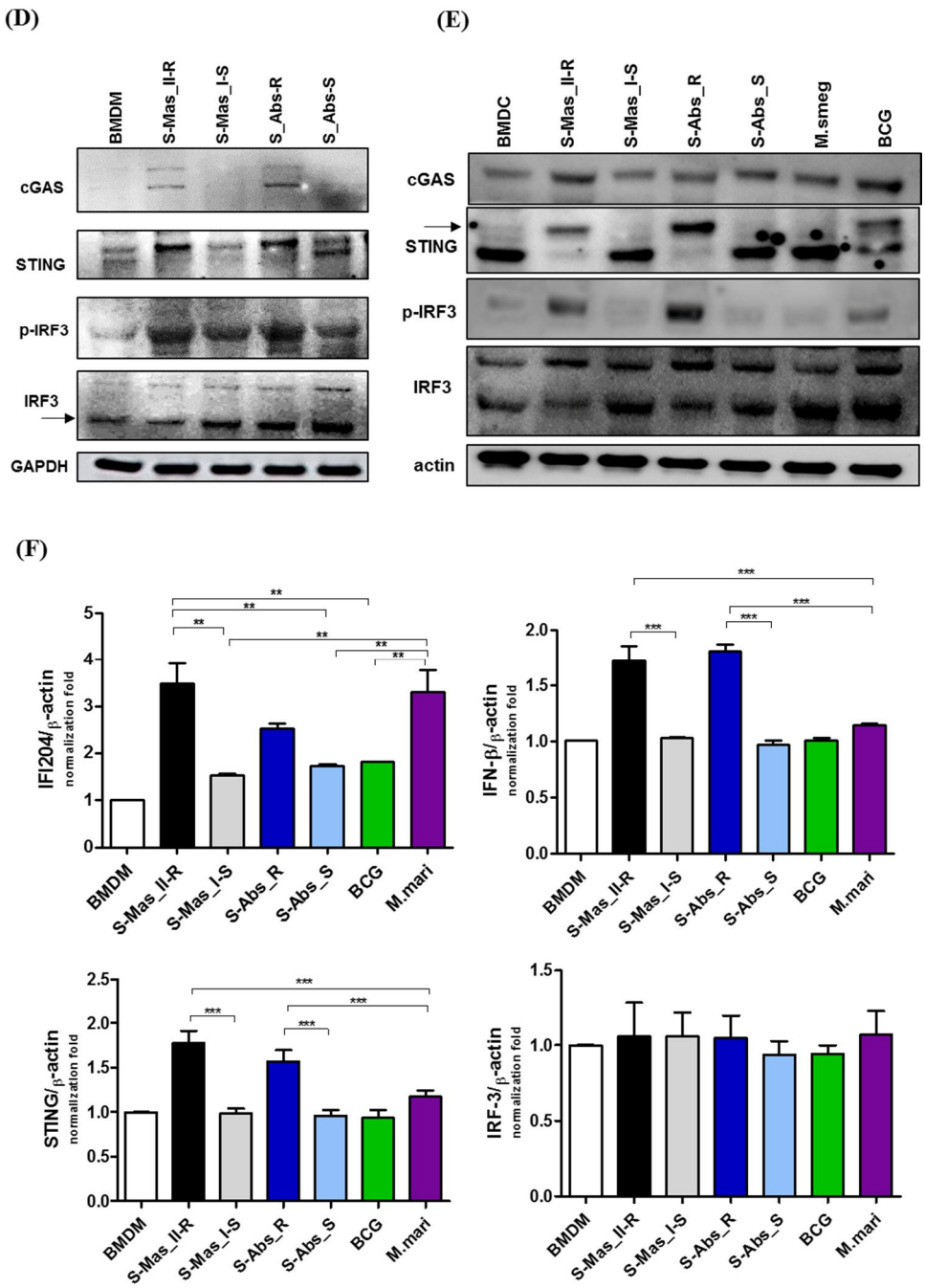

Figure 4. Live MAB-R strains induce Type I IFN secretion via the cGAS-STING-IRF3 axis. (A-B) Supernatants were harvested 24 h.p.i., and their Type I IFN levels were analyzed by IFN-β ELISA (A) and L929-ISRE luciferase bioassay

(B) (33). The luciferase bioassay units are relative light units (RLUs). (C) J774A.1 cells were either uninfected (control) or infected with live or heat-killed (HK) bacteria, the supernatants of the infected cells were collected, and Type I IFN levels measured by IFN-β ELISA. (D-E) Western blot of IRF3, p-IRF3, STING, and cGAS induced by MAB-R [S-Abs_R (*M. abscessus* type strain ATCC 19977 rough strain)] and MAB-S strains [S-Abs_S (*M. abscessus* type strain ATCC 19977 smooth strain) and S-Mas_I-S (Asan 51843)], *M. smegmatis*, and BCG infection (10 M.O.I.) of BMDMs(D) and BMDCs(E) for 24 h. (F) qRT-PCR was used to measure the expression levels of *IFI204*, *IFN-β*, *STING* and *IRF-3* mRNA in the BMDMs infected with rough strains [S-Abs_R (*M. abscessus* type strain ATCC 19977 rough strain)] and S-Mas_II-R (Asan 50594)] and smooth strains [S-Abs_S (*M. abscessus* type strain ATCC 19977 smooth strain) and S-Mas_I-S (Asan 51843)], *M. bovis* BCG, or *M. marinum* (10 M.O.I.). The expression levels represent relative fold changes based on the *β-actin* level. The results are representative of two independent experiments and represent means ± SD. P values were determined by one-way ANOVA with Tukey's multiple comparison test (A and B, E, F) and paired Student's *t*-test (C) using GraphPad prism program: ns, nonsignificant; $*P < 0.05$; $**P < 0.01$, and $***P < 0.001$.

Live MAB-R stains enhance cell death in murine macrophage

Phagosomal rupture in macrophage by virulent mycobacteria has been reported to induce cell death followed by cell-to-cell spread of cytosolic bacteria into neighboring cells via cell membrane rupture (24, 25). To address whether MAB-R strains capable of inducing phagosomal rupture also enhance the cell death of

infected macrophages, I first examined the cytotoxicity of BMDMs infected with various mycobacteria by lactate dehydrogenase (LDH) assay for 4 and 24 h.p.i. As shown in Figure 5A, there were no significant differences in cytotoxicity between MAB-S and MAB-R infected cells in early infection time (4 h.p.i), however, MAB-R strains showed more cytotoxicity in 24 h.p.i. than other mycobacterial strains. Next, to address whether cell death induced by MAB-R is due to its active replication, I compared cell death-inducing capacity of various live and HK mycobacteria in infected J774A.1 cells (Figure 5B). this data showed that only live MAB-R strains led to significantly greater cell cytotoxicity than HK bacteria, although in other mycobacterial strains (MAB-S, *M. smegmatis* or BCG), no significant difference in cell death-inducing capacity between live and HK bacteria was found, suggesting that the active multiplication of MAB-R strains may contribute to enhanced cell cytotoxicity.

Next, to determine what type of cell death is induced by infection of MAB-R strains, I compared features of induced cell death between various mycobacteria, including MAB-R strains. FACS analysis was conducted by using double staining with both annexin V (for apoptotic cell death) and 7-AAD (for necrotic cell death). This data showed that two MAB-R strains more induced both apoptotic and necrotic cell death than other mycobacterial strains in a time dependent manner (Figure 5C-D). In contrast, macrophage infected by two MAB-S strains appear to be resistant to both apoptotic and necrotic cell death even more than those infected by *M. smegmatis* in all the infected time points than MAB-R strains (Figure 5C-D).

Furthermore, I also found that live MAB-R strains but not HK strains induced apoptotic and necrotic cell deaths (Figure 5E). Together, these data indicate that

active multiplication of MAB-R strains contribute to the cell death (including apoptosis and necrosis) of infected murine macrophage.

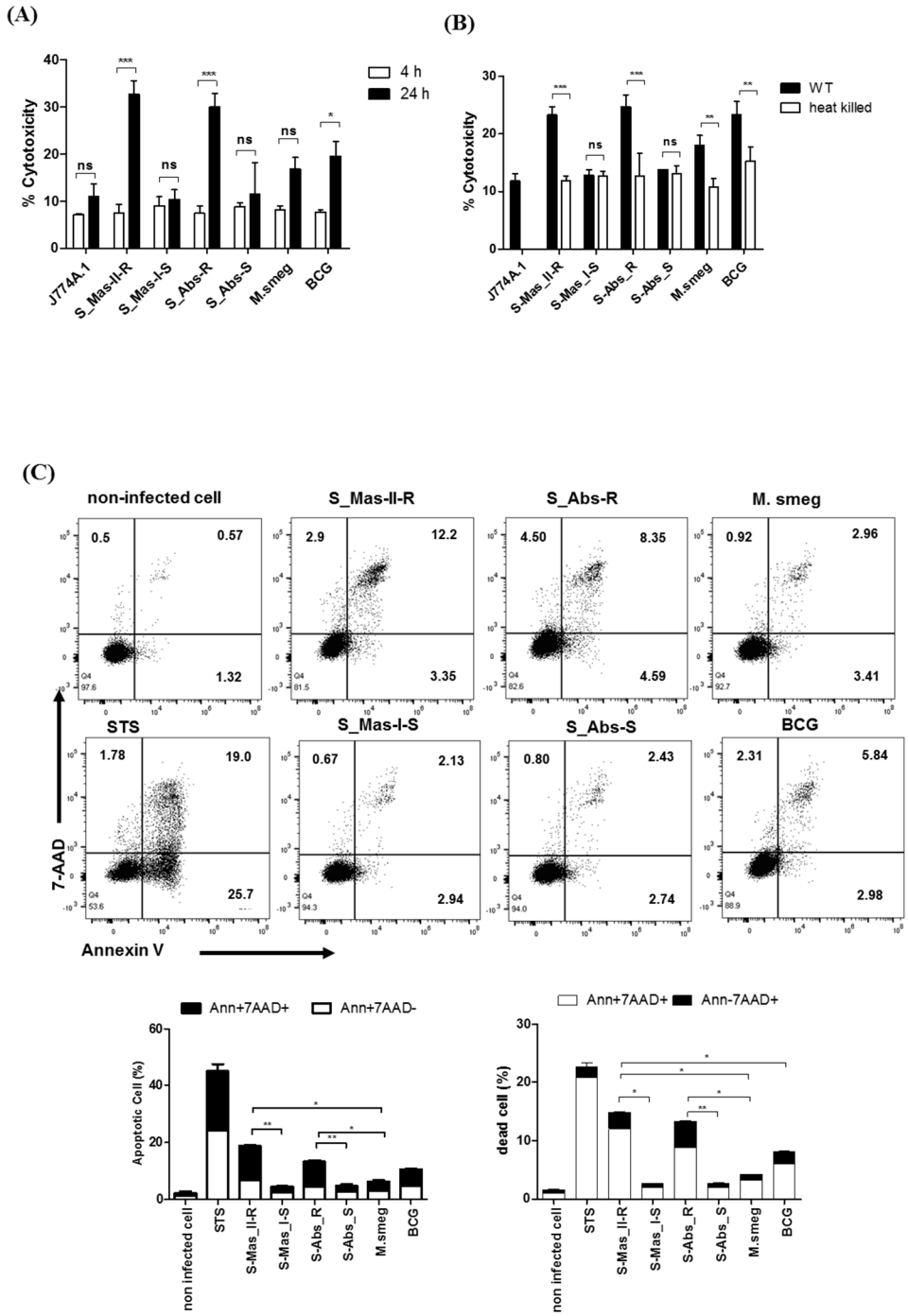

(D)

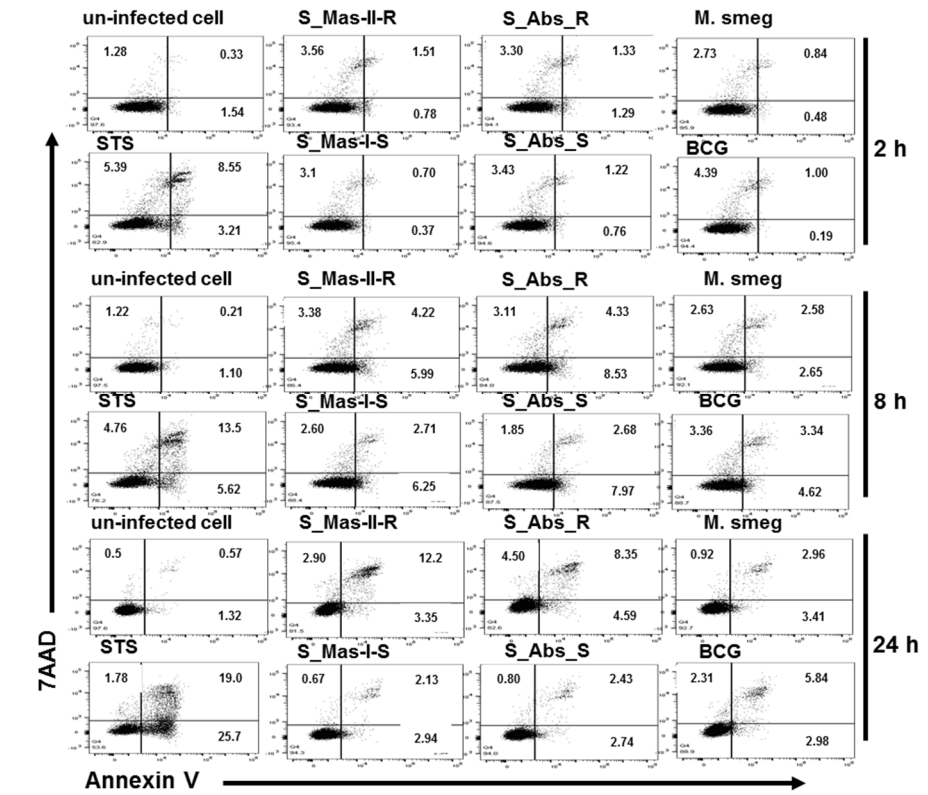
un-infected cell
S_Mas-II-R
S_Abs_R
M. smeg
STS
S_Mas-I-S
S_Abs_S
BCG
2 h
8 h
24 h
7AAD
Annexin V

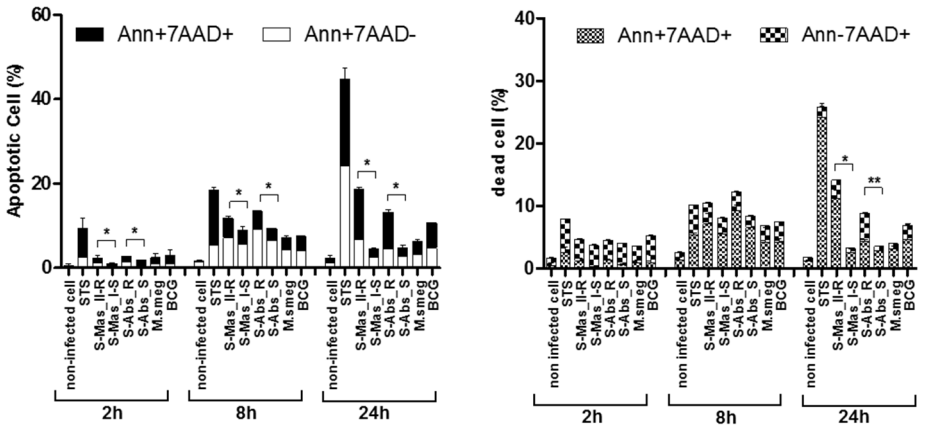
Ann+7AAD+
Ann+7AAD-
Apoptotic Cell (%)
Ann-7AAD+
dead cell (%)
non-infected cell
STS
S-Mas_II-R
S-Mas_I-S
S-Abs_R
S-Abs_S
M.smeg
BCG
2h
8h
24h

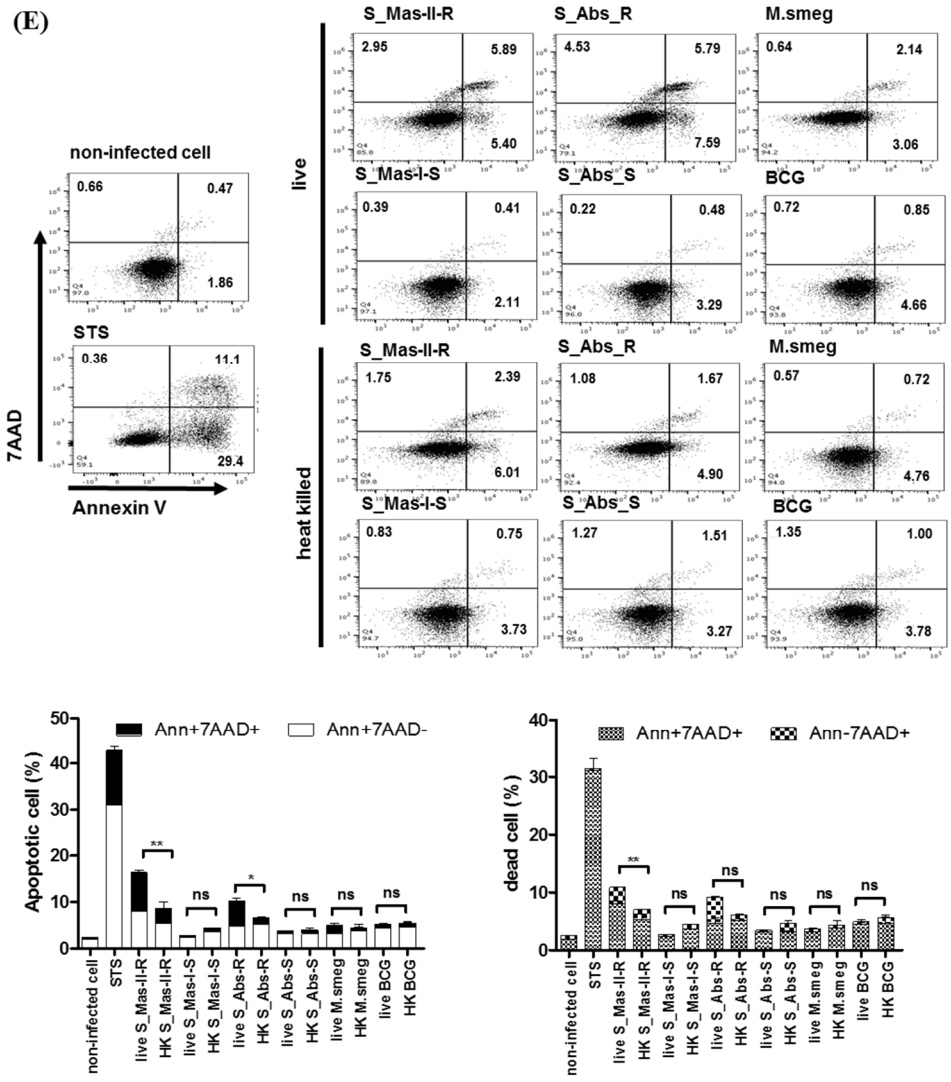

Figure 5. Live MAB-R stains enhance apoptotic cell death in murine macrophage. (A) To evaluate cytotoxic effects, cells were infected with S-Mas_II-R (Asan 50594), S-Mas_I-S (Asan 51843), S-Abs_R (*M. abscessus* type strain ATCC 19977 rough strain), S-Abs_S (*M. abscessus* type strain ATCC 19977 smooth strain), *M. smegmatis*, and *M. bovis* BCG (10 M.O.I.) in BMDM for 4 and 24 h. Cytotoxicity was quantitated by measurement of LDH activity in the culture supernatants using a CytoTox 96 assay kit (Promega) according to the

manufacturer's protocol. Error bars represent the standard deviation of at least three independent experiments. (*P < 0.05, **P < 0.01, ***P < 0.001; one-way ANOVA with Tukey's correction). (B) J774A.1 cells were either uninfected (control) or infected with live or heat-killed (HK) bacteria, supernatants of the infected cells were collected and cytotoxicity was measured by LDH assay. (C) J774A.1 cells were pre-treated with 100 nM staurosporine (apoptosis inducer) used as a positive control and infected (M.O.I. 10) with the indicated bacterial strains for 24 h.p.i. (D) J774A.1 cells were pretreated with 100 nM staurosporine (apoptosis inducer) and infected with MAB-R strains [S-Abs_R (*M. abscessus* type strain ATCC 19977 rough strain) and S-Mas_II-R (Asan 50594)] and MAB-S strains [S-Abs_S (*M. abscessus* type strain ATCC 19977 smooth strain) and S-Mas_I-S (Asan 51843)], *M. smegmatis*, and *M. bovis* BCG (10 M.O.I) at different time points (2, 8, and 24 h). (E) J774A.1 cells were either uninfected (control) or infected with live or heat-killed (HK) bacteria (10 M.O.I) of the indicated bacterial strains for 24 h. (C-E) The infected cells were stained with Annexin V and 7-AAD, after then analyzed by flow cytometry (FACS LSRFortessa X-20). The results are representative of two independent experiments and represent means ± SD. P values were determined by the Student's t-test using GraphPad prism program: ns, nonsignificant; *P < 0.05; **P < 0.01, and ***P < 0.001

The caspase dependent apoptotic cell death by MAB-R strains contribute into their cell-to-cell spread

Previously, cell death by virulent mycobacterial strains such as *M. tuberculosis* H37Rv has been reported to contribute to bacteria cell-to-cell spreading, thus

leading to increased bacterial growth (25). Therefore, to address whether cell death by MAB-R strains also contributes to enhanced intracellular bacterial growth via cell-to-cell spreading, I first compared the cell-to-cell spreading capacity of EGFP-expressing recombinant strains of MAB-R (Asan 50594), *M. smegmatis* and BCG infecting J774A.1 cells for 24 h.p.i. The cell spreading capacity was analyzed via FACS analysis as previously reported (25). This data showed that the MAB-R strain induced greater cell-to-cell spreading than *M. smegmatis* or BCG, reflecting the above finding that MAB-R strains induce cell death (Figure 6B). Next, to analyze the time kinetics and M.O.I. dependency of the cell spreading of the MAB-R strain, I investigated bacterial cell spreading in J774A.1 cells infected with the MAB-R strain at different time points (0, 6, 24, and 48 h) with different M.O.I. (1, 5, 10, and 50). I found that the spreading of bacteria into new cells was gradually increased in the period between 0 to 48 h.p.i. In addition, the cell spreading was increased in an M.O.I. and a cell death-dependent manner (Figure 6C). I found that the treatment of MAB-R-infected J774A.1 cells with staurosporine enhanced cell-to-cell spreading of bacteria in a dose-dependent manner (Figure 6E). In contrast, the treatment with SB202190 decreased the cell-to-cell spreading of bacteria in a dose-dependent manner (Figure 6F). Also, the cell-to-cell spreading induced by MAB-R strains was also decreased in the presence of pan-caspase inhibitor (Z-VAD-FMK) in a time dependent manner (Figure 6G), suggesting that apoptotic cell death may in part contributes to the macrophage cell-to-cell spreading of MAB-R strains.

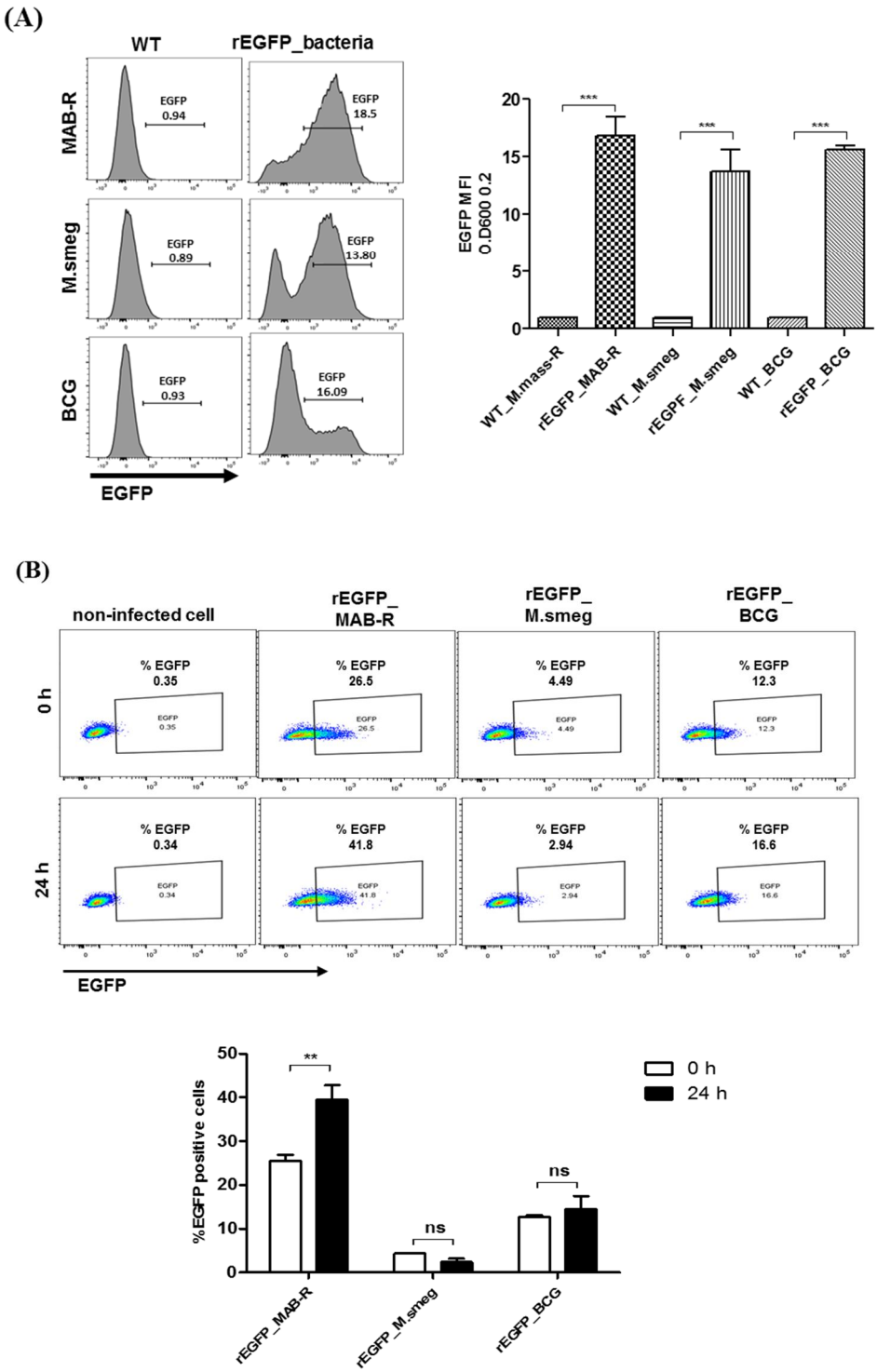
(A)
WT
rEGFP_bacteria
MAB-R
M.smeg
BCG
EGFP
0.94
EGFP
18.5
EGFP
0.89
EGFP
13.80
EGFP
0.93
EGFP
16.09
EGFP
EGFP M FI
0.D600 0.2
20
15
10
5
0
***
***
***
WT_M.mass-R
rEGFP_MAB-R
WT_M.smeg
rEGFF_M.smeg
WT_BCG
rEGFP_BCG
(B)
non-infected cell
rEGFP_
MAB-R
rEGFP_
M.smeg
rEGFP_
BCG
0 h
24 h
% EGFP
0.35
% EGFP
26.5
% EGFP
4.49
% EGFP
12.3
% EGFP
0.34
% EGFP
41.8
% EGFP
2.94
% EGFP
16.6
EGFP
%EGFP positive cells
50
40
30
20
10
0
**
ns
ns
0 h
24 h
rEGFP_MAB-R
rEGFP_M.smeg
rEGFP_BCG

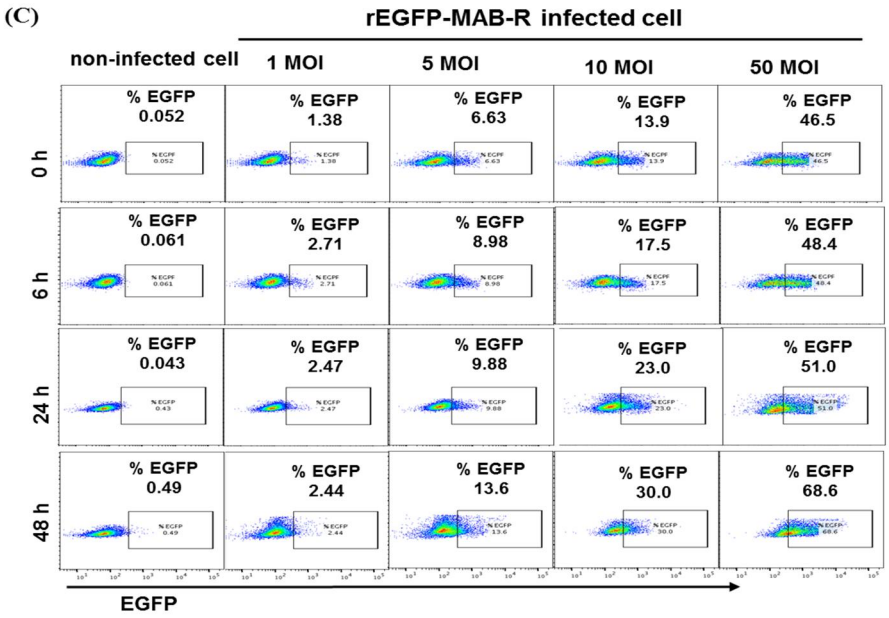
(C)
rEGFP-MAB-R infected cell
non-infected cell
1 MOI
5 MOI
10 MOI
50 MOI
0 h
6 h
24 h
48 h
% EGFP 0.052
% EGFP 1.38
% EGFP 6.63
% EGFP 13.9
% EGFP 46.5
% EGFP 0.061
% EGFP 2.71
% EGFP 8.98
% EGFP 17.5
% EGFP 48.4
% EGFP 0.043
% EGFP 2.47
% EGFP 9.88
% EGFP 23.0
% EGFP 51.0
% EGFP 0.49
% EGFP 2.44
% EGFP 13.6
% EGFP 30.0
% EGFP 68.6
EGFP

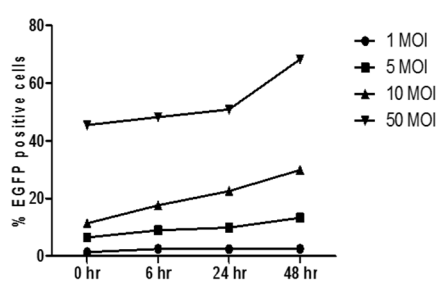
% EGFP positive cells
80
60
40
20
0
0 hr
6 hr
24 hr
48 hr
1 MOI
5 MOI
10 MOI
50 MOI

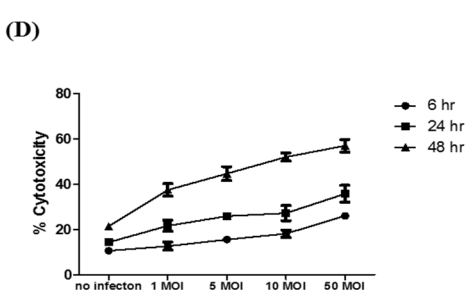
(D)
% Cytotoxicity
80
60
40
20
0
no infecton
1 MOI
5 MOI
10 MOI
50 MOI
6 hr
24 hr
48 hr

(E)

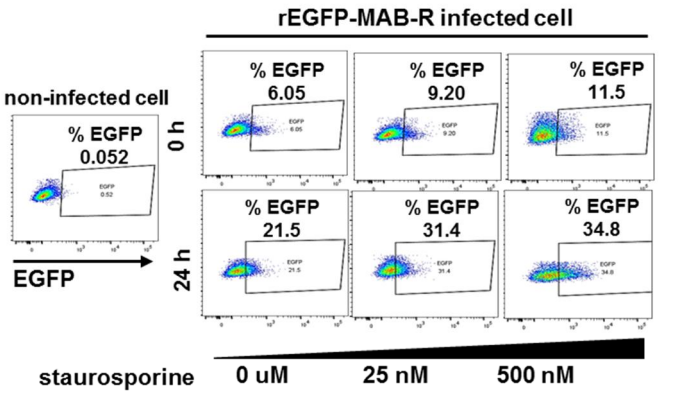
rEGFP-MAB-R infected cell
non-infected cell
% EGFP
0.052
EGFP
0 h
24 h
% EGFP
6.05
% EGFP
9.20
% EGFP
11.5
% EGFP
21.5
% EGFP
31.4
% EGFP
34.8
staurosporine
0 uM
25 nM
500 nM

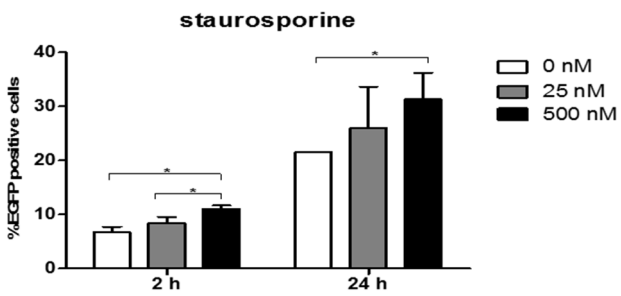
staurosporine
%EGFP positive cells
40
30
20
10
0
2 h
24 h
0 nM
25 nM
500 nM

(F)

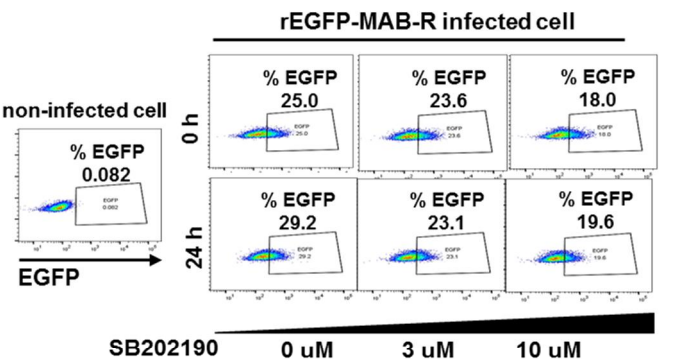
rEGFP-MAB-R infected cell
non-infected cell
% EGFP
0.082
EGFP
0 h
24 h
% EGFP
25.0
% EGFP
23.6
% EGFP
18.0
% EGFP
29.2
% EGFP
23.1
% EGFP
19.6
SB202190
0 uM
3 uM
10 uM

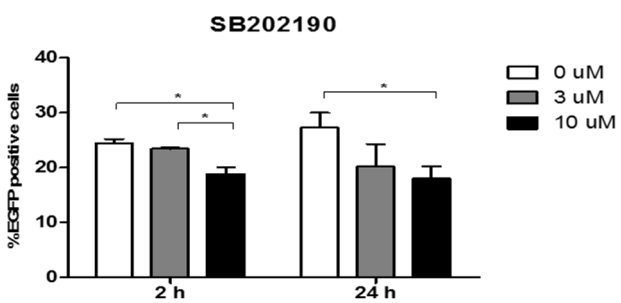
SB202190
%EGFP positive cells
40
30
20
10
0
2 h
24 h
0 uM
3 uM
10 uM

(G)

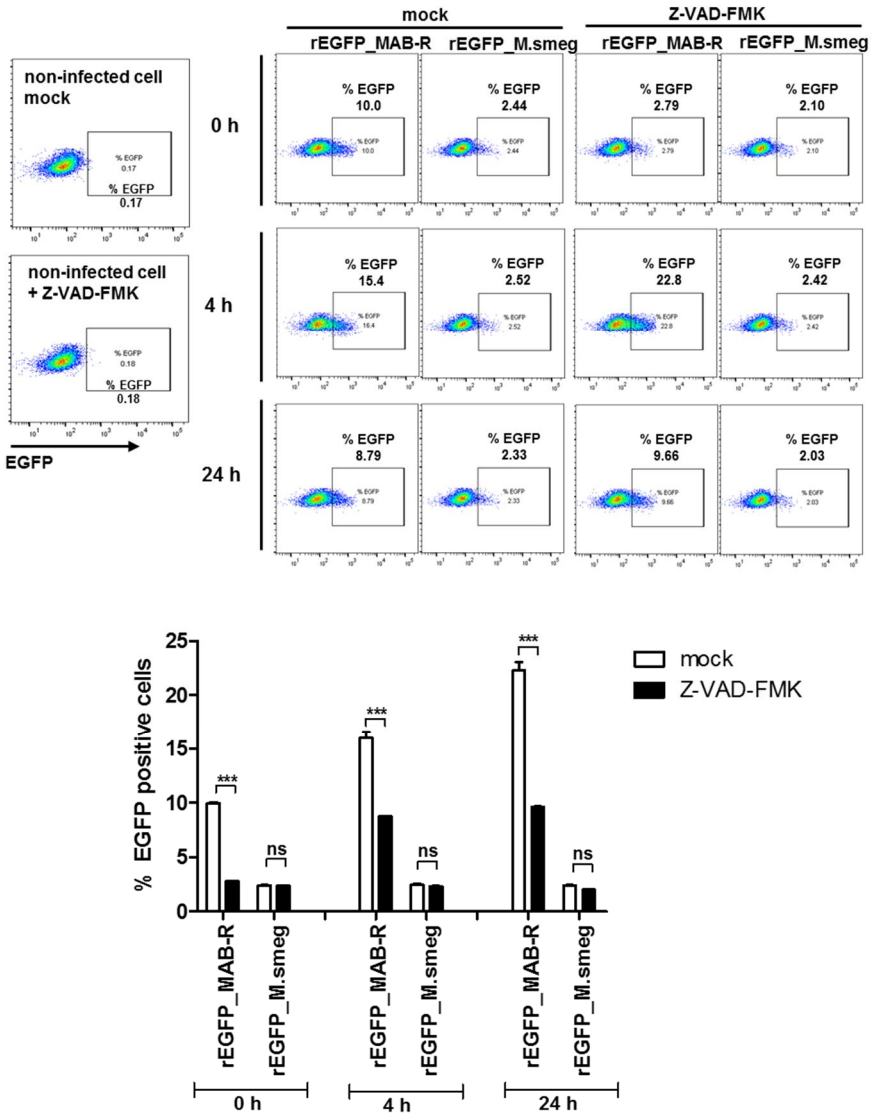

Figure 6. Enhanced apoptotic cell death by a MAB-R strain contributes to its cell-to-cell spread. (A) Recombinant mycobacteria expressing EGFP [rEGFP_MAB-R (Asan 50594), rEGFP_M.smeg, rEGFP_BCG) and wild-type mycobacteria were cultured for 3~5 days in 7H9 broth medium supplemented with 0.5% glycerol, 0.05% Tween-80, and 10% ADC, and 100 μg/ml kanamycin was added for recombinant mycobacteria. The growth rate of the recombinant

mycobacterial strains was determined by measuring the OD value at 600 nm. Bacterial pellets were washed 3 times with PBS and resuspended in FACS buffer, and recombinant mycobacteria of expressing EGFP were measured by FACScalibur (BD biosciences). (B) BMDMs infected with EGFP-expressing bacteria for 0 and 24 h. EGFP-positive cells were analyzed by flow cytometry. (C-D) J774A.1 cells were infected with MAB-R [rEGFP_M.mass-R (Asan 50594)], and analysis was performed on data at different time points (0, 6, 24, and 48 h) or M.O.I.s (1, 5, 10, and 50). The percentage of EGFP-positive cells (C) was evaluated by flow cytometry (FACScalibur). Cytotoxicity was quantitated by measurement of LDH activity in the infected cell supernatants (D). (E-F) J774A.1 cells were pretreated with staurosporine (apoptosis inducer) or SB202190 (p38 MAPK inhibitor) and infected with MAB-R [rEGFP_MAB-R (Asan 50594)] (10 M.O.I.), and the percentage of EGFP-positive cells was measured by flow cytometry (FACScalibur). (G) J774A.1 cells were pre-treated with 10 uM Z-VAD-FMK (pan-caspase inhibitor) for 2 hr and infected with rEGFP_MAB-R and rEGFP_M.smeg (10 M.O.I) for and the percentage of EGFP-positive cells was measured by flow cytometry (FACScalibur). The results are representative of two independent experiments and represent means ± SD. P values were determined by the Student's *t*-test using GraphPad prism program: ns, nonsignificant; $*P < 0.05$; $**P < 0.01$, and $***P < 0.001$.

Enhanced cell-to-cell spreading of MAB-R strains is due to an IFNAR1-dependent pathway

Type I IFN signaling induces apoptosis in the splenocytes from mice and

contributes to its virulence via cell-to-cell spreading in *Listeria monocytogenes* infections (48, 49). Therefore, I sought to explore whether Type I IFN induced by MAB-R infection could also contribute to bacterial cell-to-cell spreading via enhanced cell death. First, I compared the Type I IFN-dependent survival capacity in macrophage infected with various mycobacteria. To this end, I infected BMDMs from wild or IFNAR1 KO mice with mycobacteria and then compared their intracellular survival capacities. The result showed that only two MAB-R strains (not MAB-S, *M. smegmatis*, or BCG) led to significantly lower survival capacity in infected BMDM cells from IFNAR1 KO mice than in infected BMDMs from wild mice (Figure 7A), suggesting that Type I IFN signaling may contribute to the enhanced intracellular growth in MAB-R-infected macrophages

Next, to determine the Type I IFN dependency of MAB-R-induced cytotoxicity, I infected various mycobacterial strains into BMDMs from wild-type or IFNAR1 KO mice with 10 M.O.I. and examined them 24 h.p.i. As a result, I found that only two MAB-R strains led to significantly less cell cytotoxicity in BMDMs from IFNAR1 KO than those from wild mice; however, there were no significant changes in other mycobacteria, including two MAB-S strains, *M. smegmatis* and BCG (Figure 7B), suggesting that the Type I IFN dependency of MAB-R strains induces cell cytotoxicity.

Next, to check whether Type I IFN dependency in MAB-R strains induced cell-to-cell spread, I compared the cell-to-cell spreading capacity of EGFP-expressing recombinant strains of MAB-R [rEGFP_MAB-R (Asan 50594)] strain, *M. smegmatis* (rEGFP_M.smeg), and *M. bovis* BCG (rEGFP_BCG) after their infection into BMDMs from wild mice or IFNAR1 KO mice. I found that MAB-R

but not *M. smegmatis* and BCG led to significantly less cell-to-cell spreading in BMDMs of IFNAR1 KO mice at the 24 and 48 h.p.i. than in BMDMs of wild type (Figure 7C), suggesting a partial contribution of Type I IFN signaling to MAB-R-induced cell-to-cell spreading. Together, these data demonstrated that apoptotic cell death by MAB-R strains contributes to enhanced intracellular bacterial growth via providing a new niche for bacterial growth resulting from cell-to-cell spread. In addition, Type I IFN signaling induced by MAB-R infection partially contributes to their cell spreading.

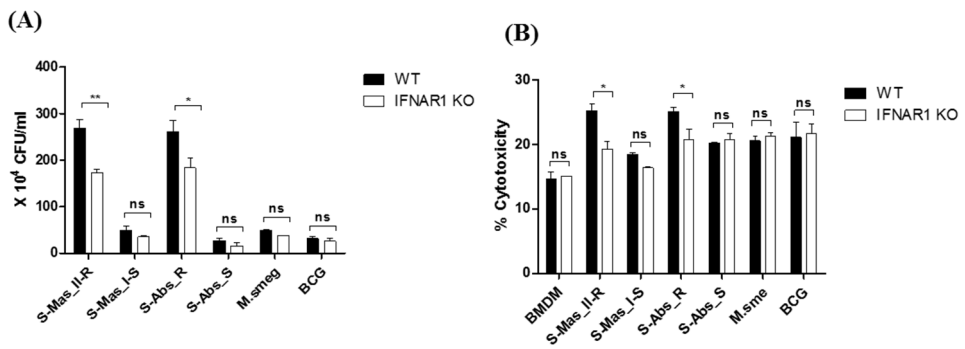

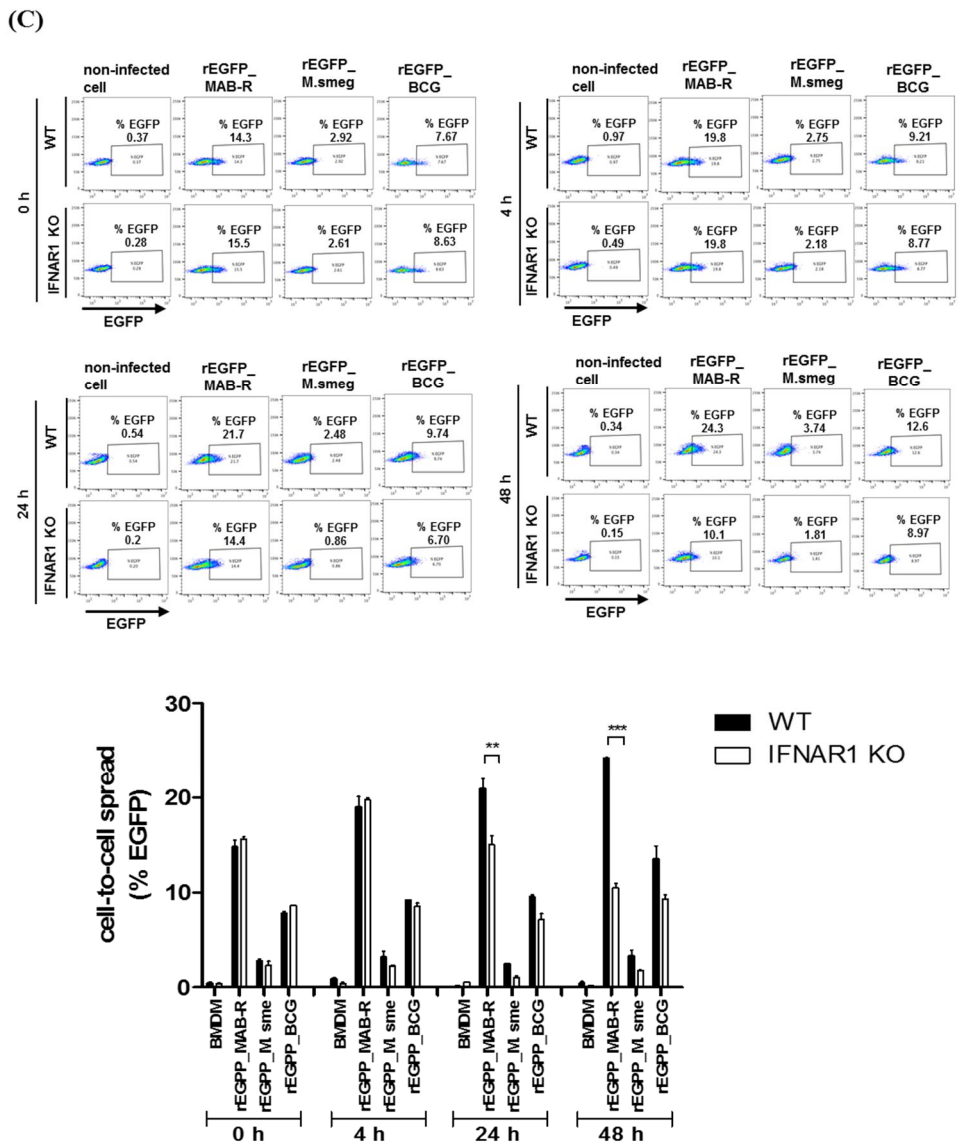

Figure 7. The cell-to-cell spread in MAB-R infection depends on Type I IFN signaling. (A and B) BMDMs (WT and IFNAR1 KO mice) infected with rough strains R [S-Abs_R (M. abscessus type strain ATCC 19977 rough strain)] and smooth strains [S-Abs_S (M. abscessus type strain ATCC 19977 smooth strain) and S-Mas_I-S (Asan 51843)], *M. smegmatis*, or M. bovis BCG (10 M.O.I) for 24 h. Infected cell lysate was used for CFU assays. Supernatants were collected and

cytotoxicity was measured by LDH assay. (C) BMDMs (WT and IFNAR1 KO mice) infected with EGFP-expressing bacteria [rEGFP_MAB-R (Asan 50594), rEGFP_M.smeg, rEGFP_BCG] (10 M.O.I), measured at different time points (0, 4, 24, and 48 h). Infected cells were collected and the percentage of EGFP-positive cells was evaluated by flow cytometry (FACScalibur). The results are representative of two independent experiments and represent means ± SD. P values were determined by the Student's *t*-test using GraphPad prism program: ns, nonsignificant; $*P < 0.05$; $**P < 0.01$, and $***P < 0.001$.

MAB-R strains exert enhance mitochondrial stress compared to MAB-S strains

Mitochondrial damage triggers the release of mitochondrial DNA (mtDNA), which is recognized by the cGAS/STING-mediated cytosolic DNA sensing pathway (50). This leads to the induction of IFN-β transcription and IFN-β secretion. I examined whether mitochondrial stress during infection of MAB-R strain into murine macrophages could induced Type I IFNs. First, mitochondria morphology was observed by means transmission electron microscopy (Figure 8A). Transmission electron microscopy images showed that normal mitochondria in macrophage, geometrical spheroid shaped or a reticulated morphology. In contrast, mitochondria morphology in infected around area infected with MAB-R strains is shrinked or distorted and lengthened. But mitochondria morphology in infected around area infected with MAB-S strains were similar to normal mitochondria or mitochondrial damage is relatively low compared to MAB-R strains infected cell. I next examined the involvement of the mitochondrial membrane potential and

mitochondrial ROS (mtROS), a kind of markers of mitochondria stress (Figure 8B-C). Infected cells were stained with the cationic dye mitochondrial superoxide indicator MitoSOX (Invitrogen) or TMRM (Invitrogen) as described in the manufacturer's protocol and fluorescence intensity was measured by flow cytometry. Rotenone, a common mitochondrial ROS inducer, was used as a positive control. Level of mitochondrial ROS and mitochondrial membrane potential were increased in MAB-R strains infected cells. Next, to check whether mtROS induction of MAB-R strains could depend on active multiplication, I compared mtROS levels between live and heat-killed (HK) MAB-R strains (Figure 8D). Only live, not HK, MAB-R strains induced mtROS. Furthermore, MAB-S, *M. smegmatis* and BCG did not also cause mtROS induction irrespective of whether they were HK or live cells, suggesting that phagosomal rupture of MAB-R strains via active multiplication in macrophage phagosome may contribute to mtROS induction.

(A)

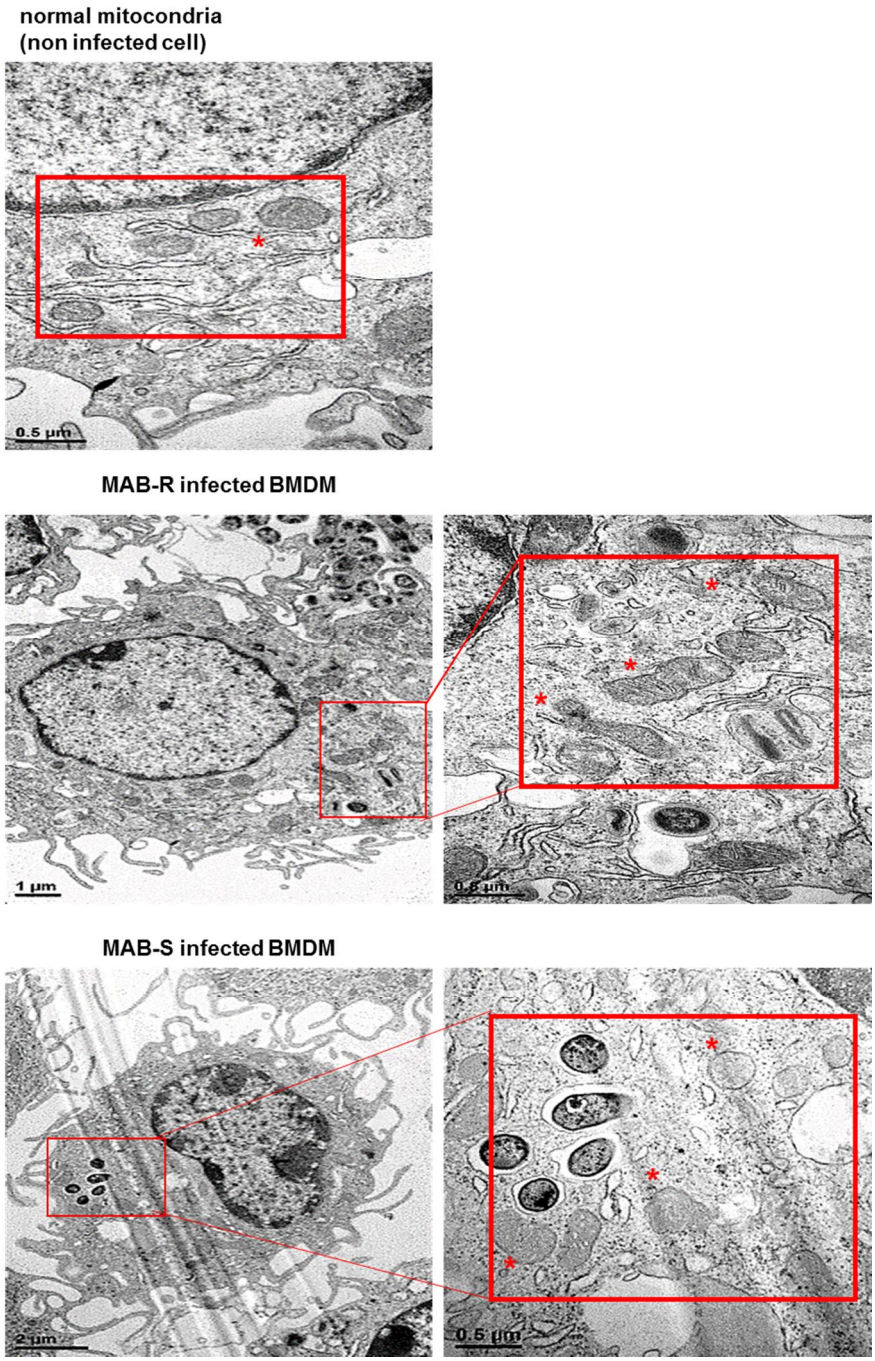
normal mitocondria
(non infected cell)
0.5 μm
MAB-R infected BMDM
1 μm
0.5 μm
MAB-S infected BMDM
2 μm
0.5 μm

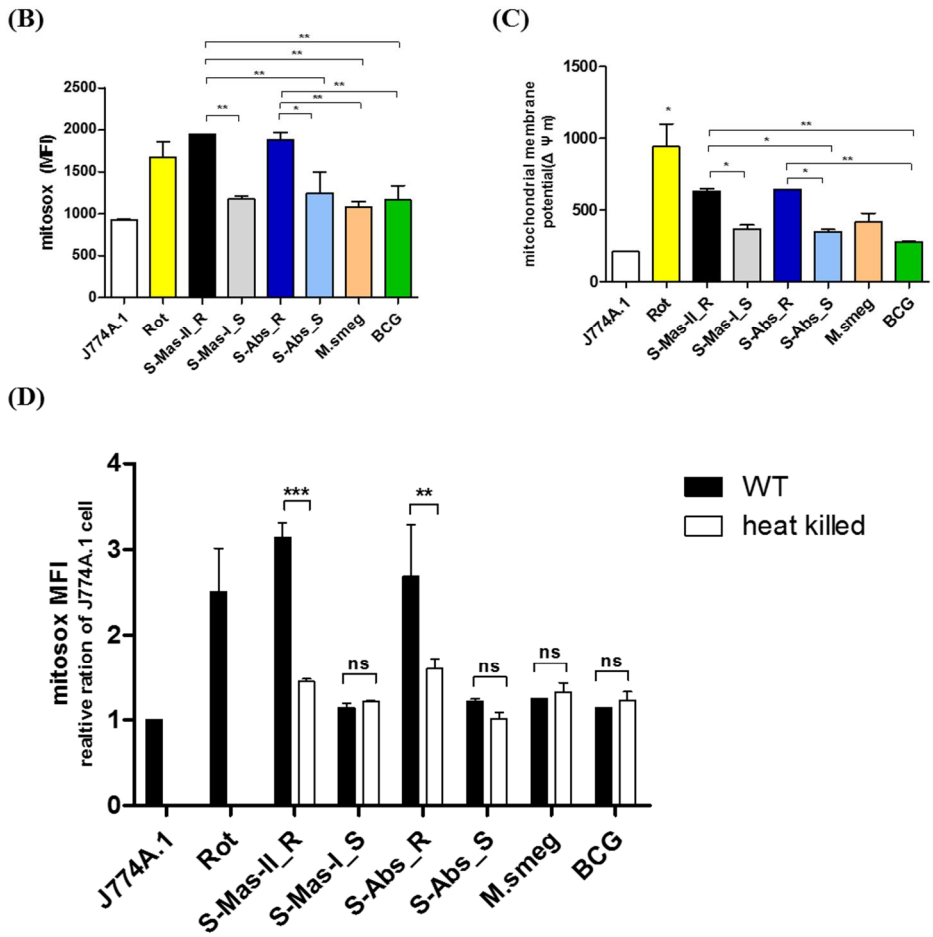

Figure 8. MAB-R strains induce severe mitochondrial damages compared to MAB-S strains. (A) Representative TEM images of J774A.1 cells infected with S-Abs_R (*M. abscessus* type strain ATCC 19977 rough strain) and S-Abs_S (*M. abscessus* type strain ATCC 19977 smooth strain) strains at 10 M.O.I. for 24 h.p.i. As a control, representative image of non-infected cells were shown. The mitochondrial morphology in infected cell and magnified images are shown (red box region and marked a red asterisk). Bar indicates 0.5 or 1 μm. (B-C) To evaluate mitochondrial ROS and mitochondrial membrane potential, BMDM cells were infected with S-Mas_II-R (Asan 50594), S-Mas_I-S (Asan 51843), S-Abs_R

(*M. abscessus* type strain ATCC 19977 rough strain), S-Abs_S (*M. abscessus* type strain ATCC 19977 smooth strain), *M. smegmatis*, *M. bovis* BCG, *M. marinum* (10 M.O.I.) at 10 M.O.I for 24 h. Also, cells were pre-treated with rotenone (Rot; 5 uM) served as a positive control (induction of ROS product) for 30 min. The infected cells were stained with MitoSox or TMRM reagents, after then analyzed by flow cytometry (FACS Calibur). (D) Representative analysis of oxidative stress in infected with live or heat-killed mycobacteria (10 M.O.I) in J774A.1 cells for 24 h measured by flow cytometry (FACS Calibur)**.** The results are representative of two independent experiments and represent means ± SD. *P* values were determined by the Student's *t*-test using GraphPad prism program: ns, nonsignificant; **P* < 0.05; ** *P* < 0.01, and *** *P* < 0.001.

MAB-R strains lead to increased cytosolic mtDNA and cytosolic oxidized mtDNA compared to MAB-S strains

Since mitochondrial stress can trigger the release of mtDNA into the cytosol to engage the NLRP3 inflammasome (30). So, I checked cytosolic mtDNAs between macrophage cells infected with MAB-R and S strains via qRT-PCR. As shown in Figure 9A, this results showed that all cytosolic mtDNA genes (Dloop-1,-2,-3 and CytB, ND4, 16S) were highly expressed in two MAB-R strains [S-Abs_R (*M. abscessus* type strain ATCC 19977 rough strain) and S-Mas_II-R (Asan 50594)] compared to MAB-S strains [S-Abs_S (*M. abscessus* type strain ATCC 19977 smooth strain) and S-Mas_I-S (Asan 51843)], or even compared to *M. marinum*, which is known to be capable of phagosomal escape (21, 46). It has been reported that mtROS generation can result in oxidized mtDNA, which can be proved to

check increased mitochondrial 8-hydroxy-2-deoxyguanosine (8-OHdG), a marker of the DNA damage (30). Consistently, I found that the quantification of 8-OHdG was significantly increased in cells infected with MAB-R strains versus MAB-S strains, even cells infected with other mycobacteria, *M. smegmatis* or BCG (Figure 9B). These results collectively indicate that MAB-R strains versus MAB-S could exert enhanced release of oxidized mtDNAs into cytosol in infected macrophages.

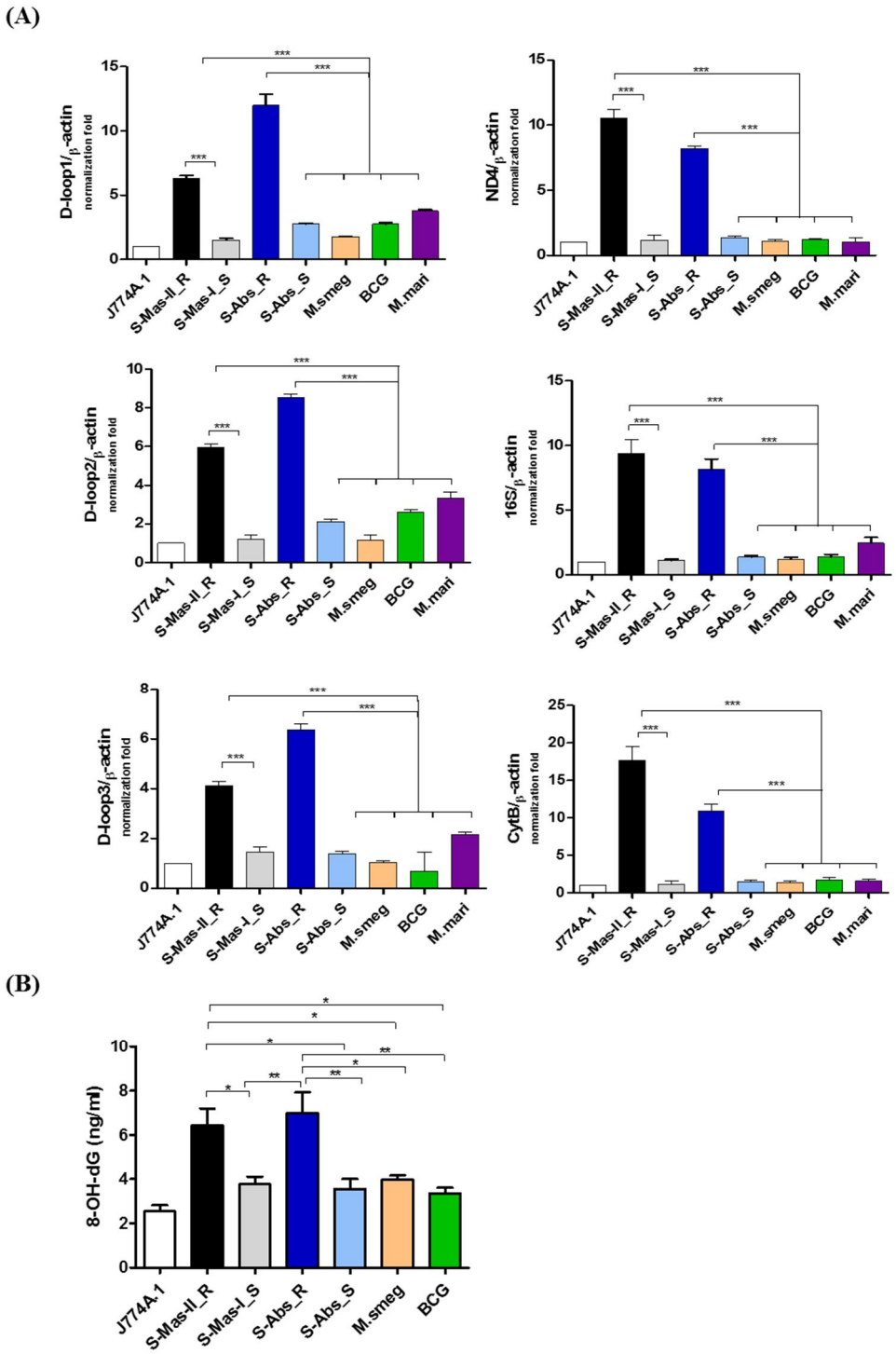

Figure 9. Increased cytosolic mtDNA and oxidized DNA by MAB-R strains in

macrophage cell. (A) Cytosolic mtDNA was extracted from nuclear and cytosolic extracts of S-Abs_R [(*M. abscessus* type strain ATCC 19977 rough strain) and S-Mas_II-R (Asan 50594)], smooth strains [S-Abs_S (*M. abscessus* type strain ATCC 19977 smooth strain) and S-Mas_I-S (Asan 51843)], *M. smegmatis*, *M. bovis* BCG, and *M. marinum* (10 M.O.I.) infected in J774A.1 cells for 24 h. Cytosolic mtDNA was quantitated via qRT-PCR using a mitochondrial Dloop primer set (Dloop-1,-2,-3 and CytB, ND4, 16S). Normalization was performed as described in the materials and methods. (B) Extracted DNAs from infected J774A.1 cells were enzymatically hydrolyzed into nucleosides, and levels of 8-OHdG were measured by ELISA kit. The results are representative of two independent experiments and represent means ± SD. *P* values were determined by the Student's *t*-test using GraphPad prism program: ns, nonsignificant; *$P < 0.05$; ** $P < 0.01$, and *** $P < 0.001$.

Enhanced IL-1ß secretion by MAB-R strains is due to both increased NLRP3 expression and inflammasome activation

Other studies have indicated that mtROS might play an important role in NLRP3 activation (51, 52). Indeed, my results showed that upon stimulation with two MAB-R strains [S-Abs_R (*M. abscessus* type strain ATCC 19977 rough strain) and S-Mas_II-R (Asan 50594)], mtROS was increased (Figure 8B). And MAB-R strains led to increased IL-1β secretion in macrophage cells, compared to MAB-S strains. *M. smegmatis* or BCG (Figure 11A). As shown in Figure 10, these results indicated that live MAB-R, but not H.K. strains led to enhanced IL-1β secretion in macrophages, suggesting IL-1β secretion of MAB-R strains may depend on their active replication. On the other hand, IL-6 and IL-10 production was no significant

differences in cytokine productions between live and H.K. MAB-R strains, suggesting that IL-6 and IL-10 production of MAB infection may not be dependent on active replication (Figure 10).

Consistently, immunoblots of cell lysates from infected BMDM for 24 h.p.i showed that two MAB-R strains [S-Abs_R (*M. abscessus* type strain ATCC 19977 rough strain) and S-Mas_II-R (Asan 50594)] led to enhanced expression of pro–IL-1β and NLRP3 compared to two MAB-S strains [S-Mas_I-S (Asan 51843) and S-Abs_S (*M. abscessus* type strain ATCC 19977 smooth strains)], suggesting that enhanced expression of pro–IL-1β and NLRP3 may contribute into enhanced IL-1β secretion of MAB-R strains. Furthermore, I also found that MAB-R strains led to enhanced production of mature IL-1β (17-kDa) proteins as well as expression of pro–IL-1β (35-kDa) in infected cells, compared to MAB-S strains and *M. smegmatis* or BCG infected cell (Figure 11B), suggesting not only expression of NLRP3 inflammasome, but also its activation could contribute into enhanced IL-1β secretion of MAB-R strains. Furthermore, enhanced production of mature caspase-1 found in cells infected with MAB-R strains further supported that above finding (Figure 11B).

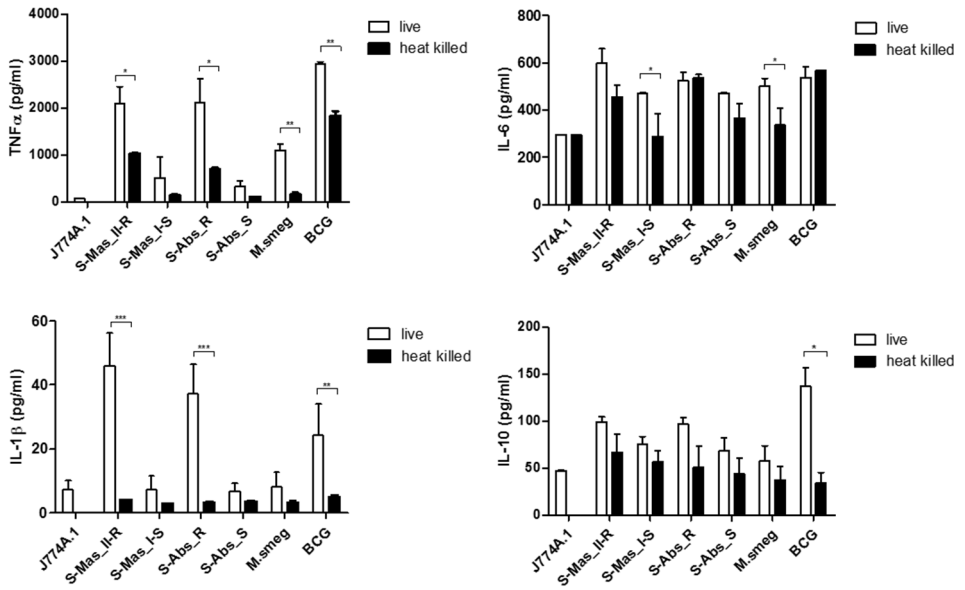

Figure 10. Cytokine production by live or heat-killed mycobacteria in murine macrophages. Live or heat-killed MAB-R strains [S-Abs_R (*M. abscessus* type strain ATCC 19977 rough strain) and S-Mas_II-R (Asan 50594)] and MAB-S strains [S-Abs_S (*M. abscessus* type strain ATCC 19977 smooth strain) and S-Mas_I-S (Asan 51843)], *M. smegmatis*, and BCG (10 M.O.I. infection) infecting J774A.1 cells for 24 h. Infected cell supernatants and TNF-α, IL-6, IL-1β and IL-10 cytokine levels were analyzed by ELISA. The results are representative of two independent experiments and represent means ± SD. *P* values were determined by the Student's *t*-test using GraphPad prism program: ns, nonsignificant; **P* < 0.05; ***P* < 0.01, and ****P* < 0.001.

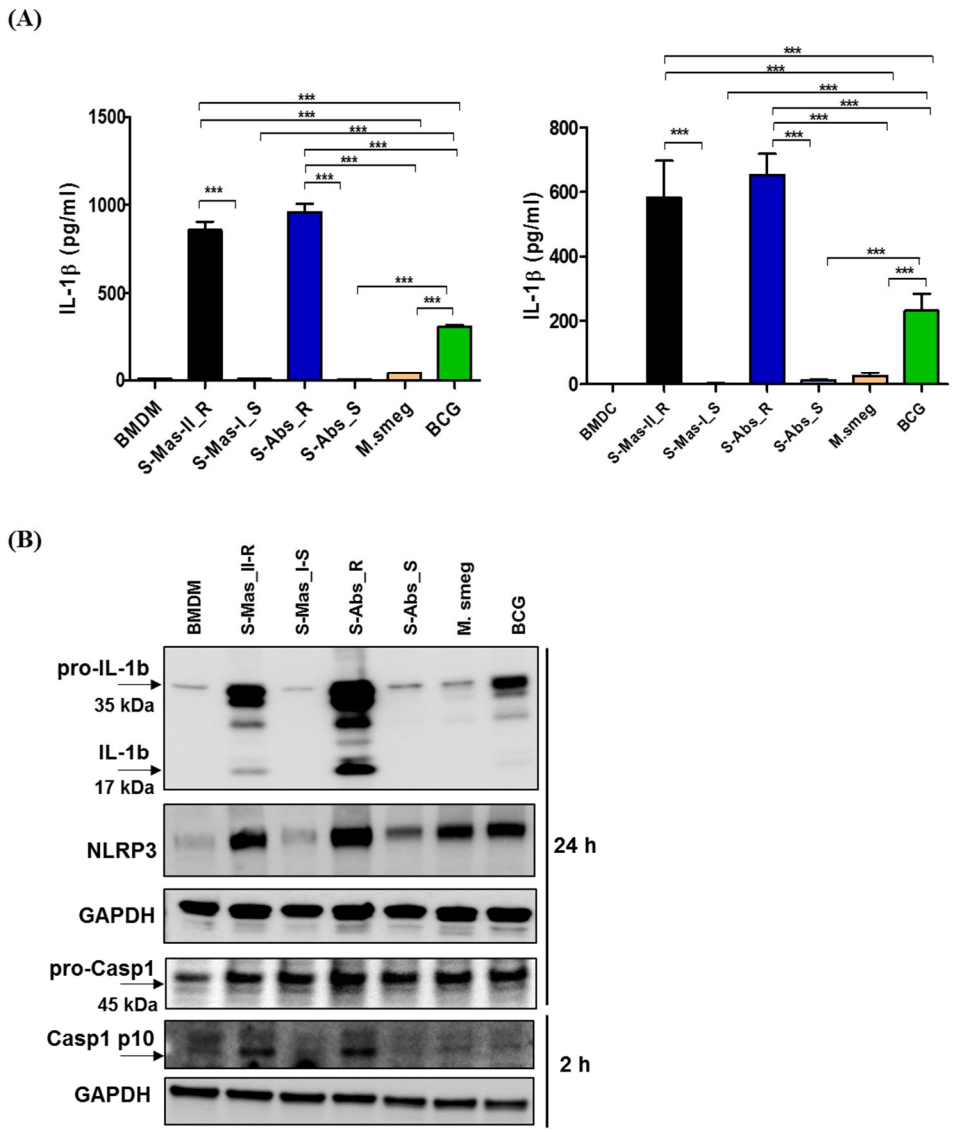

Figure 11. Production of IL-1β induced MAB-R via NLRP3 inflammasome. (A) BMDMs (left panel) and BMDCs (right panel) were infected with indicated bacteria at 10 M.O.I for 24 h, the supernatants of the infected cells were collected, and IL-1 β levels measured by IL-1 β ELISA. The results are representative of two independent experiments and represent means ± SD. *P* values were determined by the Student's *t*-test using GraphPad prism program: ns, nonsignificant; *$P < 0.05$;

**$P < 0.01$, and ***$P < 0.001$. (B) Western blot of NLRP3, IL- 1β and capase-1 induced by S-Abs_R [(*M. abscessus* type strain ATCC 19977 rough strain) and S-Mas_II-R (Asan 50594)], smooth strains [S-Abs_S (*M. abscessus* type strain ATCC 19977 smooth strain) and S-Mas_I-S (Asan 51843)], *M. smegmatis*, *M. bovis* BCG (10 M.O.I.) infected BMDM for 2 h or 24 h.

MAB-R strains increase Type I IFNs via mitochondrial ROS induction

To further support my hypothesis that MAB-R strains could cause NLRP3 inflammasome activation via mtROS, I treated cells infected with mycobacteria strains with mito-TEMPO, the mitochondria-targeted antioxidant. As shown in Figure 12A, level of mtROS induced by MAB-R strains [S-Abs_R (*M. abscessus* type strain ATCC 19977 rough strain) and S-Mas_II-R (Asan 50594)] were decreased by treatment of mito-TEMPO. But, it did not lead to any significant differences in mtROS levels in infected cells by MAB-S strains [S-Mas_I-S (Asan 51843) and S-Abs_S (*M. abscessus* type strain ATCC 19977 smooth strains)] or *M. smegmatis*. I next investigated whether inhibition of mtROS by treatment of mito-TEMPO could affect enhanced Type I IFNs and other cytokines found in MAB-R infected cells. I found that treatment of mito-TEMPO could lead to complete reversion of enhanced Type I IFN productions found in cells infected by MAB-R strains (Figure 12B). The similar trends were also found in IL-6 and IL-1β productions of cells infected with MAB-R strains, suggesting that Type I IFN, IL-6 and IL-1β productions in cells infected by MAB-R strains may depend on mtROS, However, treatment of mito-TEMPO could not affect production of TNF-α, suggesting that its production may not depend on mtROS.

Next, I checked whether treatment of mito-TEMPO could affect released cytosolic mtDNA in cells infected with MAB-R strains. To this end, I analyzed cytosolic mtDNA via qRT-PCR. As shown in Figure 12C, treatment of mito-TEMPO led to decreased releases of all the cytosolic mtDNA genes (Dloop and CytB, ND4) in J774A.1 cells infected by two MAB-R strains [S-Abs_R (*M. abscessus* type strain ATCC 19977 rough strain) and S-Mas_II-R (Asan 50594)], but not by other mycobacteria strains [S-Mas_I-S (Asan 51843) and S-Abs_S (*M. abscessus* type strain ATCC 19977 smooth strains) and *M. smegmatis*], suggesting increased mtDNAs may be due to the enhanced mtROS in cells infected by MAB-R strains. Next, to check the effect of mtROS on Type I IFN dependent cell-to-cell spread in J774A.1 cells infected by MAB-R strains, I analyzed cell-to-cell spread in J774A.1 cells infected with recombinant rEGFP_MAB-R [rEGFP_M.mass-R (Asan 50594)] and rEGFP_M.smeg (*M. smegmatis*) after mito-TEMPO treatment. As shown previously (Figure 6D), MAB-R strains induced cell-to-cell spreading, shown in Figure 12D but, its cell-to-cell spread capacity was inhibited in mito-TEMPO treated macrophage cells. Also, I found that treatment with mito-TEMPO could significantly decreased the intracellular growth of MAB-R, but not MAB-S (Figure 12E). These results suggest that antioxidant targeting mtROS could have the potential for the treatment in infection of MAB-R strains to control bacterial growth via inhibiting its Type I IFN dependent cell to cell spreading.

(A)

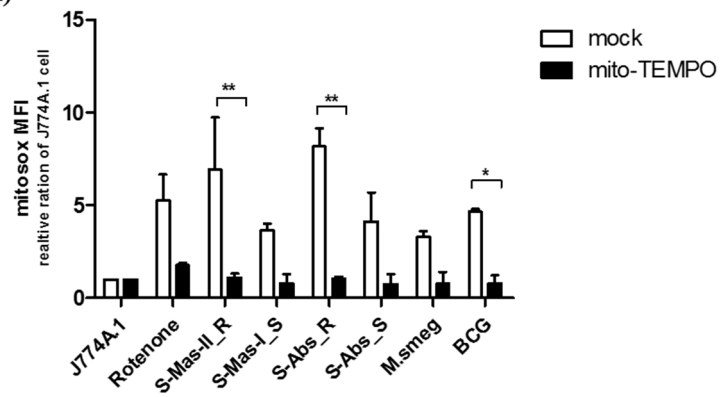
mitosox MFI
realtive ration of J774A.1 cell
15
10
5
0
mock
mito-TEMPO
**
**
*
J774A.1
Rotenone
S-Mas-II_R
S-Mas-I_S
S-Abs_R
S-Abs_S
M.smeg
BCG

(B)

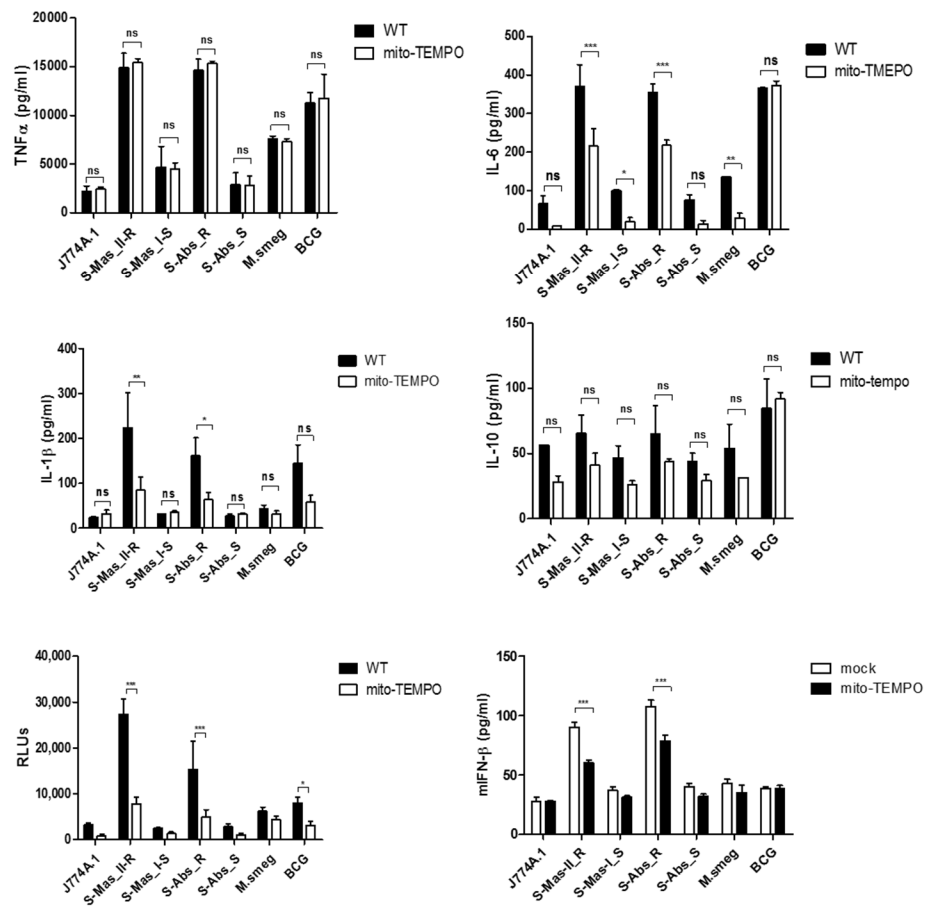
TNFα (pg/ml)
WT
mito-TEMPO
IL-6 (pg/ml)
WT
mito-TMEPO
IL-1β (pg/ml)
WT
mito-TEMPO
IL-10 (pg/ml)
WT
mito-tempo
RLUs
WT
mito-TEMPO
mIFN-β (pg/ml)
mock
mito-TEMPO
J774A.1
S-Mas_II-R
S-Mas_I-S
S-Abs_R
S-Abs_S
M.smeg
BCG

(C)

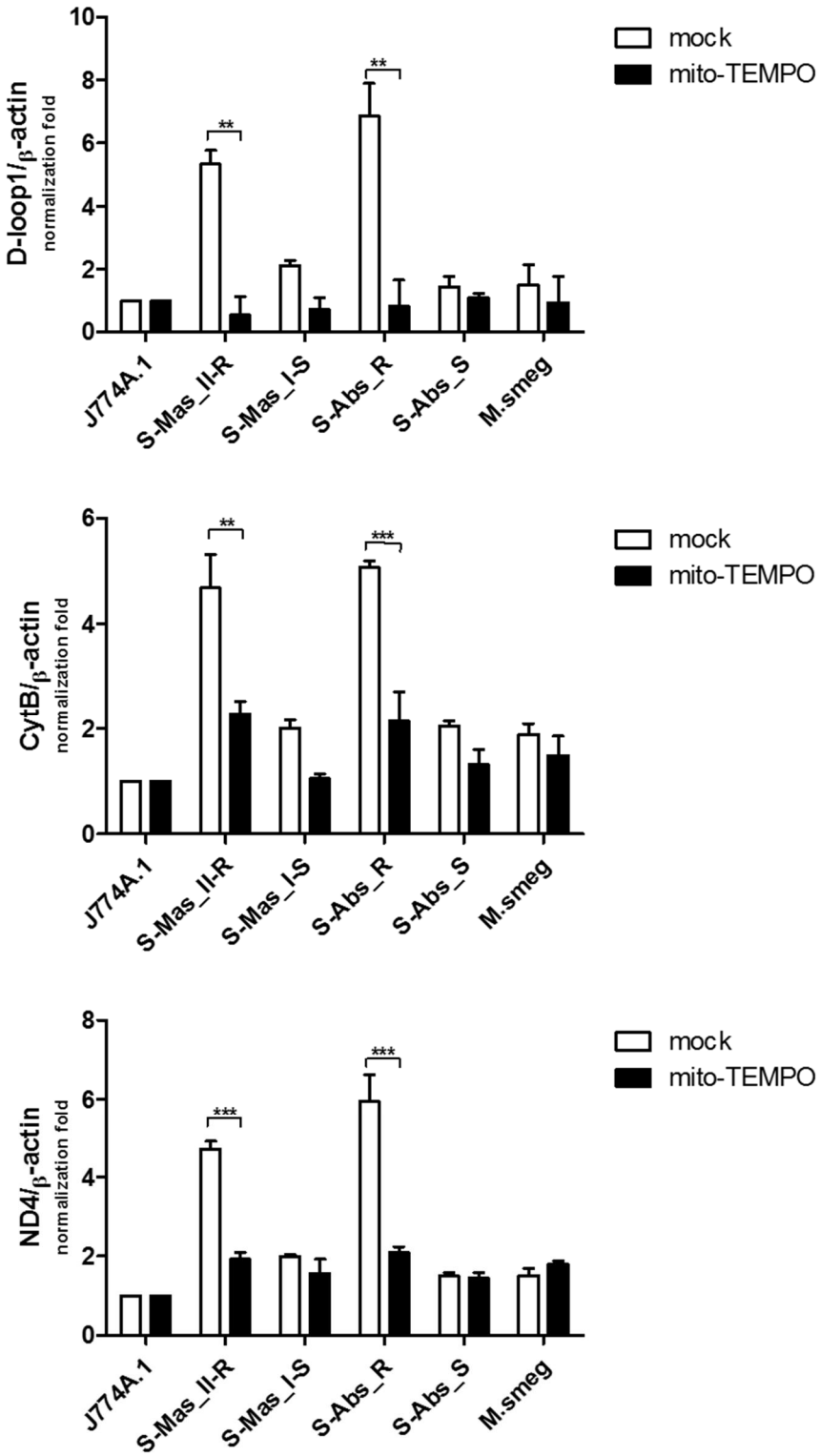
D-loop1/β-actin
normalization fold
10
8
6
4
2
0
**
**
mock
mito-TEMPO
J774A.1
S-Mas_II-R
S-Mas_I-S
S-Abs_R
S-Abs_S
M.smeg
CytB/β-actin
normalization fold
6
4
2
0
**
***
mock
mito-TEMPO
J774A.1
S-Mas_II-R
S-Mas_I-S
S-Abs_R
S-Abs_S
M.smeg
ND4/β-actin
normalization fold
8
6
4
2
0
***
***
mock
mito-TEMPO
J774A.1
S-Mas_II-R
S-Mas_I-S
S-Abs_R
S-Abs_S
M.smeg

(D)

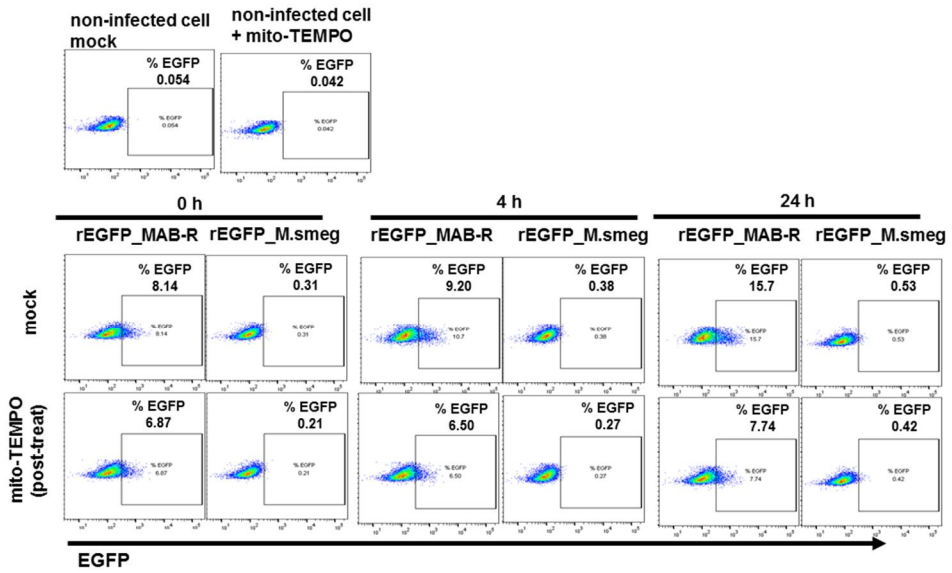
non-infected cell
mock
% EGFP
0.054
non-infected cell
+ mito-TEMPO
% EGFP
0.042
0 h
4 h
24 h
rEGFP_MAB-R
rEGFP_M.smeg
mock
mito-TEMPO
(post-treat)
% EGFP
8.14
% EGFP
0.31
% EGFP
9.20
% EGFP
0.38
% EGFP
15.7
% EGFP
0.53
% EGFP
6.87
% EGFP
0.21
% EGFP
6.50
% EGFP
0.27
% EGFP
7.74
% EGFP
0.42
EGFP

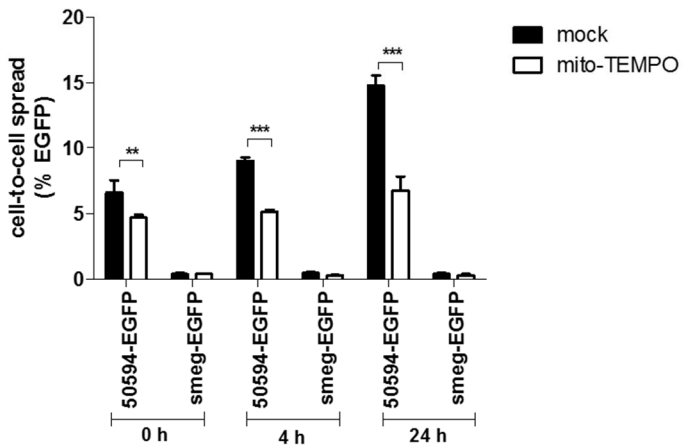
cell-to-cell spread
(% EGFP)
20
15
10
5
0
**
***
***
mock
mito-TEMPO
50594-EGFP
smeg-EGFP
50594-EGFP
smeg-EGFP
50594-EGFP
smeg-EGFP
0 h
4 h
24 h

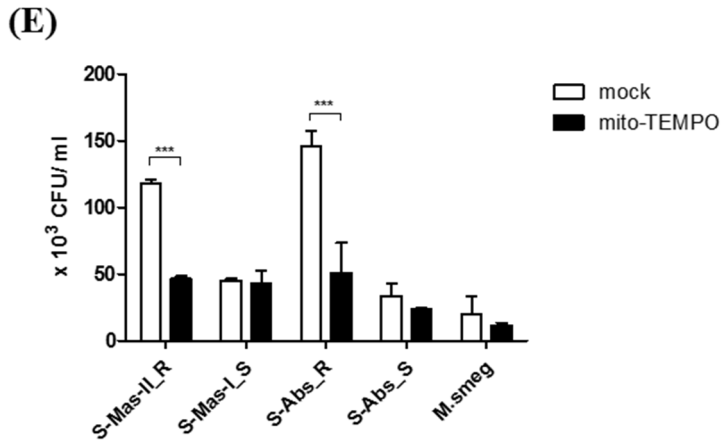

Figure 12. mtROS enhance type I IFN production and cell-to-cell spread in MAB-R infection macrophage cells. (A) mito-tempo post-treated (100 uM) J774A.1 cells and normal J774A.1 cells infected with infected with S-Abs_R [(*M. abscessus* type strain ATCC 19977 rough strain) and S-Mas_II-R (Asan 50594)], smooth strains [S-Abs_S (*M. abscessus* type strain ATCC 19977 smooth strain) and S-Mas_I-S (Asan 51843)], *M. smegmatis*, and *M. bovis* BCG (10 M.O.I.) for 24 h. cells were pre-treated with rotenone (5 uM) served as a positive control (induction of ROS product) for 30 min. The infected cells were stained with MitoSox after then analyzed by flow cytometry (FACS Calibur). (B) Supernatants from the infected cells were collected, TNF-α and IL-6, IL-1β, IL-10, and IFN- β cytokine levels were analyzed by ELISA or IFN bioassay. (C) Cytosolic mtDNA was extracted from nuclear and cytosolic extracts of S-Abs_R [(*M. abscessus* type strain ATCC 19977 rough strain) and S-Mas_II-R (Asan 50594)], smooth strains [S-Abs_S (*M. abscessus* type strain ATCC 19977 smooth strain) and S-Mas_I-S (Asan 51843)], *M. smegmatis*, *M. bovis* BCG, and *M. marinum* (10 M.O.I.) infected in mito-tempo post-treated (100 uM) J774A.1 cells or normal J774A.1

cells for 24 h. Cytosolic mtDNA was quantitated via qRT-PCR using a mitochondrial Dloop primer set (Dloop-1, CytB, and ND4). (D) J774A.1 cells were infected with rEGFP_MAB-R [rEGFP_M.mass-R (Asan 50594)] and rEGFP_M.smeg (*M. smegmatis*) at 10 M.O.I, and analysis was performed on post-treatment with mito-TEMPO (100 uM). The percentage of EGFP-positive cells was evaluated by flow cytometry (FACScalibur). (E) J774A.1 cells (mock and mito-TEMPO 100 uM post-treatment) infected with rough strains R [S-Abs_R (M. abscessus type strain ATCC 19977 rough strain)] and smooth strains [S-Abs_S (M. abscessus type strain ATCC 19977 smooth strain) and S-Mas_I-S (Asan 51843)], *M. smegmatis*, for 24 h. Infected cell lysate was used for CFU assays. The results are representative of two independent experiments and represent means ± SD. *P* values were determined by the Student's *t*-test using GraphPad prism program: ns, nonsignificant; *$P < 0.05$; ** $P < 0.01$, and *** $P < 0.001$.

MAB-R strains lead to enhanced Type I IFNs in infected murine macrophages via actin dependent phagocytosis

It was recently reported that several intracellular bacterial pathogens, including species of *Listeria*, *Rickettsia*, *Shigella*, *Mycobacteria*, and *Burkholderia*, have developed mechanisms to exploit the actin polymerization strategies of their hosts to induce actin-based motility, for these pathogens to capable of entering into other host cells (53, 54). As MAB-R could induce phagosomal rupture, I hypothesized that MAB-R strains could lead to mitochondrial stress mediated Type I IFN production via actin dependent phagocytosis. To prove it, I checked that treatment of Cytochalasin D (phagocytosis inhibitor), an inhibitor of actin polymerization

could affect several Type I IFN mediated biological activities found in J774A.1 cells infected by MAB-R strains [(*M. abscessus* type strain ATCC 19977 rough strain) and S-Mas_II-R (Asan 50594)]. I found that treatment of Cytochalasin D led to decreased mtROS (Figure 13A) and mtROS mediated cytosol mtDNA (Dloop and CytB, ND4) (Figure 13C) in cell infected by MAB-R strains [S-Abs_S (*M. abscessus* type strain ATCC 19977 smooth strain) and S-Mas_I-S (Asan 51843)], but it is not true in cells infected by other mycobacteria strains including MAB-S strains or *M. smegmatis*. Moreover, it also led to significant decrease of IL-1β and IFN-β production in J774A.1 cells infected with MAB-R strains (Figure 13B). Consistently, I examined effect of treatment of Cytochalasin D on cell-to-cell spreading in cells infected with MAB-R strains. I found that it also led to inhibition of cell-to-cell spreading in infected J774A.1 cells (Figure 13C). As shown in Figure 13E, treatment with Cytochalasin D could significantly decreased the intracellular growth of MAB-R, but not MAB-S. These result suggest that actin dependent phagocytosis could function as upstream signal of mitochondrial stress mediated Type I IFN production found in macrophages infected with MAB-R strains and also suggest its potential as a drug target of MAB infection.

(A)

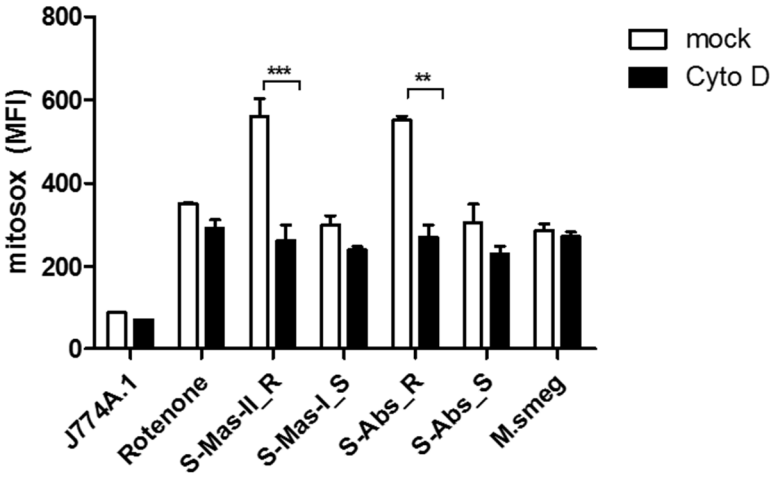
mitosox (MFI)
800
600
400
200
0
***
**
mock
Cyto D
J774A.1
Rotenone
S-Mas-II_R
S-Mas-I_S
S-Abs_R
S-Abs_S
M.smeg

(B)

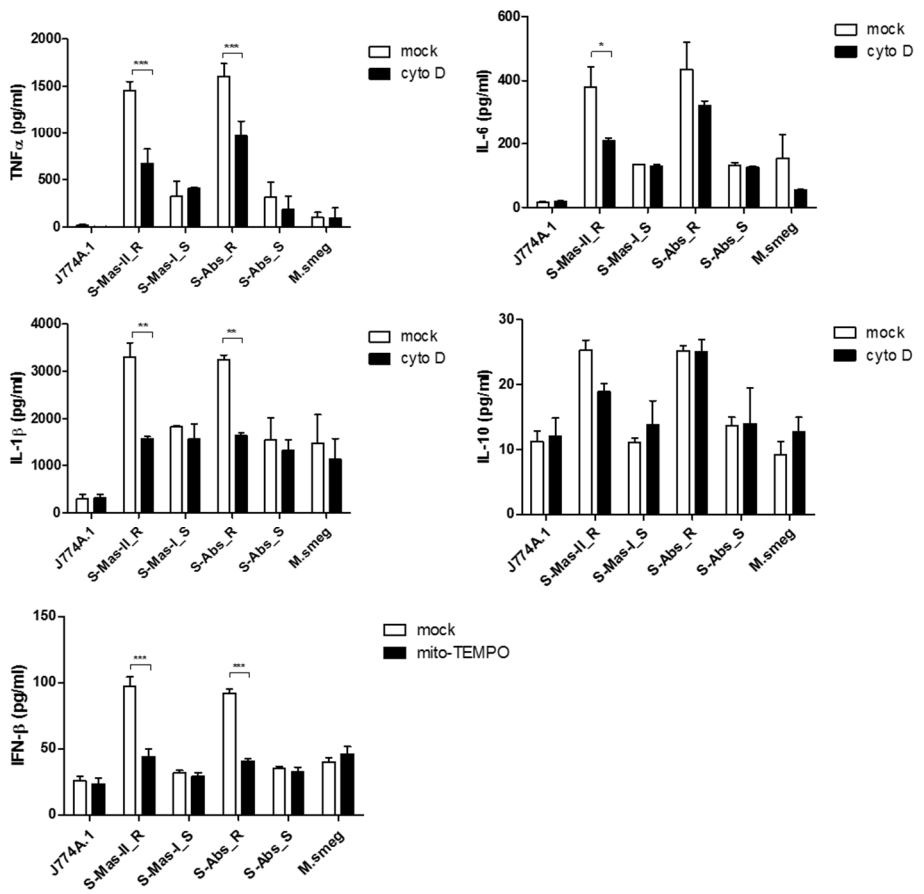
TNFα (pg/ml)
IL-6 (pg/ml)
IL-1β (pg/ml)
IL-10 (pg/ml)
IFN-β (pg/ml)
mock
cyto D
mito-TEMPO
J774A.1
S-Mas-II_R
S-Mas-I_S
S-Abs_R
S-Abs_S
M.smeg

(C)

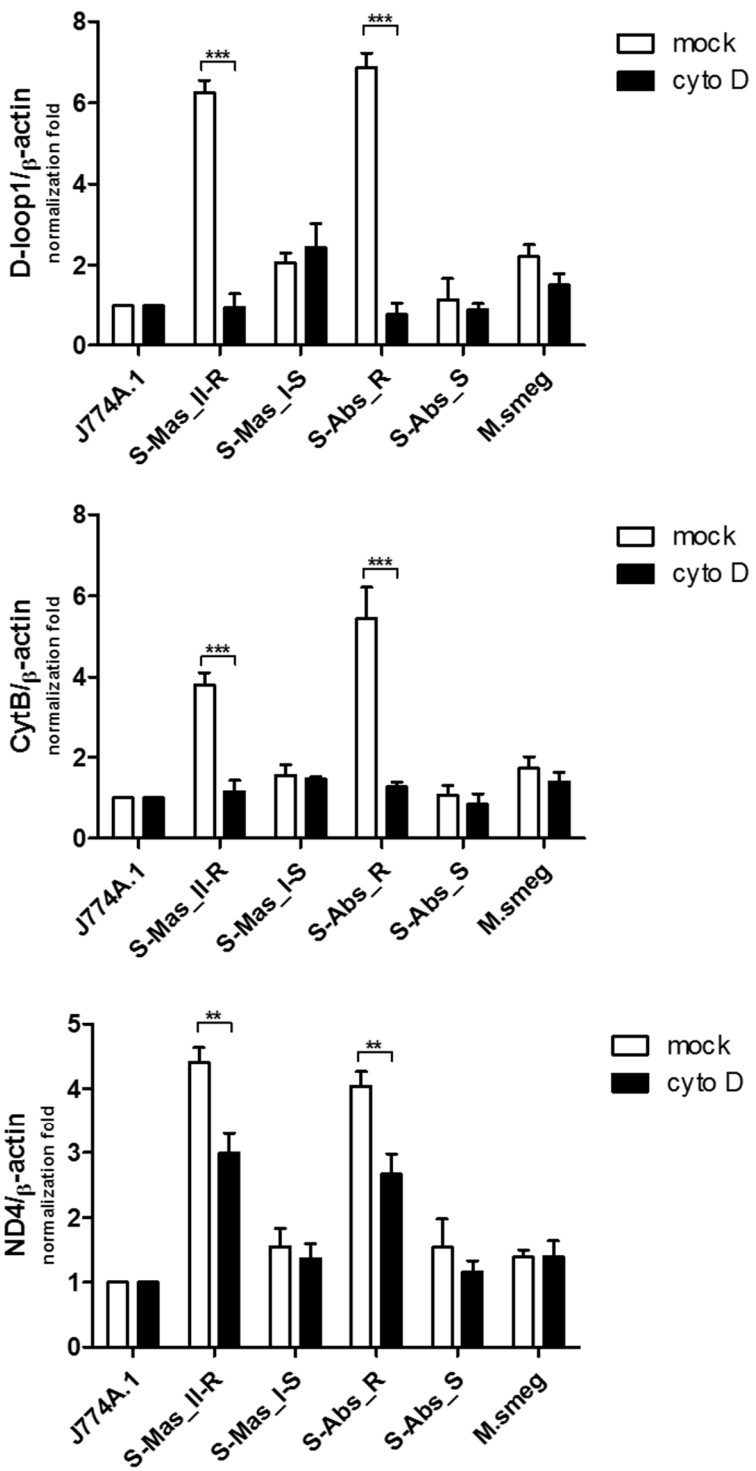
D-loop1/β-actin
normalization fold
mock
cyto D
***
***
J774A.1
S-Mas_II-R
S-Mas_I-S
S-Abs_R
S-Abs_S
M.smeg
CytB/β-actin
normalization fold
mock
cyto D
***
***
J774A.1
S-Mas_II-R
S-Mas_I-S
S-Abs_R
S-Abs_S
M.smeg
ND4/β-actin
normalization fold
mock
cyto D
**
**
J774A.1
S-Mas_II-R
S-Mas_I-S
S-Abs_R
S-Abs_S
M.smeg

(D)

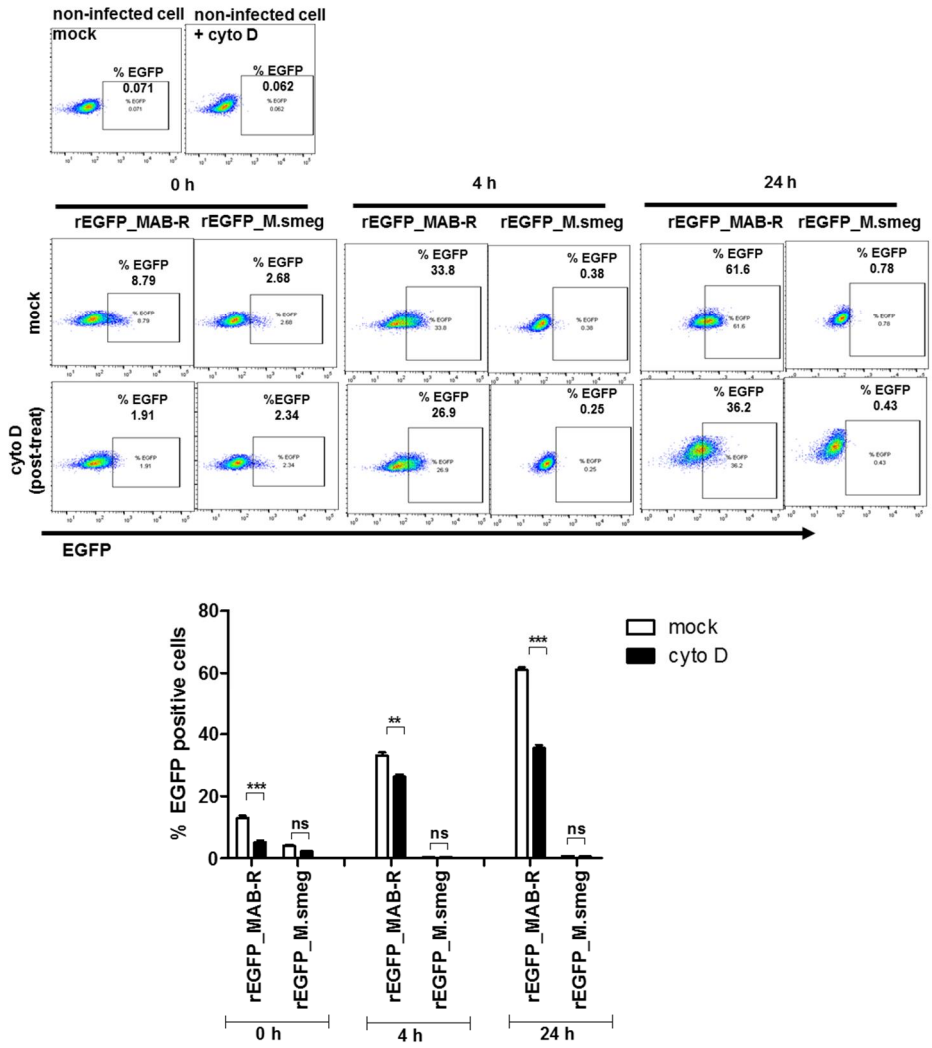
non-infected cell
mock
% EGFP
0.071
non-infected cell
+ cyto D
% EGFP
0.062
0 h
4 h
24 h
rEGFP_MAB-R
rEGFP_M.smeg
mock
cyto D
(post-treat)
% EGFP
8.79
% EGFP
2.68
% EGFP
33.8
% EGFP
0.38
% EGFP
61.6
% EGFP
0.78
% EGFP
1.91
%EGFP
2.34
% EGFP
26.9
% EGFP
0.25
% EGFP
36.2
% EGFP
0.43
EGFP
% EGFP positive cells
mock
cyto D
***
ns
**
ns
***
ns
rEGFP_MAB-R
rEGFP_M.smeg
0 h
4 h
24 h

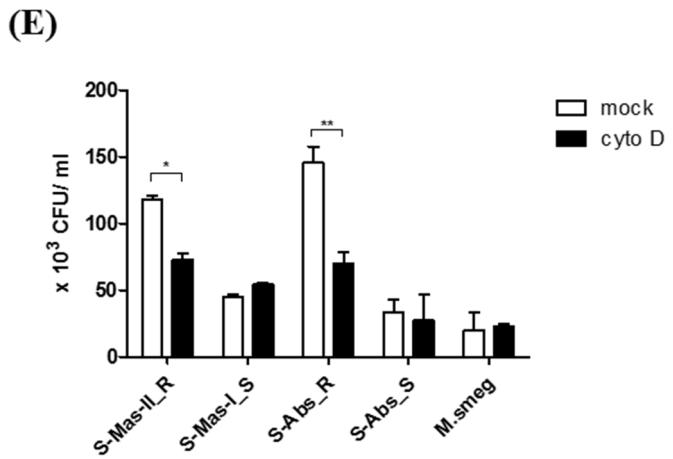

Figure 13. Actin-dependent phagocytosis contributes to cell-to-cell spreading by MAB-R strains. (A) Cytochalasin D post-treated (cyto D; 1 ug/ml) J774A.1 cells and normal J774A.1 cells infected with infected with S-Abs_R [(*M. abscessus* type strain ATCC 19977 rough strain) and S-Mas_II-R (Asan 50594)], smooth strains [S-Abs_S (*M. abscessus* type strain ATCC 19977 smooth strain) and S-Mas_I-S (Asan 51843)], *M. smegmatis*, and *M. bovis* BCG (10 M.O.I.) for 24 h. cells were pre-treated with rotenone (5 uM) served as a positive control (induction of ROS product) for 30 min. The infected cells were stained with MitoSox after then analyzed by flow cytometry (FACS Calibur). (B) Supernatants from the infected cells were collected, TNF-α and IL-6, IL-1β, IL-10 and IFN- β cytokine levels were analyzed by ELISA. (C) Cytosolic mtDNA was extracted from nuclear and cytosolic extracts of S-Abs_R [(*M. abscessus* type strain ATCC 19977 rough strain) and S-Mas_II-R (Asan 50594)], smooth strains [S-Abs_S (*M. abscessus* type strain ATCC 19977 smooth strain) and S-Mas_I-S (Asan 51843)], *M. smegmatis*, *M. bovis* BCG, and *M. marinum* (10 M.O.I.) infected in post-treated

with cytochalasin D (cyto D; 1 ug/ml) J774A.1 cells or normal J774A.1 cells for 24 h. Cytosolic mtDNA was quantitated via qRT-PCR using a mitochondrial Dloop primer set (Dloop-1, CytB, and ND4). (D) J774A.1 cells were infected with rEGFP_MAB-R [rEGFP_M.mass-R (Asan 50594)] and rEGFP_M.smeg (*M. smegmatis*) at 10 M.O.I, and analysis was performed on treatment with cytocahasin D (cyto D; 1 ug/ml). (E) J774A.1 cells (mock and cytochalasin D 1ug/ml post-treatment) infected with rough strains R [S-Abs_R (M. abscessus type strain ATCC 19977 rough strain)] and smooth strains [S-Abs_S (M. abscessus type strain ATCC 19977 smooth strain) and S-Mas_I-S (Asan 51843)], *M. smegmatis* for 24 h. Infected cell lysate was used for CFU assays. The percentage of EGFP-positive cells was evaluated by flow cytometry (FACScalibur). The results are representative of two independent experiments and represent means ± SD. *P* values were determined by the Student's *t*-test using GraphPad prism program: ns, nonsignificant; *$P < 0.05$; ** $P < 0.01$, and *** $P < 0.001$.

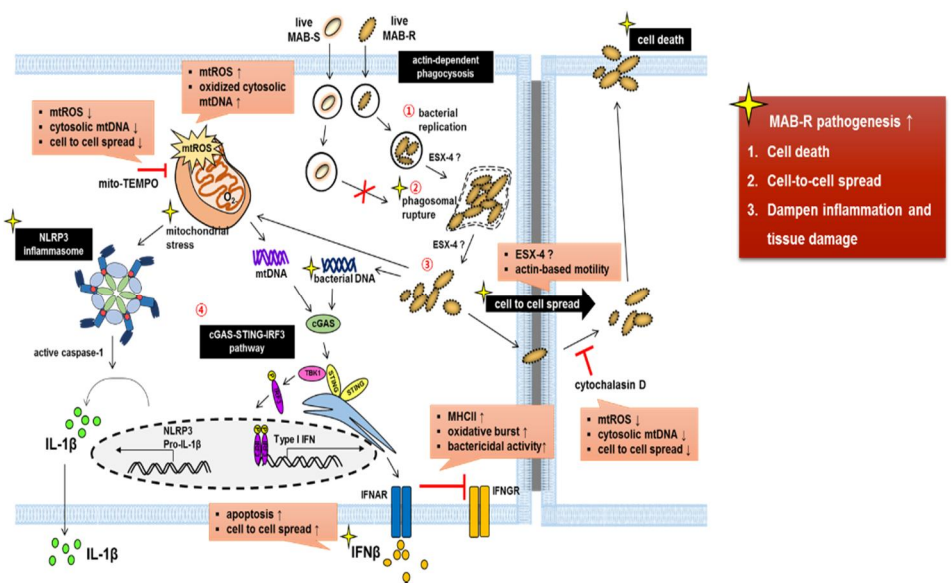

Figure 14. Schematic of a phagocyte infected with MAB and the different events related Type I IFN production and NLRP3 inflammasome. The schematic image showed that phagosomal rupture-mediated phagosomal escape of MAB-R in infected murine macrophage, leading to Type I INF production via the cGAS-STING-IRF3 axis and activate NLRP3 inflammasome via mitochondrial stress mediated release of oxidized mitochondrial DNA into cytosol. Live *M. abscessus* (MAB-R and -S) move into macrophage cells by phagocytosis. However, different life styles within macrophages were found between MAB-R and MAB-S strains. MAB-S strains remain silent in the phagosome and cannot lead to phagosomal rupture mediated escape to cytosol. So, MAB-S strains also cannot activate Type I IFN production via the cGAS-STING-IRF3 pathway. However, MAB-R can replicate in the phagosome (1) and cause phagosomal rupture (2). MAB-R can escape to the cytosol (3), which produce Type I IFN (IFNβ) via the cGAS-STING-IRF3 pathway (4). Furthermore, MAB-R can move to adjacent cells by Type I IFN receptor-dependent cell-to-cell spreading. ESX-4 locus, which has been recently reported to be related to phagosomal rupture (55), may contribute into replication in phagosome (1), phagosome rupture (2), and escape into cytosol of MAB-R (3). Next, secreted IFN-β by MAB-R infections could also contribute into bacteria proliferation by interfering with IFN-γ signaling pathway (56). The phagosomal rupture induced mitochondrial stress (mitochondrial ROS induction) and oxidized mtDNA release into cytosol, which lead to activate NLRP3 inflammasome.

DISCUSSION

Previously reported that the S-Mas type II genotype (rough type) leads to the production of a higher level of CFUs and TNF-α secretion from human monocytes than the Type I genotype (smooth type) (26). It was recently reported that highly virulent clinical MAB strains lead to more cell death than nonvirulent strains (2). Furthermore, virulent *M. tuberculosis* strains have been reported to survive better than attenuated strains because of their cell-to-cell spreading and bacterial cytosol access via ESX-1-derived active phagosomal rupture (20-22). In this process, bacterial DNA exposed in the cytosol induces Type I IFN signaling, resulting in apoptotic cell death (22-25). These previous findings prompt me to hypothesize that the higher pathogenic potential in MAB-R strains versus MAB-S strains may also be due to mechanisms similar to those in virulent *M. tuberculosis*. Indeed, in the present study, I found that irrespective of different subspecies or genotypes, virulent MAB-R strains have cytosolic stages that are followed by phagosomal replication and rupture in the course of infecting murine macrophages (Figure 2), consequently leading to the induction of Type I IFN signaling (Figure 4) and cell death-mediated cell-to-cell spreading (Figure 5-7).

Unlike virulent *M. tuberculosis* or *M. marinum* strains harboring the ESX-1 locus (20-22) or some specialized intracellular bacteria such as *Shigella flexneri* (57), *Listeria monocytogenes* (42) or *Francisella tularensis* (58) that can actively destroy the phagosome membrane, MAB strains without an ESX-1 ortholog in their genome (28) have to utilize an alternative strategy for bacterial cytosol access.

Recently, the orthologous ESX-4 locus in *M. abscessus* genome has been reported to be capable of elicit phagosome membrane rupture and be essential for the intracellular survival of *M. abscessus* in amoeba or macrophage, strongly supporting the possibility that ESX-4 may operate as a surrogate for ESX-1 in *M. tuberculosis* (55). Indeed, I found via TEM and AFB staining that abrupt increases in the intracellular growth of MAB-R strain during the initial phase of infecting macrophages (6 to 24 h.p.i.) was due to their active multiplication in phagosome, leading to phagosomal rupture via their overgrowth beyond phagosome capacity (Figure 2E-G), which could consequently lead to their escape into the cytosol. These TEM and AFB staining data indicated that even in some MAB-R-infected cells, bacterial release into the extracellular medium from destroyed cell membranes occurred (Figure 2F-G), suggesting a possible link between the phagosomal escape of MAB-R strains by phagosomal rupture to cell death-mediated bacterial cell-to-cell spreading. The bacterial escape into the cytosol via overgrowth in phagosomes that was exhibited by MAB-R strains has not been previously reported. However, whether ESX-4 locus of *M. abscessus* could contribute into active replication in phagosome, phagosome escape and intracellular survival of MAB-R strains in infected macrophages should be elucidated in the future.

In contrast to MAB-R strains, the MAB-S strains rarely increased their intracellular growth in the initial stage of infection (Figure 1C), suggesting a lack of growth in the phagosome, which is consistent with the TEM data showing a single bacterium per vacuole in most vacuoles and no evidence of phagosomal rupture (Figure 2C). The disparity in phagosomal rupture-inducing capacity

between MAB-R and -S types can lead to distinct damage-associated molecular pattern (DAMP) responses between the two groups. Indeed, I found that MAB-S strains produced lower amounts of proinflammatory cytokines such as TNF-α and IL-6 than MAB-R strains in infections of murine macrophage or dendritic cells (Figure 1D-F). Furthermore, the contrast in produced cytokines between live and HK bacteria was less pronounced in MAB-S-infected macrophage than in MAB-R-infected macrophage (Figure 10). It has been reported that MAB-S infection is more prevalent during initial infection from environments, but after infection, a morphotype change from the MAB-S type into the MAB-R type frequently follows (2, 17, 18). Therefore, in macrophage infections with both morphotypes, MAB-S strains may enable the initial infection and the colonization into macrophage by minimally evoking host immune responses like a latent infection of *M. tuberculosis*, and their transition into the MAB-R type could broaden its niche for intracellular survival in the late phase of infection at the expense of evoking host immune responses.

In addition to TEM-based evidence, there are two other findings (biochemical evidence and PCR-based detection) supporting the presence of cytosol stages of MAB-R strains in infected macrophage. First, I also found that irrespective of the types of their subspecies (S-Abs or S-Mas) or genotypes (Type I or Type II of S-Mas), MAB-R strains but not MAB-S strains induced IFN-β secretion (Figure 4A), ISRE-dependent luciferase activity (Figure 4B) and the transcriptional expression of downstream interferon-related genes (Figure 4E) in an IRF3-dependent manner in infected BMDMs or BMDCs, further providing clear biochemical evidence for their cytosol access. Moreover, the finding that only their live strains and not HK

strains induce IFN-β secretion (Figure 4C) proves that their induction of Type I IFN may be due to DAMP (cytosolic bacterial DNAs)-dependent intracellular signaling rather than extracellular signaling by membrane-associated pattern recognition receptors (PRRs) such as TLR3 or TLR9. Indeed, I also found an increase in activated STING proteins in MAB-R-infected BMDM or BMDCs (Figure 4D), suggesting the direct sensing of cytosolic bacterial DNA. For the second piece of evidence supporting the cytosol stages of MAB-R strains, I directly detected the presence of cytosolic MAB DNA by a PCR method targeting mycobacterial *hsp65* genes in MAB-R-infected murine macrophages (J774A.1 cells and BMDMs) (Figure 3A-B).

Type I IFN plays a pivotal role in immunity and inflammation in an autocrine or a paracrine manner via interactions with its receptor, IFNAR1, which is ubiquitously expressed in a variety of cells (59, 60). Although the host-protective functions of Type I IFNs have been well described in viral infections, they are also generally considered to have a detrimental effect on diseases caused by intracellular bacteria, such as *M. tuberculosis* (61-63). For example, in humans, a comparable IFN-inducible gene signature was observed in the blood of TB patients as well as in 10~25% of latently infected individuals, suggesting that the whole-blood IFN signature could be useful in identifying active TB disease (64). Furthermore, a recent *in vivo* mice study proved that coinfection with a virulent *M. tuberculosis* infection could increase the severity of other viral infections such as influenza in a Type I IFN signaling-dependent manner (65). Since avirulent or saprophytic mycobacteria cannot induce type I IFNs, it is hypothesized that Type I IFN production is associated with mycobacterial virulence and increased host

susceptibility (66). Furthermore, Induction of Type I IFN has also been reported to lead to proliferation of intracellular bacteria such as *L. monocytogenes* within macrophage via inhibiting macrophage activation by IFN-γ (56) (Figure 15). Indeed, these findings of enhanced Type I IFN production in virulent strains (MAB-R) strains but not in the less virulent type (MAB-S) (Figure 7A-B) also support the above hypothesis. Therefore, chronic stimulation of the Type I IFN signaling pathway, induced by MAB-R infection, could compromise host-defense immune responses against its infection and affect disease progression by other infections co-infecting with MAB-R, such as *M. tuberculosis* or influenza.

Apoptotic cell death via phagosomal rupture in pathogenic mycobacterial infection can lead to cell-to-cell spreading, which contributes to their survival in macrophage (25, 46, 67, 68). A recent study showed that Type I IFN signaling induced by *Listeria monocytogenes* infections contributes to their virulence via cell-to-cell spreading (49). Indeed, in this study, I proved that enhanced apoptotic cell death by MAB-R strains leads to cell-to-cell spreading in an IFNAR1-dependent manner (Figure 7C), suggesting that Type I IFN in MAB-R strains contributes to their enhanced virulence via providing a niche for their survival within macrophage (Figure 7A).

Recently, it has been reported that Type I IFN can promote cell-to-cell spreads of *L. monocytogenes* in *in vitro* macrophage or in livers of infected mice, which is mediated by formation of actin comet tails via IFNRR1 (49). So it is tempting to speculate that Type I IFN dependent cell-to-cell spread of MAB-R strains as shown in this study (Figure 7C), may also be due to the similar mechanism as shown in *L. monocytogenes* (56). However, issue regarding actin based motility or actin comet

formation of MAB-R strains for cell-to-cell spread remain to be addressed in the future.

A recent study has reported that Type I IFN secretion was varied depending on *M. tuberculosis* strains despite there being no difference in bacterial cytosol access via phagosome rupture between them, suggesting the presence of other factors affecting Type I IFN secretion in *Mtb* infection (29). So, I hypothesized that MAB-R strains may also have other mechanism to induce Type I INF productions distinct from one mediated via cytosolic bacterial DNAs described above. Here, I proved that actin-dependent bacteria phagocytosis could also exert an enhanced Type I IFN production via evoking mitochondrial stress mediated release of oxidized mtDNAs into cytosols in MAB-R infected murine macrophages. Furthermore, mitochondrial stress induced by MAB-R infection can also lead to NLRP3 inflammasome mediated IL-1β productions, which were mediated by two arms, one for the enahnced expression of pro IL-1β and NLRP3 and the other for inflammasome activations. I also proved that anti-oxidant treatment to inhibit mtROS or drug targeting phagocytosis stage of bacteria as upstream of mtROS could inhibit Type I IFN production and Type I IFN mediated biological actions such as increased production of pro-inflammatory cytokines or cell-to-cell spreads, suggesting their promise for the control of MAB infections.

In conclusion, this study indicated that MAB-R strains versus MAB-S could lead to enahnced Type I IFN productions in infected macrophages via both mechanisms, one for cGAS-STING dependent recognition of bacterial cytosolic DNAs and the other for mitochondrial stress mediated release of oxidized mtDNAs in an actin dependent phagocytosis. Type I IFN induced by MAB-R strains could contribute to

pathogenesis in MAB infections in following three actions. First, Type I IFN could lead to apoptotic or necrotic cell death in infected macrophage, which could compromise innate systems in infected patients, Second, Type I IFN mediated apoptotic cell death could lead to cell-to-cell spreading in infected macrophage, which could provied a broaden niche for the bacterial growth. Third, mitochondrial stress mediated Type I IFN and NLRP3 dependent IL-1β productions could contribute into pathogenesis in infected patients via dampening local inflammation and tissue damage. In addition, this study also suggested that treatment targeting stages involved in mitochondrial ROS generation or actin dependent phagocytosis may be very effective for the control of MAB infections.

REFERENCES

1. Brown-Elliott BA, Wallace RJ, Jr. Clinical and taxonomic status of pathogenic nonpigmented or late-pigmenting rapidly growing mycobacteria. *Clin Microbiol Rev* (2002) 15(4):716-46. PubMed PMID: 12364376; PubMed Central PMCID: PMCPMC126856.

2. Whang J, Back YW, Lee KI, Fujiwara N, Paik S, Choi CH, et al. Mycobacterium abscessus glycopeptidolipids inhibit macrophage apoptosis and bacterial spreading by targeting mitochondrial cyclophilin D. *Cell Death Dis* (2017) 8(8):e3012. doi: 10.1038/cddis.2017.420. PubMed PMID: 28837151; PubMed Central PMCID: PMCPMC5596598.

3. Collins AC, Cai HC, Li T, Franco LH, Li XD, Nair VR, et al. Cyclic GMP-AMP Synthase Is an Innate Immune DNA Sensor for Mycobacterium tuberculosis. *Cell Host Microbe* (2015) 17(6):820-8. doi: 10.1016/j.chom.2015.05.005. PubMed PMID: WOS:000356101600013.

4. Sanguinetti M, Ardito F, Fiscarelli E, La Sorda M, D'Argenio P, Ricciotti G, et al. Fatal pulmonary infection due to multidrug-resistant Mycobacterium abscessus in a patient with cystic fibrosis. *J Clin Microbiol* (2001) 39(2):816-9. doi: Doi 10.1128/Jcm.39.2.816-819.2001. PubMed PMID: WOS:000166776100077.

5. Lee MR, Sheng WH, Hung CC, Yu CJ, Lee LN, Hsueh PR. Mycobacterium abscessus Complex Infections in Humans. *Emerg Infect Dis* (2015) 21(9):1638-46. doi: 10.3201/2109.141634. PubMed PMID: 26295364; PubMed Central PMCID: PMCPMC4550155.

6. Piersimoni C, Scarparo C. Pulmonary infections associated with non-tuberculous mycobacteria in immunocompetent patients. *Lancet Infect Dis* (2008) 8(5):323-34. doi: 10.1016/S1473-3099(08)70100-2. PubMed PMID: 18471777.

7. Kim HY, Kook Y, Yun YJ, Park CG, Lee NY, Shim TS, et al. Proportions of Mycobacterium massiliense and Mycobacterium bolletii strains among Korean Mycobacterium chelonae-Mycobacterium abscessus group isolates. *J Clin Microbiol* (2008) 46(10):3384-90. doi: 10.1128/Jcm.00319-08. PubMed PMID: WOS:000259758900030.

8. Choi G-E, Jo Y, Shin SJ. Current understanding of Mycobacterium abscessus infection. *Journal of Bacteriology and Virology* (2012) 42(1):17-28.

9. Phillips MS, von Reyn CF. Nosocomial infections due to nontuberculous mycobacteria. *Clin Infect Dis* (2001) 33(8):1363-74. doi: Doi 10.1086/323126. PubMed PMID: WOS:000171235600014.

10. Zhang Z, Lu J, Liu M, Wang Y, Zhao Y, Pang Y. In vitro activity of clarithromycin in combination with other antimicrobial agents against Mycobacterium abscessus and Mycobacterium massiliense. *Int J Antimicrob Agents* (2017) 49(3):383-6. doi: 10.1016/j.ijantimicag.2016.12.003. PubMed PMID: 28188830.

11. van Ingen J, Boeree MJ, van Soolingen D, Mouton JW. Resistance mechanisms and drug susceptibility testing of nontuberculous mycobacteria. *Drug*

Resistance Updates (2012) 15(3):149-61.

12. Leao SC, Tortoli E, Euzeby JP, Garcia MJ. Proposal that Mycobacterium massiliense and Mycobacterium bolletii be united and reclassified as Mycobacterium abscessus subsp bolletii comb. nov., designation of Mycobacterium abscessus subsp abscessus subsp nov and emended description of Mycobacterium abscessus. *Int J Syst Evol Micr* (2011) 61:2311-3. doi: 10.1099/ijs.0.023770-0. PubMed PMID: WOS:000295432300048.

13. Tortoli E, Kohl TA, Brown-Elliott BA, Trovato A, Leao SC, Garcia MJ, et al. Emended description of Mycobacterium abscessus, Mycobacterium abscessus subsp. abscessus and Mycobacteriumabscessus subsp. bolletii and designation of Mycobacteriumabscessus subsp. massiliense comb. nov. *Int J Syst Evol Microbiol* (2016) 66(11):4471-9. doi: 10.1099/ijsem.0.001376. PubMed PMID: 27499141.

14. Kim BJ, Yi SY, Shim TS, Do SY, Yu HK, Park YG, et al. Discovery of a Novel hsp65 Genotype within Mycobacterium massiliense Associated with the Rough Colony Morphology. *Plos One* (2012) 7(6). doi: ARTN e38420 10.1371/journal.pone.0038420. PubMed PMID: WOS:000305343900040.

15. Kim BJ, Kim BR, Lee SY, Kook YH, Kim BJ. Rough colony morphology of Mycobacterium massiliense Type II genotype is due to the deletion of glycopeptidolipid locus within its genome. *Bmc Genomics* (2013) 14. doi: Artn 890 10.1186/1471-2164-14-890. PubMed PMID: WOS:000329365700001.

16. Pawlik A, Garnier G, Orgeur M, Tong P, Lohan A, Le Chevalier F, et al. Identification and characterization of the genetic changes responsible for the characteristic smooth-to-rough morphotype alterations of clinically persistent Mycobacterium abscessus. *Mol Microbiol* (2013) 90(3):612-29. doi:

10.1111/mmi.12387. PubMed PMID: 23998761.

17. Bernut A, Herrmann JL, Kissa K, Dubremetz JF, Gaillard JL, Lutfalla G, et al. Mycobacterium abscessus cording prevents phagocytosis and promotes abscess formation. *Proc Natl Acad Sci U S A* (2014) 111(10):E943-52. doi: 10.1073/pnas.1321390111. PubMed PMID: 24567393; PubMed Central PMCID: PMCPMC3956181.

18. Catherinot E, Clarissou J, Etienne G, Ripoll F, Emile JF, Daffe M, et al. Hypervirulence of a rough variant of the Mycobacterium abscessus type strain. *Infect Immun* (2007) 75(2):1055-8. doi: 10.1128/IAI.00835-06. PubMed PMID: 17145951; PubMed Central PMCID: PMCPMC1828507.

19. Simeone R, Bobard A, Lippmann J, Bitter W, Majlessi L, Brosch R, et al. Phagosomal rupture by Mycobacterium tuberculosis results in toxicity and host cell death. *PLoS Pathog* (2012) 8(2):e1002507. doi: 10.1371/journal.ppat.1002507. PubMed PMID: 22319448; PubMed Central PMCID: PMCPMC3271072.

20. Houben D, Demangel C, van Ingen J, Perez J, Baldeon L, Abdallah AM, et al. ESX-1-mediated translocation to the cytosol controls virulence of mycobacteria. *Cell Microbiol* (2012) 14(8):1287-98. doi: 10.1111/j.1462-5822.2012.01799.x. PubMed PMID: 22524898.

21. Smith J, Manoranjan J, Pan M, Bohsali A, Xu J, Liu J, et al. Evidence for pore formation in host cell membranes by ESX-1-secreted ESAT-6 and its role in Mycobacterium marinum escape from the vacuole. *Infect Immun* (2008) 76(12):5478-87. doi: 10.1128/IAI.00614-08. PubMed PMID: 18852239; PubMed Central PMCID: PMCPMC2583575.

22. Wassermann R, Gulen MF, Sala C, Perin SG, Lou Y, Rybniker J, et al.

Mycobacterium tuberculosis Differentially Activates cGAS- and Inflammasome-Dependent Intracellular Immune Responses through ESX-1. *Cell Host Microbe* (2015) 17(6):799-810. doi: 10.1016/j.chom.2015.05.003. PubMed PMID: WOS:000356101600011.

23. Majlessi L, Brosch R. Mycobacterium tuberculosis Meets the Cytosol: The Role of cGAS in Anti-mycobacterial Immunity. *Cell Host Microbe* (2015) 17(6):733-5. doi: 10.1016/j.chom.2015.05.017. PubMed PMID: 26067600.

24. Augenstreich J, Arbues A, Simeone R, Haanappel E, Wegener A, Sayes F, et al. ESX-1 and phthiocerol dimycocerosates of Mycobacterium tuberculosis act in concert to cause phagosomal rupture and host cell apoptosis. *Cell Microbiol* (2017) 19(7). doi: 10.1111/cmi.12726. PubMed PMID: 28095608.

25. Aguilo JI, Alonso H, Uranga S, Marinova D, Arbues A, de Martino A, et al. ESX-1-induced apoptosis is involved in cell-to-cell spread of Mycobacterium tuberculosis. *Cellular Microbiology* (2013) 15(12):1994-2005. doi: 10.1111/cmi.12169. PubMed PMID: WOS:000326934000005.

26. Kim BJ, Shim TS, Yi SY, Kim HC, Kim BR, Lee SY, et al. Mycobacterium massiliense Type II genotype leads to higher level of colony forming units and TNF-alpha secretion from human monocytes than Type I genotype. *APMIS* (2015) 123(10):895-902. doi: 10.1111/apm.12436. PubMed PMID: 26303945.

27. Roux AL, Viljoen A, Bah A, Simeone R, Bernut A, Laencina L, et al. The distinct fate of smooth and rough Mycobacterium abscessus variants inside macrophages. *Open Biology* (2016) 6(11). doi: ARTN 160185 10.1098/rsob.160185. PubMed PMID: WOS:000390348200005.

28. Ripoll F, Pasek S, Schenowitz C, Dossat C, Barbe V, Rottman M, et al. Non mycobacterial virulence genes in the genome of the emerging pathogen Mycobacterium abscessus. *Plos One* (2009) 4(6):e5660. doi: 10.1371/journal.pone.0005660. PubMed PMID: 19543527; PubMed Central PMCID: PMCPMC2694998.

29. Wiens KE, Ernst JD. The Mechanism for Type I Interferon Induction by Mycobacterium tuberculosis is Bacterial Strain-Dependent. *Plos Pathogens* (2016) 12(8). doi: ARTN e1005809

10.1371/journal.ppat.1005809. PubMed PMID: WOS:000383376000039.

30. Shimada K, Crother TR, Karlin J, Dagvadorj J, Chiba N, Chen S, et al. Oxidized mitochondrial DNA activates the NLRP3 inflammasome during apoptosis. *Immunity* (2012) 36(3):401-14. Epub 2012/02/22. doi: 10.1016/j.immuni.2012.01.009. PubMed PMID: 22342844; PubMed Central PMCID: PMCPMC3312986.

31. Gurung P, Lukens JR, Kanneganti TD. Mitochondria: diversity in the regulation of the NLRP3 inflammasome. *Trends Mol Med* (2015) 21(3):193-201. Epub 2014/12/17. doi: 10.1016/j.molmed.2014.11.008. PubMed PMID: 25500014; PubMed Central PMCID: PMCPMC4352396.

32. Weinberg SE, Sena LA, Chandel NS. Mitochondria in the regulation of innate and adaptive immunity. *Immunity* (2015) 42(3):406-17. Epub 2015/03/19. doi: 10.1016/j.immuni.2015.02.002. PubMed PMID: 25786173; PubMed Central PMCID: PMCPMC4365295.

33. Cai X, Chiu YH, Chen ZJ. The cGAS-cGAMP-STING pathway of cytosolic DNA sensing and signaling. *Mol Cell* (2014) 54(2):289-96. Epub

2014/04/29. doi: 10.1016/j.molcel.2014.03.040. PubMed PMID: 24766893.

34. Ma Z, Damania B. The cGAS-STING Defense Pathway and Its Counteraction by Viruses. *Cell Host Microbe* (2016) 19(2):150-8. Epub 2016/02/13. doi: 10.1016/j.chom.2016.01.010. PubMed PMID: 26867174; PubMed Central PMCID: PMCPMC4755325.

35. West AP, Khoury-Hanold W, Staron M, Tal MC, Pineda CM, Lang SM, et al. Mitochondrial DNA stress primes the antiviral innate immune response. *Nature* (2015) 520(7548):553-7. Epub 2015/02/03. doi: 10.1038/nature14156. PubMed PMID: 25642965; PubMed Central PMCID: PMCPMC4409480.

36. Lee H, Kim BJ, Kim BR, Kook YH, Kim BJ. The Development of a Novel Mycobacterium-Escherichia coli Shuttle Vector System Using pMyong2, a Linear Plasmid from Mycobacterium yongonense DSM 45126(T). *Plos One* (2015) 10(3). doi: ARTN e0122897

10.1371/journal.pone.0122897. PubMed PMID: WOS:000352134700207.

37. Snapper SB, Melton RE, Mustafa S, Kieser T, Jacobs WR. Isolation and Characterization of Efficient Plasmid Transformation Mutants of Mycobacterium-Smegmatis. *Molecular Microbiology* (1990) 4(11):1911-9. doi: DOI 10.1111/j.1365-2958.1990.tb02040.x. PubMed PMID: WOS:A1990EJ57800014.

38. Jiang ZF, Georgel P, Du X, Shamel L, Sovath S, Mudd S, et al. CD14 is required for MyD88-independent LPS signaling. *Nat Immunol* (2005) 6(6):565-70. doi: 10.1038/ni1207. PubMed PMID: WOS:000229385900010.

39. Kim BJ, Lee KH, Park BN, Kim SJ, Bai GH, Kim SJ, et al. Differentiation of mycobacterial species by PCR-restriction analysis of DNA (342 base pairs) of the RNA polymerase gene (rpoB). *J Clin Microbiol* (2001)

39(6):2102-9. doi: Doi 10.1128/Jcm.39.6.2102-2109.2001. PubMed PMID: WOS:000169097100011.

40. Kim H, Kim SH, Shim TS, Kim MN, Bai GH, Park YG, et al. Differentiation of Mycobacterium species by analysis of the heat-shock protein 65 gene (hsp65). *Int J Syst Evol Micr* (2005) 55:1649-56. doi: 10.1099/ijs.0.63553-0. PubMed PMID: WOS:000230828200040.

41. Carroll EC, Jin L, Mori A, Munoz-Wolf N, Oleszycka E, Moran HBT, et al. The Vaccine Adjuvant Chitosan Promotes Cellular Immunity via DNA Sensor cGAS-STING-Dependent Induction of Type I Interferons. *Immunity* (2016) 44(3):597-608. doi: 10.1016/j.immuni.2016.02.004. PubMed PMID: WOS:000372784200017.

42. Bierne H, Milohanic E, Kortebi M. To be cytosolic or vacuolar: the double life of Listeria monocytogenes. *Frontiers in Cellular and Infection Microbiology* (2018) 8:136.

43. Rhoades ER, Archambault AS, Greendyke R, Hsu F-F, Streeter C, Byrd TFJTJoI. Mycobacterium abscessus glycopeptidolipids mask underlying cell wall phosphatidyl-myo-inositol mannosides blocking induction of human macrophage TNF-α by preventing interaction with TLR2. (2009):jimmunol. 0802181.

44. Roux AL, Viljoen A, Bah A, Simeone R, Bernut A, Laencina L, et al. The distinct fate of smooth and rough Mycobacterium abscessus variants inside macrophages. *Open Biol* (2016) 6(11). doi: 10.1098/rsob.160185. PubMed PMID: 27906132; PubMed Central PMCID: PMCPMC5133439.

45. Baltierra-Uribe SL, García-Vásquez MdJ, Castrejón-Jiménez NS, Estrella-Piñón MP, Luna-Herrera J, García-Pérez BEJCjom. Mycobacteria entry and

trafficking into endothelial cells. (2014) 60(9):569-77.

46. Stamm LM, Morisaki JH, Gao LY, Jeng RL, McDonald KL, Roth R, et al. Mycobacterium marinum escapes from phagosomes and is propelled by actin-based motility. *J Exp Med* (2003) 198(9):1361-8. doi: 10.1084/jem.20031072. PubMed PMID: WOS:000186423700008.

47. Hartlova A, Erttmann SF, Raffi FA, Schmalz AM, Resch U, Anugula S, et al. DNA damage primes the type I interferon system via the cytosolic DNA sensor STING to promote anti-microbial innate immunity. *Immunity* (2015) 42(2):332-43. doi: 10.1016/j.immuni.2015.01.012. PubMed PMID: 25692705.

48. O'Connell RM, Saha SK, Vaidya SA, Bruhn KW, Miranda GA, Zarnegar B, et al. Type I interferon production enhances susceptibility to Listeria monocytogenes infection. *J Exp Med* (2004) 200(4):437-45. doi: 10.1084/jem.20040712. PubMed PMID: WOS:000223455700004.

49. Osborne SE, Sit B, Shaker A, Currie E, Tan JM, van Rijn J, et al. Type I interferon promotes cell-to-cell spread of Listeria monocytogenes. (2017) 19(3):e12660.

50. White MJ, McArthur K, Metcalf D, Lane RM, Cambier JC, Herold MJ, et al. Apoptotic caspases suppress mtDNA-induced STING-mediated type I IFN production. *Cell* (2014) 159(7):1549-62.

51. Choi AM, Nakahira K. Dampening insulin signaling by an NLRP3'meta-flammasome'. *Nat Immunol* (2011) 12(5):379.

52. Zhou R, Yazdi AS, Menu P, Tschopp J. A role for mitochondria in NLRP3 inflammasome activation. *Nature* (2011) 469(7329):221.

53. Carlsson F, Brown EJ. Actin-based motility of intracellular bacteria, and

polarized surface distribution of the bacterial effector molecules. *J Cell Physiol* (2006) 209(2):288-96. Epub 2006/07/11. doi: 10.1002/jcp.20721. PubMed PMID: 16826602.

54. Gouin E, Welch MD, Cossart P. Actin-based motility of intracellular pathogens. *Curr Opin Microbiol* (2005) 8(1):35-45. Epub 2005/02/08. doi: 10.1016/j.mib.2004.12.013. PubMed PMID: 15694855.

55. Laencina L, Dubois V, Le Moigne V, Viljoen A, Majlessi L, Pritchard J, et al. Identification of genes required for Mycobacterium abscessus growth in vivo with a prominent role of the ESX-4 locus. (2018):201713195.

56. Rayamajhi M, Humann J, Penheiter K, Andreasen K, Lenz LLJJoEM. Induction of IFN-αβ enables Listeria monocytogenes to suppress macrophage activation by IFN-γ. (2010) 207(2):327-37.

57. Campbell-Valois FX, Sachse M, Sansonetti PJ, Parsot C. Escape of Actively Secreting Shigella flexneri from ATG8/LC3-Positive Vacuoles Formed during Cell-To-Cell Spread Is Facilitated by IcsB and VirA. *MBio* (2015) 6(3):e02567-14. doi: 10.1128/mBio.02567-14. PubMed PMID: 26015503; PubMed Central PMCID: PMCPMC4447254.

58. Ozanic M, Marecic V, Abu Kwaik Y, Santic M. The Divergent Intracellular Lifestyle of Francisella tularensis in Evolutionarily Distinct Host Cells. *PLoS Pathog* (2015) 11(12):e1005208. doi: 10.1371/journal.ppat.1005208. PubMed PMID: 26633893; PubMed Central PMCID: PMCPMC4669081.

59. Platanias LC. Mechanisms of type-I- and type-II-interferon-mediated signalling. *Nat Rev Immunol* (2005) 5(5):375-86. doi: 10.1038/nri1604. PubMed PMID: WOS:000228833700012.

60. Ivashkiv LB, Donlin LT. Regulation of type I interferon responses. *Nat Rev Immunol* (2014) 14(1):36-49. doi: 10.1038/nri3581. PubMed PMID: 24362405; PubMed Central PMCID: PMCPMC4084561.

61. Gonzalez-Navajas JM, Lee J, David M, Raz E. Immunomodulatory functions of type I interferons. *Nat Rev Immunol* (2012) 12(2):125-35. doi: 10.1038/nri3133. PubMed PMID: WOS:000300296300012.

62. Manca C, Tsenova L, Freeman S, Barczak AK, Tovey M, Murray PJ, et al. Hypervirulent M. tuberculosis W/Beijing strains upregulate type I IFNs and increase expression of negative regulators of the Jak-Stat pathway. *J Interferon Cytokine Res* (2005) 25(11):694-701. doi: 10.1089/jir.2005.25.694. PubMed PMID: 16318583.

63. Stifter SA, Feng CG. Interfering with immunity: detrimental role of type I IFNs during infection. *J Immunol* (2015) 194(6):2455-65. doi: 10.4049/jimmunol.1402794. PubMed PMID: 25747907.

64. Berry MPR, Graham CM, McNab FW, Xu ZH, Bloch SAA, Oni T, et al. An interferon-inducible neutrophil-driven blood transcriptional signature in human tuberculosis. *Nature* (2010) 466(7309):973-U98. doi: 10.1038/nature09247. PubMed PMID: WOS:000281030300034.

65. Redford PS, Mayer-Barber KD, McNab FW, Stavropoulos E, Wack A, Sher A, et al. Influenza A virus impairs control of Mycobacterium tuberculosis coinfection through a type I interferon receptor-dependent pathway. *J Infect Dis* (2014) 209(2):270-4. doi: 10.1093/infdis/jit424. PubMed PMID: 23935205; PubMed Central PMCID: PMCPMC3873785.

66. Mayer-Barber KD, Andrade BB, Oland SD, Amaral EP, Barber DL,

Gonzales J, et al. Host-directed therapy of tuberculosis based on interleukin-1 and type I interferon crosstalk. *Nature* (2014) 511(7507):99-103. doi: 10.1038/nature13489. PubMed PMID: 24990750; PubMed Central PMCID: PMCPMC4809146.

67. Hagedorn M, Rohde KH, Russell DG, Soldati T. Infection by tubercular mycobacteria is spread by nonlytic ejection from their amoeba hosts. *Science* (2009) 323(5922):1729-33.

68. Gao LY, Guo S, McLaughlin B, Morisaki H, Engel JN, Brown EJ. A mycobacterial virulence gene cluster extending RD1 is required for cytolysis, bacterial spreading and ESAT-6 secretion. *Molecular Microbiology* (2004) 53(6):1677-93. doi: 10.1111/j.1365-2958.2004.04261.x. PubMed PMID: WOS:000223662100010.

국문 초록

Mycobacterium abscessus (MAB)는 비결핵 항산균 (nontuberculous mycobacteria, NTM) 중 신속 발육 마이코박테리아(rapidly grow mycobacteria, RGM)에 속하는 인체 감염 병원균으로서 전 세계적으로 감염과 질환이 증가함에 따라 그의 임상적 중요성이 높아지고 있다. MAB는 집락형에 따라 높은 glycopeptidolipid(GPL) 함량을 가지는 활면 집락형(smooth, S)과 낮은 수준의 GPL을 생산하는 조면 집락형(rough, R)으로 나뉘며, 조면 집락형의 병원성이 활면 집락형에 비해 높다고 알려져 있다. 그러나 MAB의 집락형 차이에 따른 병원성 인자 및 기전은 잘 알려져 있지 않다. 이에 본 연구에서는 제1형 인터페론을 중심으로 한 MAB의 병원성 기전을 설명 하고자 하였다.

MAB 조면 집락형 균주는 액틴 의존적인 식세포작용을 통해 세포 안으로 유입된 후, 파고좀 내에서 능동적인 균 증식을 유도 하였다. 결핵

균과는 다른 방법으로 파고좀 파열(phagosomal rupture)을 이끌어 두 가지 기전으로 제1형 인터페론을 생산함을 확인 하였다. 활면 집락형 균주와 달리 조면 집락형 균주는 1)파고좀에서 세포질로 탈출(phagosomal escape) 후, 이로 인해 세균 DNA가 세포질에 유입되는 기전과 2)더 활발히 미토콘드리아 스트레스를 유도하여 산화된 미토콘드리아 DNA를 세포질로 방출시키는 기전을 통해 cGAS-STING 수용체 인지(recognition)를 유도, 결과적으로 내제적 제1형 인터페론의 생산을 유도한다.

조면 집락형 균주는 제1형 인터페론 의존적으로, 감염된 대식세포의 세포사멸을 유도하고, 세포사멸을 매개로 한 세포 간 전파를 통하여 세균증식을 위한 새로운 서식처(niche)를 제공함으로써 세균의 병원성을 향상 시킬 수 있다. 뿐만 아니라 산화된 미토콘드리아 DNA는 NLRP3 인플라마좀 활성화를 증가시켜 염증성 사이토카인의 일종인 인터루킨-1β(IL-1β)의 생산을 유도함으로써 제1형 인터페론과 상승적으로 조면 집락형 균주의 병원성을 증가시킬 수 있다는 것을 확인하였다. 또한 조면 집락형 균주의 제1형 인터페론 생산의 상위 신호전달 체계인 액틴 의존성 식세포작용 및 미코콘드리아 스트레스를 억제함으로써 대식세포에서의 세균의 증식이 줄어듦을 확인하였다.

따라서, 본 연구 결과는 제1형 인터페론을 중심으로 조면 집락형 균주가 활면 집락형 균주에 비해 높은 병원성을 지니는 기전을 설명하였고, 이를 토대로 조면 집락형 균주와 활면 집락형 균주 변이 간의 병원성 차

이에 대한 새로운 이해 및 MAB 감염 치료 전략을 제시하였다.

주요어: 마이코박테리움 압세수스, 조면 집락형 균주, 파고좀 파열, 제 1 형 인터페론, 세포사, 세포간 전파, 미토콘드리아 스트레스, 인플라마좀

학 번: 2012-21785